INVESTIGATION OF A FLUID-FILLED CELLULAR COMPOSITE FOR RADIATION SHIELDING IN MEDIUM EARTH ORBIT AND INTERPLANETARY SPACE

By

Gabriel D. Maestas

Submitted in Partial Fulfillment
of the Requirements for the Degree of
Master of Science in Mechanical Engineering
with Specialization in Solid Mechanics

New Mexico Institute of Mining and Technology
Socorro, New Mexico
December, 2021

ABSTRACT

One of the primary challenges associated with manned deep space missions is the danger imposed on crew and sensitive electronics by ionizing radiation. There are multiple methods NASA has determined that reduce radiation exposure risk including decreasing transit time, adding active radiation shielding, and increasing passive shielding, among others. Of these methods, it has been determined that the addition of passive radiation shielding with multiuse materials is one of the most viable when considering size and weight constraints necessary for interplanetary travel. It is understood that hydrogen-dense materials perform exceptionally well for radiation shielding purposes, though the materials with the highest density of hydrogen tend to be difficult to implement, as they are: polyethylene, liquid water, and liquid hydrogen. Often discounted for use or retrofitted as an afterthought, the shielding capability of these materials is substantial and would provide noticeable benefits if applicable in multiuse materials.

These hydrogen-dense materials have potential implementation in the Fluid-Filled Cellular Composite (FFCC) for improved radiation shielding capabilities over that of traditional shielding materials like lead, tantalum, and aluminum. The FFCC is a layered composite material inspired by the human skull, where skin layers surround a porous core whose interstitial space is filled with a fluid chosen on a mission-wise basis. From this biomimetic structure, as determined from prior testing, the FFCC has been found to have multiple functions including mechanical structure, acoustic dampening, high strain rate impact resistance, thermal management, and potential in radiation shielding. As the skull maintains a strong housing and a safe, consistent environment for the mammalian brain, the FFCC can be designed to provide similar protection for crew on a spacecraft.

One of the difficulties associated with prior investigations of the FFCC as well as other investigations of nonhomogeneous materials is in modeling the heterogenous layers for analysis in the Space Environment Information System (SPENVIS). In a past investigation, the fluid-filled porous core was modeled as multiple stacked layers of its homogenous components, however this method is suboptimal since layer order affects results in SPENVIS. This is remedied in the current investigation by use of a homogenization process, as discussed in Section Chapter 3, allowing for a more accurate analysis of the FFCC.

Here, the FFCC has been considered for Total Ionizing Dose (TID) after shielding in a silicon detector by computation with the Multi-Layered Shielding Simulation (MULASSIS) tool from GEANT4 in SPENVIS. This has been done in an effort to model the FFCC radiation shielding capabilities in two space environments, Medium Earth Orbit and Interplanetary Space. It has been found that a variety of the tested FFCC compositions have outperformed traditional shielding materials by a Quality Function Deployment (QFD) methodology of shielding, density, and cost. Dependent on specific composition, the FFCC either meets or exceeds the shielding capability of polyethylene, the NASA standard for shielding materials, while maintaining its broad range of multifunctionality [4]. It is this combination of improved shielding with multifunctionality that advances the FFCC as a potential Mars-class material for use as a spacecraft structural layer or within an off-world habitat.

Keywords: Fluid-Filled Cellular Composite; Composite; Radiation Shielding; Simulation; SPENVIS

ACKNOWLEDGEMENTS

I would like to thank my advisor, Dr. Ashok Ghosh, for his support in my pursuit of this investigation. He stepped out a limb accepting me as a student, as I had emailed him with a research inquiry out of nowhere. His work with the Fluid-Filled Cellular Composite has been influential in how I have come to think about physical world. His focus on nature as an example for functional design has brought an amazing material to light in the FFCC. I am happy to have been able to work with him over the course of the last two years, and hope to continue with him for a Doctorate.

I would also like to extend a great thanks to Dr. Cheol Park of NASA Langley Research Center for his advice as my research advisor and radiation shielding subject matter expert. I am constantly amazed at how much Dr. Park knows about the field of radiation shielding and I am appreciative of his willingness to direct my efforts.

Additionally, I would like to thank Dr. Curtis O'Malley and Dr. Jamie Kimberley for joining my committee as advisors for the Solid Mechanics aspect of my work. The courses these professors have taught and the input they provided has been of particular use in my pursuit of this research and my Master's degree. Both have acted to not only improve my education in my time at New Mexico Tech, but have also been excellent examples in how engineers should conduct themselves.

I would like to thank Paul Reimann, for his assistance in providing me a means of connecting Python to the online version of SPENVIS. This code has allowed me to obtain many times more data than I could otherwise by manual input of parameters. Other than being a great computer scientist, Paul has been an excellent friend to me since our days as undergraduates.

Lastly, I would like to thank Dr. Paulo Oemig and the New Mexico Space Grant Consortium for providing partial funding for this research.

This research has been conducted at the New Mexico Institute of Mining and Technology.

This project was partially supported by the New Mexico Space Grant Consortium (NMSGC), NASA Training Grant #NNX15AL51H S010.

CONTENTS

LIST OF TABLES

Table Page

LIST OF FIGURES

LIST OF ABBREVIATIONS AND SYMBOLS

AU	Astronomical Unit
BN	Boron Nitride
BNNTs	Boron Nitride Nano Tubes
ESA	European Space Agency
FFCC	Fluid-Filled Cellular Composite
GCR	Galactic Cosmic Rays
GEANT4	GEometry ANd Tracking
GRAS	GEANT4 Radiation Analysis for Space
HZE	High Atomic Weight and Energy
HZETRN	High Charge and Energy Transport
LET	Linear Energy Transfer
MEO	Medium Earth Orbit
MULASSIS	Multi-Layered Shielding Simulation
NASA	National Aeronautics and Space Administration
NMT	New Mexico Tech
OLTARIS	On-Line Tool for the Assessment of Radiation in Space
SPE	Solar Particle Events
SPENVIS	Space Environment Information System
TID	Total Ionizing Dose
TRL	Technology Readiness Level

The dissertation is accepted on behalf of the faculty Institute by the following committee:

Ashok Kumar Ghosh

_____

Academic and Research Advisor

Cheol Park

_____

Research Advisor

Curtis O'Malley

_____

Jamie Kimberley

_____

I release this document to the New Mexico Institute of Mining and Technology.

Gabriel D. Maestas December 14, 2018

_____

CHAPTER 1: RADIATION SHIELDING CHALLENGES

1. Introduction

A primary challenge for deep space exploration is the inherent risk of extreme levels of ionizing radiation for humans as well as sensitive electronics. The harsh radiation environment of space comes in multiple forms dependent on mission type and duration. Short duration, low earth orbit missions are primarily subject to trapped electron and trapped proton radiation associated with the Van Allen Belts. Long duration, interplanetary missions are at risk from Solar Particle Events (SPEs) and Galactic Cosmic Rays (GCRs) where highly accelerated, light and heavy particles and high-energy EM waves make shielding difficult. Earth's magnetic field effectively shields earth orbits from GCR and SPE, though outside earth's sphere of influence, spacecraft are subject to the full bombardment of the GCR and SPE spectrum. The different space missions and various types of radiation environments necessitate the use of different materials for radiation attenuation. A sheet of paper will effectively shield alpha particles, while many feet of concrete or several inches of lead are required to stop gamma rays. Heavy ions (high Z) from GCR or SPE are the most difficult to shield and can cause secondary radiation from ionization of shielding materials. High-density hydrogen rich materials (such as water) have been shown to provide considerable shielding in this respect. Here, shielding materials are compared to pure polyethylene since NASA considers polyethylene's shielding response as the line dividing traditional radiation shielding materials from state-of-the-art materials [4].

1.1. The Types of Radiation

Radiation is the release of energy from matter and can be either ionizing or non-ionizing. Non-ionizing radiation is low energy, and cannot break bonds in molecules or atoms it interacts with. Examples of non-ionizing radiation are light and heat, which may transfer energy but can only excite molecules. Ionizing radiation on the other hand, carries high enough levels of energy that it can break bonds in molecules and atoms upon interaction. Ionizing radiation comes in two primary forms, each with their own sub-variety. These two forms are electromagnetic radiation which has no mass, and particle radiation which does have mass.

1.2. Electromagnetic Radiation

Electromagnetic radiation is a massless energy, which travels at the speed of light in waves of a given frequency. Light is an example of non-ionizing electromagnetic radiation, while x-rays and gamma rays are examples of ionizing electromagnetic radiation. X-rays and gamma rays are high energy waves that occur from the radioactive decay of nuclei that can travel through great distances of space and through large thickness of materials. To shield x-rays and gamma rays, high atomic number materials with high density are commonly employed, such as lead or tantalum.

1.3. Particle Radiation

Particle radiation is composed of subatomic particles, who's energy is defined by the kinetic energy associated with their mass and speed. Particle radiation can come in a variety of forms, with varying levels of difficulty in shielding, respectively. They are:

1.3.1. Alpha Particles

Alpha particles are identical to helium-4 nuclei, as they are composed of two protons and two neutrons. These charged particles are generally simple to shield, and can be stopped by a sheet of paper or the outermost layers of skin. Higher energy alpha particles, such as those seen ejected in Solar Particle Events are more difficult to shield than those seen emitted from alpha decay on Earth.

1.3.2. Beta Particles

Beta particles are high energy electrons that have been ejected from an atom via beta decay. These can generally be shielded with a thin sheet of plastic or aluminum.

1.3.3. HZE Ions

HZE stands for high atomic number and energy. These charged particles are nuclei of elements larger than helium, traveling close to the speed of light. HZE ions are primarily carbon, oxygen, magnesium, silicon, and iron nuclei ejected from Galactic Cosmic Rays and Solar Particle Events and are one of the most difficult to shield. Though, because they make up less than one percent of SPE, protons present more of a danger to astronauts.

1.3.4. Protons

High energy protons are the primary type of particle radiation from GCRs, making up roughly 90% of the particles. Protons are identical to hydrogen nuclei, as both are a single proton. The earth's magnetic field is strong enough that solar protons are not able to penetrate it, so the majority of GCR and SPE effects are only seen outside of earth's magnetic field.

1.3.5. Neutrons

Neutrons have neutral charge and are one of the most difficult radiation particles to stop. They are a result of nuclear fission or fusion, and cannot be stopped by mass alone. To effectively shield neutron radiation, high hydrogen content material is necessary as it slows the neutrons by complex interactions that are beyond the scope of this research. This is commonly done on earth by the use of water, or by many feet of concrete. Neutrons are also known to impart radioactivity in shielding materials, which is then released in the form of secondary radiation.

.

1.4. Hydrogen Content for Radiation Shielding

Materials with high hydrogen content are considered desirable for radiation shielding purposes. Hydrogen is advantageous as a shielding material for having the greatest ratio of charge to mass of any element [4], where the ratio of electrons to neutrons is equal to 1. This ratio of charge to mass places more molecules in the path of incident ionizing particles than

materials with higher atomic mass, translating to greater fragmentation of incident high Z neutrons present in GCR and SPE [5]. Hydrogen also has the distinct advantage of having a low tendency of creating secondary neutrons or electrons [5]. Secondary neutron radiation is a known danger associated with the use of higher atomic mass materials like aluminum for shielding materials [4][6].

1.5. Radiation Environments

Radiation environments are dependent on mission type and duration. The primary mission types come in the form of orbits around earth or other planets, surface missions, such as those for habitats on the moon, and interplanetary travel like missions to Mars. Each of these missions have different radiation environments associated with them, with each environment being composed of a particular selection of the various radiation types.

1.5.1. Earth Orbit Radiation Environments

Earth orbits are primarily affected by trapped particle radiation from the Van Allen Belts, because the Earth's magnetic field effectively shields the other types of radiation. Trapped particle radiation is composed of electrons and protons that have been trapped in Earth's magnetic field, and are distributed in different sections around Earth. An example of this can be seen in Figure 1.1.

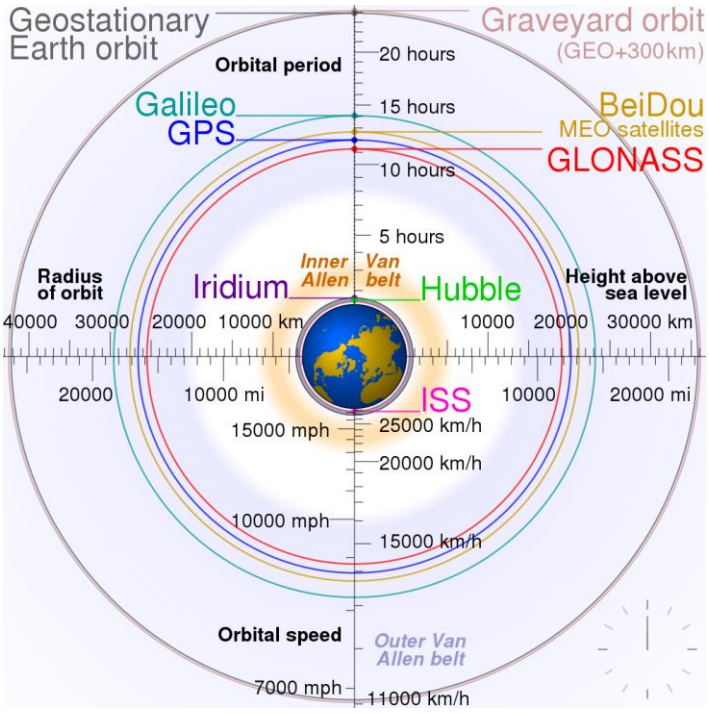

Figure 1.1. Earth Orbits and Altitudes, Van Allen Belts
Image Credit: Wikimedia Commons/Cmglee, Geo Swan
https://commons.wikimedia.org/wiki/File:Comparison_satellite_navigation_orbits.svg

Trapped protons generally have energies ranging from 100keV to hundreds of MeV, while trapped electrons have energies ranging from tens of keV to 10MeV [7]. The location of a

specific orbit dictates how much of each will be present and at what energy. This is determined by the use of various radiation models dependent on the orbit type, as seen in Figure 1.2.

1.5.2. **Interplanetary Radiation Environments**

Interplanetary missions are the harshest type of mission, as no protection is provided by the Earth's magnetic field, so a spacecraft traveling between planets will see the full spectrum of space radiation. The radiation environments of interplanetary space come primarily in the form of Galactic Cosmic Rays and Solar Particle Events. GCR are the constant background radiation of the galaxy, and are composed of high energy protons (90%), high energy helium ions (9%), and HZE (1%). SPE are occasional, but the worst-case scenario for space missions, as they are the radiation emitted from the sun during solar flares or coronal mass ejections. These are primarily composed of protons, but can also include HZE ions as well. A variety of radiation models are available for GCR and SPE, with those used in this research shown in Figure 1.2. The SPE models are often utilized in the form of worst-case scenario as they are not a constant source of radiation, while the GCR models can be used with minimum or maximum average over a particular amount of time.

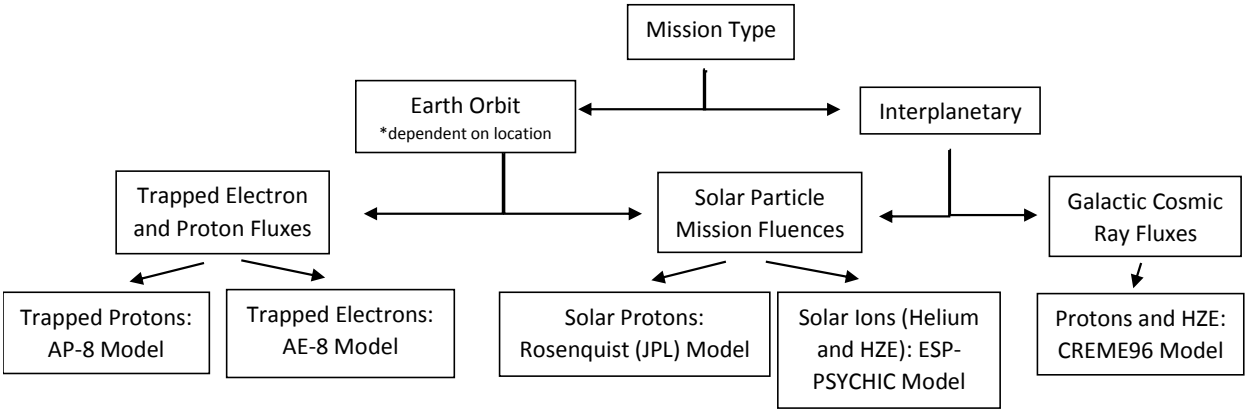

Figure 1.2. Flowchart for Radiation Sources and Models Dependent on Mission Type

Figure 1.2. shows the Flowchart of the radiation models utilized in this research, for the two missions and three radiation environments investigated. This is discussed further in section 3.1., with explanations of why each model and environment were chosen and what settings are associated with their use.

CHAPTER 2: THE FLUID FILLED CELLULAR COMPOSITE

2. Composites as Multifunctional Materials

Bulky shielding materials make extended space travel difficult as constraints on size, weight, and cost limit the distances spacecraft can travel. Composites are particularly useful materials in this realm as they can be made to perform multiple functions, thus reducing constraints, associated costs, and improving overall capabilities. The Fluid-Filled Cellular Composite of this investigation has multiple uses determined from prior testing, including impact resistance [2], acoustic damping [1], and thermal management [8], in addition to mechanical structure [1,2].

2.1. The Fluid-Filled Cellular Composite

The proposed research is focused on the Fluid-Filled Cellular Composite (FFCC), an adaptable composite material inspired by the skeletal structure of humans. Much like the human skull, the FFCC is composed of a sandwiched construction of skin layers surrounding a fluid-filled porous core structure as seen in Figure 2.1

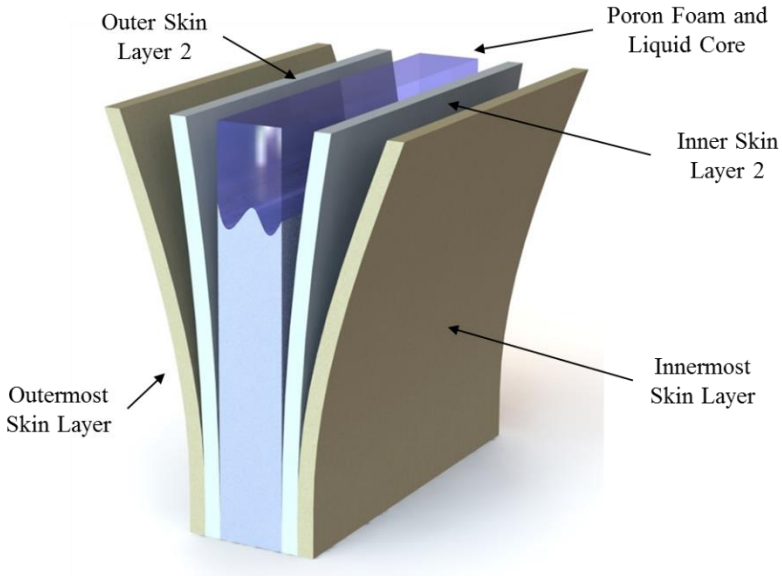

Figure 2.1. The Fluid-Filled Cellular Composite

The core layer is an open-cell, polyurethane foam whose interstitial space is filled with a liquid (generally water, but engineered for each mission). The outermost skin is traditionally a thin film, which protects the other layers from UV radiation, though this can be adjusted for purposes of structural or thermal properties. The outer and inner secondary skin layers are variable with multiple candidate materials available from previous testing, and are generally a structural layer made out of a Kevlar or Nextel [1]. The innermost skin layer can be the same as the outermost for a symmetric composite, or varied for other desirable properties.

2.2. Prior Investigation- Experimental Radiation Analysis [1]

Garley/Ghosh [3] were the first to look at the FFCC for radiation shielding purposes. This was done by experimental testing of a select handful of FFCC samples with a Cobalt-60 radiation source at Sandia National Labs 2.1(d). With a base structure of Kevlar, epoxy, and poron foam, other materials with desirable shielding properties were added to tailor the composite for shielding against gamma radiation. The materials also considered were distilled water, Tyvek, and Boron Nitride. Tyvek is a brand of high-density polyethylene fibers, flash spun into a fabric with potential to shield against alpha and beta particles. Boron Nitride is a nanocomposite and was utilized as a powder that could be suspended in the interstitial water of the poron foam. The goal being to improve the neutron shielding capabilities of the composite via doping with light elements Boron, Nitrogen, Carbon, and Hydrogen without additional material layers. The radiation dosage was varied with the greatest exposure being equivalent to over 100 trips to Mars. Materials were then tested for front and rear face strength to understand the radiation attenuation by comparison of degradation between the front and back layers. Meaning, the gamma radiation was fully shielded if the front face strength was greatly deteriorated while the rear face strength was not.

Out of the 30 samples tested, the (Tyvek/ Kevlar/ Poron/ Water/ Boron Nitride/ Kevlar) sample performed the best in rear face strength (no deterioration), showing the most gamma radiation shielding. This research showed the potential for radiation shielding properties of a layered composite material, and the ability of fluid filled foam to shield radiation even at high doses.

2.3. Prior Investigation- SPENVIS Simulation [3a]

Sid/Ghosh [3a] then explored the implementation of multiple other materials for use in the FFCC as a radiation shield for an Earth orbit. In the selected GPS orbit, trapped electrons are the primary radiation environment the composite needed to attenuate. Considered materials were: Kevlar, Nextel, Tyvek, Boron Nitride, Poron 4701-30 Foam, and polyethylene, which were modeled in the Space Environment Information System (SPENVIS), a Monte Carlo based code, and tested for individual shielding properties. After these materials were simulated and understood individually, random combinations there-in were simulated as layered composites with Kevlar, Poron, and Nextel showing the greatest shielding potential in a five-layer composite. With this, a handful of designs were tested for overall shielding capability via Total Ionizing Dose (TID) in comparison to aluminum and tantalum.

	Layered Composite Material						Traditional Materials	
	Design 1 (areal density, g/cm^2)	Design 2 (areal density, g/cm^2)	Design 3 (areal density, g/cm^2)	Design 4 (areal density, g/cm^2)	Design 5 (areal density, g/cm^2)	Design 6 (areal density, g/cm^2)	Aluminum (areal density, g/cm^2)	Tantalum (areal density, g/cm^2)
Layer 1	Nextel (0.324)	Poron (0.0405)	Kevlar (0.081)	Nextel (0.648)	Kevlar (0.0405)	Kevlar (0.0405)	0.81	0.81
Layer 2	Kevlar (0.0504)	Kevlar (0.0405)	Nextel (0.324)	Kevlar (0.081)	Poron (0.081)	Poron (0.0405)		
Layer 3	Poron (0.081)	Poron (0.0405)	Poron (0.0405)	Poron (0.0405)	Nextel (0.324)	Nextel (0.324)		
Layer 4	Kevlar (0.081)	Kevlar (0.0405)	Poron (0.0405)	Poron (0.0405)	Kevlar (0.0405)	Kevlar (0.081)		
Layer 5	Nextel (0.324)	Nextel (0.648)	Nextel (0.324)	None	Nextel (0.324)	Nextel (0.324)		
TID after shielding (rad)	1871	1655	2271	2511	**1612**	1893	**5483**	**1518**

Table 2.1. Initial Analysis of FFCC Designs in Comparison to Aluminum and Tantalum [3], Copyright 2016, NMT, reprinted with permission.

The best of these (Design 5 in Table 1) was shown to be 1.54 and 1.8 times more effective than aluminum and tantalum respectively, as determined by a Quality Function Deployment analysis of primary radiation, secondary radiation, density, and cost.
Lastly a layer-wise investigation of the design 5 FFCC suggests that this composite can be made to selectively attenuate portions of the GPS orbit radiation spectrum. This is seen in the plot below, where fluence across the energy spectrum is seen to decrease across each layer of material. Moreover, each layer of material is associated with a decrease in a select portion of the spectrum of radiation.

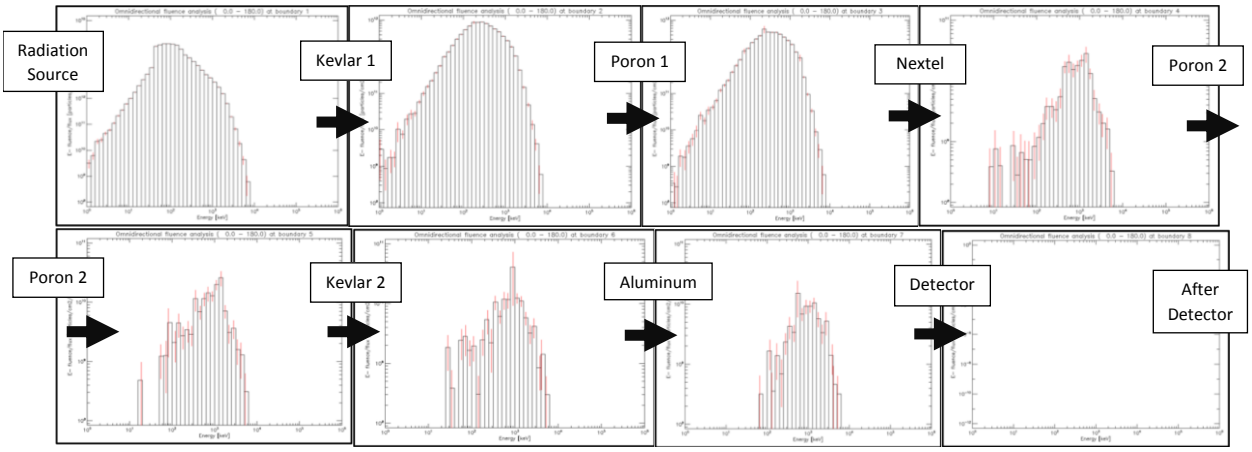

Figure 2.2. Layer-Wise Radiation Filtering with a FFCC [3], Copyright 2016, NMT, reprinted with permission.

It is the discovery of this potential for layer-wise attenuation of portions of the radiation spectrum that make the FFCC a candidate material for radiation shielding. This allows the structural composite to be designed for specific radiation environments, thus optimizing the shielding capabilities on a mission by mission basis and driving down size and cost associated with radiation shielding.

2.4. The Current Investigation

The current investigation begins where the last left off. That is, research is being conducted to determine the FFCC radiation shielding capabilities for use in space. This is done computationally by a layer-wise engineering of the composition of the FFCC in SPENVIS. To do this, first the heterogenous FFCC will be modeled as a combination of homogenous layers for analysis with the Multi-Layered Shielding Simulation (MULASSIS) tool in SPENVIS. It is this homogenization aspect which was ignored in the prior investigations, but will now be addressed. The previously explored materials will be reconsidered, as well as a lunar regolith material that NASA Kennedy Space Center is considering as an in-situ resource. These will make up a database of available materials from which it will be possible to optimize the composition of the FFCC for desired missions. The primary space missions investigated in this research are a Medium Earth Orbit as well as an interplanetary mission, thus covering the two primary portions of a prospective space mission. In a manner similar to the prior investigation, dose after shielding in a silicon detector will be used for a comparative analysis of the various FFCC trials in each environment.

2.5. Goals Associated with this Research

The ultimate goal for the FFCC project as a whole is to develop a multifunctional material for space use. That is, to optimize the design of the FFCC in respect to strength, impact resistance, acoustic dampening, thermal management, and radiation shielding to address space needs for multifunctional, structural materials.

The goal for this research is to determine the applicability or adaptability of the FFCC for radiation shielding purposes alone. This can be more specifically formulated with the goals below:

- To address the issue of modeling the heterogenous core layer of the FFCC.
- To determine FFCC radiation shielding capabilities for optimization to specific space missions.
- To create a material database for consideration in the construction of the FFCC and use in mission-wise optimization.
- To determine shielding characteristics of lunar regolith materials for consideration/ use in the FFCC as a structural habitat material.

CHAPTER 3: SPENVIS SIMULATION

3. Monte Carlo Simulation

The software used to simulate the two primary radiation environments investigated in this research is the Space Environment Information System developed by the European Space Agency, ESA, and the Belgian Institute for Space Aeronomy. SPENVIS is an online tool that utilizes a built-in coordinate generator to determine mission paths and parameters. These parameters are then used in conjunction with select radiation models to determine incident flux associated with the various radiation types present, discussed further in the next section. When a mission and radiation source are defined, the Multi-Layered Shielding Simulation (MULASSIS) tool is used to model materials for shielding analysis. MULASSIS is a tool for analyzing dose and fluence of shielding materials that utilizes and simplifies the application of GEometry ANd Tracking (GEANT4) code which was originally developed in C++. GEANT4 employs Monte Carlo methods for statistical mechanics-based simulation of charged particle interactions in passing through matter.

In comparison to deterministic methods of similar software like NASA's On-Line Tool for the Assessment of Radiation in Space (OLTARIS) and High Charge and Energy Transport (HZETRN), GEANT4 is noted as having good agreement (within 15%) with HZETRN, though without the underestimation of low energy neutrons (below 1 MeV) [9]. GEANT4 is also noted as having multithreading capability for decreased computation times, though that is not implemented in the online version of SPENVIS [9].

SPENVIS allows for the simple generation of macro files for particle sources and implementation with MULASSIS/ GEANT4. For the purposes of this research, MULASSIS is a particularly applicable tool for FFCC analysis as materials are modeled on a layer wise basis, with one dimensional planar geometry as opposed to the three-dimensional geometry as modeled in the GEANT4 Radiation Analysis for Space (GRAS) package which is also available. This planar geometry is more applicable to the FFCC as a low Technology Readiness Level (TRL) plate material without specific geometry.

3.1. The Modeled Radiation Environments

The prior investigation considered the FFCC in a Medium Earth Orbit, per reference with the European Space Agency (ESA) document, "Investigation on the effects of combinations of shielding materials on the total ionising dose for the LAPLACE mission" by Giovanni Santin, Marie Ansart [10]. This research starts with further consideration of the FFCC in the same MEO of the LAPLACE mission, allowing for simple verification and comparison to the layered shielding method outlined by Santin et al. This simulation utilizes orbit information from the appendix of Santin et al defined as: 23528 km Circular Orbit, 56.07 degree Inclination, 1 year duration starting at 01/01/2010.

The AP-8 and AE-8 radiation models in SPENVIS are used for trapped proton and electron fluxes as determined by the mission path. An updated model for trapped proton and electron radiation is available as the AP-9 and AE-9 models, though was not implemented in this research in keeping with Santin et al. [11][12].

The trapped electron spectrum, as generated in SPENVIS per the above orbit definition, can be seen in Figure 3.1, in comparison to the Santin Figure 6 values. It can be seen that the radiation environment defined in this research is in complete agreement with the environment defined by Santin et al. [10]

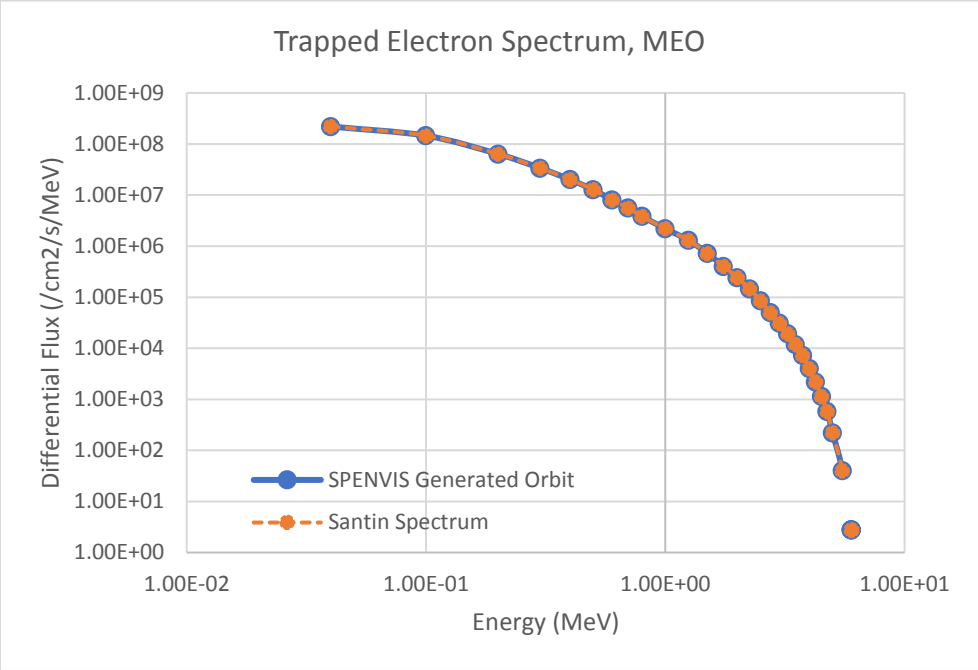

Figure 3.1. Comparison of Generated Radiation Environment with Santin Reference Values

As space missions may extend beyond the Earth's sphere of influence, where SPEs and GCR present a more formidable radiation environment, additional analysis of the FFCC in interplanetary space has been conducted. Here, the mission modeled is based off that of the Mars Science Laboratory Mission [13], with a Hohmann Transfer from Earth (1 AU) to Mars (1.54 AU). The mission modeled in SPENVIS is in interplanetary space, at 1AU, with a duration of 254 days, beginning on 11/26/2011.

This initial investigation in interplanetary space is placed at 1 AU because SPENVIS is not capable of modeling a Hohmann transfer mission (though a mission path could be uploaded to be able to do so). Feynmann et al. have outlined a method to extend the 1 AU proton radiation models to greater heliocentric distances via an inverse square dependence [14], though this is not utilized in this initial investigation and corresponding results are expected to be more conservative. SPENVIS does automatically apply this scaling dependent on heliocentric radius, though a manual example of this radially dependent fluence estimation is seen utilized by Yoon et al. [15] in analysis of dose in a CubeSat on a mission to Mars. This investigation uses the same mission parameters as those outlined by Yoon et al, though without the radial dependence estimation.

A variety of radiation models are available through SPENVIS, with some models being specific to GCR and others being for Solar Particles, as seen in the mission to radiation model flowchart of Figure 1.2. The CRÈME-96 model was used for analysis of proton radiation from

GCR. The Rosenquist (JPL-91) model with a confidence level of 97.7% was utilized for analysis of proton radiation due to solar particles. The ESP-PSYCHIC model with 97.7% confidence was used to analyze Helium-4 radiation from solar particle events. The SPENVIS generated radiation models are shown below.

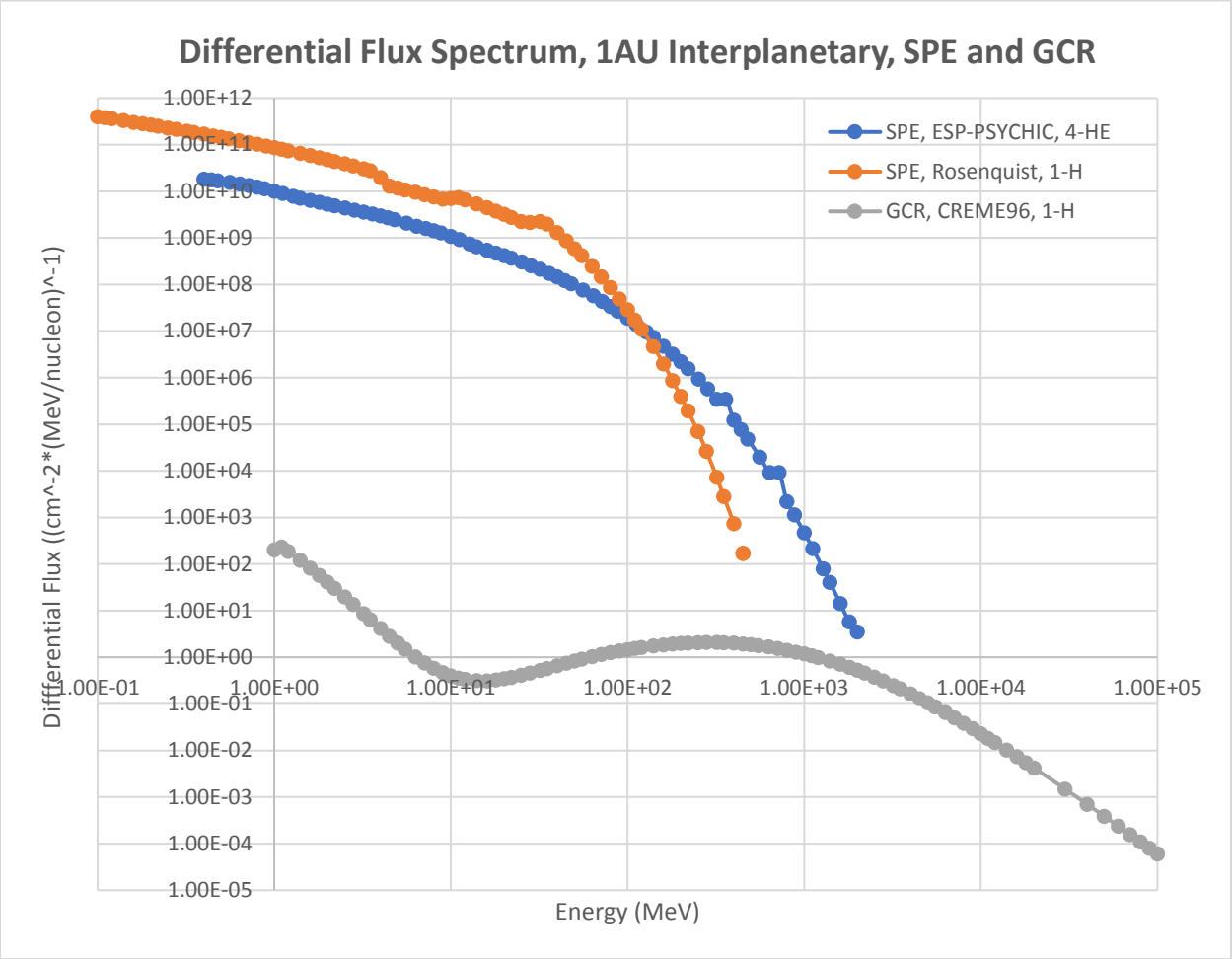

Figure 3.2. GCR and SPE Radiation Spectrum Generated in SPENVIS

It can be seen in Figure 3.2., that the primary concern for a 254-day duration mission at 1AU is likely to be SPE. Here, the Rosenquist model is used primarily for analysis of charged protons (hydrogen nuclei). This model is equivalent to the JPL model developed by Feynmann et al., though with an updated list of solar proton events to decrease the underestimation in fluence associated with the JPL model [7]. SPENVIS recommends that confidence levels for the JPL models should be increased with longer mission durations, as seen below.

Recommended Confidence Levels for Solar Particle Models	
Mission Duration	Confidence Level
1 year	97
2 years	95
3 years	95
4 years	90
5 years	90
6 years	90

Figure 3.3. JPL Confidence Level Recommendations from SPENVIS [7]

For this reason, all models were generated with a confidence level of 97.7%, to account for the (less than one year) duration of a one-way Hohmann transfer. Where confidence level is associated with likelihood of exceeding a given fluence in a mission: "Locate the confidence level required, recalling that a confidence level of say 95% means that only 5% of missions identical to the one considered will have fluences larger than that determined for the 95% confidence level (i.e., probability + confidence level = 100%)." [7]. This is in accordance with Yoon et al. [15] as well.

The SPE spectrum is generally composed of 90% protons (hydrogen nuclei), followed by 9% Helium-4 nuclei, with the remaining 1% distributed in other heavier nuclei. For this reason, both solar protons and 4-He will be modeled for radiation shielding. Because the Rosenquist model only accounts for solar protons, additional use of the ESP-PSYCHIC model is necessary to analyze the effects of heavier nucleons. Single events of heavy solar ions (solar maximum) exceed the effects of GCR and are worth consideration. Alpha particles (4-He) specifically are noted as being dangerous to sensitive electronics like photovoltaics, in addition to astronauts. The 4-He particles present in SPE and GCR are commonly of very high energy, capable of penetrating meters of shielding material in comparison to the millimeters (or less) of shielding as seen with alpha decay on earth.

3.2. Total Ionizing Dose as a Measure of Shielding Effectiveness

Comparison of the Total Ionizing Dose (TID) deposited in a silicon detector after shielding will be used to determine shielding effectiveness of FFCC trials. This analysis is done in the MULASSIS tool by the method utilized by Santin et al. [10], in which a layered material is defined with the last two layers being composed of 100um of aluminum followed by 10um of silicon, representative of a silicon detector. This 100um layer of aluminum is "placed just before the Silicon layer to prevent dose enhancement effects from Auger and Coster Konig electron emission close to the sensitive volume" [10].

Total ionizing dose is the measure of energy (ε) absorbed per unit mass (m) in a shielding material, measured in Gray (J/kg) which equates to 100 rad.

$$TID = \frac{d\varepsilon}{dm}$$

Because radiation models commonly provide the charged particle spectrum in terms of fluence and flux, absorbed dose can be found in simple form from fluence by the following:

$$TID = \frac{1}{\rho} * F * LET$$

Where F is fluence (ionizing particles/cm^2), ρ is the mass density of the material, and LET is the Linear Energy Transfer. LET is the rate of energy loss of a particle traveling through matter, primarily as a function of energy (MeV) and atomic number (Z) in determining collisions in a material over a particular distance.

$$LET = \frac{d\varepsilon}{dx}$$

The multitude of interactions that occur to induce energy loss of charged particles traveling through matter are beyond the scope of this research, though are thoroughly accounted for in GEANT4. The physics of which can be found in the *GEANT4 Physics Reference Manual* [16].

3.3. Validation of Simulation Settings

All SPENVIS settings were kept consistent with the Santin et al. reference and SPENVIS recommendations. Comparison to Santin et al. Figure 5 is used for comparison of output values for aluminum in MEO. SPENVIS output values are seen to have a consistent 40% error from Santin et al. values, so an adjustment factor of 1.75 is added retroactively for direct comparison. See table 3.1. The standard formula for percent error is as follows:

$$\%err = \frac{(reference\ value) - (simulation\ value)}{(reference\ value)} * 100$$

Note a negative percent error implies a simulation value larger than the reference value, while a positive percent error implies a simulation value smaller than the reference value.

Areal Density	Santin Reference Values, Pure Al	MULASSIS Calculated Al	MULASSIS Calculated Al x1.75	%err	%err x1.75
0.81	1.50E+04	**8.95E+03**	1.57E+04	40%	-4%
0.95	7.50E+03	4.91E+03	8.58E+03	35%	-14%
1.08	4.25E+03	2.59E+03	4.54E+03	39%	-7%
1.22	2.20E+03	1.53E+03	2.68E+03	30%	-22%
1.35	1.30E+03	1.08E+03	1.89E+03	17%	-45%
2.16	4.50E+01	1.62E+02	2.83E+02	-259%	-528%
2.7	2.20E+01	3.44E+01	6.03E+01	-57%	-174%

Table 3.1. Percent Error, Compare to Santin Figure 5, TID Pure Aluminum in MEO

For values in Table 3.1, the settings for MULASSIS were kept at the recommended settings by SPENVIS. Settings were also varied in an effort to improve the MULASSIS outputs in comparison to Santin Report values, though no variation proved better than those

recommended by SPENVIS. Since 2012, updates in SPENVIS/MULASSISv1.26 provide more accurate simulation results and necessitate the use of an adjustment factor for comparison to Santin et al. because the overall trend is consistent otherwise. High percent error values at low TID values (areal densities above 1.35g/cm^2 in this case) are expected and accounted for in Chapter 5. All data is presented without adjustment factor. Additional comparison of SPENVIS aluminum shielding response (Table 2.1) to a dose depth curve of aluminum subject to trapped electrons, seen in Figure 5. of Yoon et al., provides additional validation with commensurate thickness predictions for a Medium Earth Orbit environment subject to trapped electron radiation [15].

3.4. Goals of the Analysis

- To develop a database of individual material shielding TID response to various types of radiation and environments.
- To develop/implement a method of homogenizing the polyurethane core layer (poron/water), (BN/water), ((BN/Water)/poron foam), and (liquid hydrogen/poron foam).
- To develop an initial understanding of FFCC response to various radiation environments/types based on compositions used in prior investigation, and intuition gained from individual material responses.
- To develop a FFCC composition that will offer the greatest shielding capability while maintaining perceived structural characteristics and multifunctionality for each mission.

3.5. Analysis Process

- Consider radiation environments and associated radiation types on a mission-wise basis. Starting with MEO and associated trapped proton and trapped electron radiation.
- Consider the TID and fluence response of individual materials to each radiation type. This will formulate a basis for material selection in the FFCC.
- Consider the response of simplified FFCC (Skin layer/ foam/ skin layer) to each radiation type. Compositions determined from prior research, can be used for comparison as well.
- Consider the response of the FFCC with Poron and Water (Skin layer/ water/ foam/ water/ skin layer)
    - Consider the response of FFCC with multiple skin layers and no water (Skin layer 1/ skin layer 2/ foam/ skin layer 2/ skin layer 1), Compositions determined from prior research.
    - This will shed light on influence of multiple layer materials. Interstitial fluid will be ignored to decrease noise associated with added water layers.
- Consider the response of the FFCC with interstitial liquid and suspended BNNTs Water (Skin layer/ water/ BN/ Water/ BN/ skin layer). Ignore Poron foam to decrease error stacking in response. Compositions determined from prior research.
- Consider basic FFCC with homogenized core materials (Skin layer/ homogenized core/ skin layer). Compare to non-homogenized trials from prior compositions.

- Consider FFCC with multiple skin layers and homogenized core (Skin layer 1/ skin layer 2/ homogenized core/ skin layer 2, skin layer 1). This should be representative of the full composition FFCC.
- Consider liquid hydrogen as an interstitial fluid in the porous core section.
- Determine optimal FFCC construction for MEO environment.
- Consider the response of individual materials to SPE and GCR in interplanetary space.
- Consider the response of the MEO-optimal FFCC trials in interplanetary space.
- Consider the response of the geopolymer to each radiation environment and type.

3.6. Simulation Set-Up Process

Consistent simulation set-up is obligatory to provide accurate results. The process for setting up SPENVIS is summarized below:

- Coordinate Generators >
    - Spacecraft Trajectories
        - Define a mission duration.
        - Define a mission type, parameters, and start date.
- Radiation Sources and Effects >
    - Select from:
        - Trapped proton and electron fluxes (standard models)
        - Solar particle mission fluences
        - Galactic cosmic ray fluxes
    - Define a radiation environment associated with the mission.
    - Select a radiation model that is applicable to the defined mission.
- GEANT4 Tools > Multi-Layered Shielding Simulation (MULASSIS)
    - Set MULASSIS parameters for analysis of the FFCC in the desired radiation environment.
    - Source Particle Macro
        - This should be mission based unless a particle spectrum is known, at which point a User Defined environment can be made with a tabulated Incident Energy Spectrum.
        - Set the incident particle type.
        - Use the maximum number of particles for the most accuracy in the simulation (see Chapter 5 for discussion on Error Analysis).
        - Don’t use energy biasing.
        - Linear Interpolation.
        - Omnidirectional angular distribution.
    - Geometry
        - User Defined, Planar Slab
        - Set number of layers to include the FFCC layers in front of 100um of Al and 10um of Silicon
        - Materials must be predefined in the Material Definition tab.
    - Analysis Parameters

        - Total Ionizing Dose (rad)
        - The only data that is necessary is the TID from the last layer (silicon detector), so it must be checked.
    - Cuts in Range
        - Use the default.
    - Create Macro File and use MULASSIS v1.26 to run the simulation.

3.7. Implementation of SPENVIS/MULASSIS with Python

One primary limitation to the use of the online version of SPENVIS is the lack of a batch run capability. It is possible to perform batch runs on the local version of SPENVIS, though at the time of this report it is not yet available to individuals outside of the European Union. Batch run capability is vital to this research due to the volume of calculations necessary to determine the various FFCC composition's functionality in the two radiation environments. In addition, each of these simulations generally take 10-15 minutes when the maximum number of particles are used. Because of this high simulation time and necessity for detailed attention in setting up each simulation, prior research was limited to calculations of TID for single areal density values.

To provide batch run capability, a Python code was created that could interface with the www.spenvis.oma.be website (see Appendix). The code operates by utilizing .har files of the SPENVIS/MULASSIS setup and calculation process. These .har files are essentially a recording of all the network calls made with SPENVIS servers that can later be reuploaded to make the same network calls in the order they were recorded. The .har files are recorded by pushing F12 on a given webpage, starting a recording that includes the MULASSIS setup, starting with settings for the radiation source, continuing with the layer order and materials, and ending with the simulation results output by MULASSIS. Then, when a .har file is recorded with the desired background settings, the settings for layer material, order, and thickness associated with FFCC composition in MULASSIS can be changed in the .har file to run a new composition in the same overall simulation. These steps are all completed in Python, with a batch run simply being a "for" loop cycling through a list of desired value changes in the .har file, which is then uploaded and the results recorded. The ability to change shielding materials and thicknesses also permits the option to optimize structure by iterating FFCC composition to obtain a desired level of shielding for a particular environment. This has been tested initially with limited success, and will be considered in future research.

With the newfound ability to perform batch runs, many times more simulations can be run than was possible in the previous investigations. This ultimately permits the investigators to obtain results for TID as a function of areal density, thus shining light on the trend of each FFCC trial towards complete attenuation of the incident radiation. In addition, when plotting the TID after shielding of each material as a function of areal density specifically (as opposed to TID v. thickness), a comparative analysis for radiation shielding potential can be conducted between materials. This then allows the current investigation to directly compare the various FFCC compositions for TID.

As a helpful note, the implementation of the Python code also has the added benefit of removing the potential for human error in setting up each simulation, because the simulation

only needs to be set up for each radiation environment with the recording of the .har file. This means that so long as the .har file is recorded in the desired format and with the desired settings in SPENVIS/MULASSIS, all subsequent uses of that .har file will apply the same settings.

As a word of caution, intensive use of the online version of SPENVIS through batch runs with the python code has been noted as straining the SPENVIS servers, causing them to crash when overwhelmed by both the script runs and others users. The suggestion by SPENVIS scientist, Erwin De Donder, is to compile the MULASSIS generated files for use on a local version of GEANT4.

CHAPTER 4: FFCC COMPONENT MATERIALS

4. Materials Under Consideration

As the FFCC is a composite of multiple layers, there are several NASA approved materials that will be considered for layer materials due to their various properties. These are:

- Aluminum- As a reference for a current radiation shielding material
  - Chemical Formula: Al
  - Density: 2.7g/cm^3

- Water- For interstitial use in the foam core. Water is noted to have high hydrogen content with an additional oxygen atom that tends not to break into neutrons upon impact, but instead deteriorates into helium nuclei which is a preferable alternative [5].
  - Chemical Formula: H_2O
  - Density: 1.0 g/cm^3

- Boron Nitride (Cubic) – Boron Nitride has been known to provide effective shielding for a variety of the radiation spectrum. BN exists primarily in hexagonal and cubic crystal formations, akin to carbon, with each structure having their own advantages. In this research cubic Boron Nitride will be primarily considered for doping of interstitial water for improved neutron attenuation as tested in a prior investigation, though this low Z material can also be used for doping layer materials for higher strength, thermal stability, and chemical stability. Both boron and nitrogen are noted as having a high neutron absorption cross sections, allowing for good protection from neutron radiation [5].
  - Chemical Formula: BN
  - Density: 3.49 g/cm^3

- Kevlar – an organic, structural fabric with good radiation shielding properties (roughly 80-90% that of polyethylene) [2]. Kevlar is also used for shielding against Micro Meteoroid Orbital Debris (MMOD) and functions well for the associated hypervelocity impacts [6].
  - Chemical Formula: $C_{14}H_{14}N_2O_4$
  - Density: 1.44g/cm^3

- Poron 4701-30 Foam – An open cell urethane foam with good compression set resistance for impact resistance [17].
  - Chemical Formula: $C_3H_7NO_2$
  - Density: 0.4 g/cm^3

- Polyethylene – A NASA qualified radiation shielding material with the highest hydrogen density for a solid. The possibility of laminates made from polyethylene is noted as a worthwhile investigation by NASA [5]. Polyethylene is noted as being somewhat difficult to bond to, therefore its use in laminates/composites is limited. Other research has been conducted in MULASSIS exploring the possibility of a graphite fiber reinforced

polyethylene to address structural concerns associated with pure polyethylene for space use. In addition to the improved mechanical characteristics, shielding was found to slightly improve as well [18].
    - Chemical Formula: $[CH_2\text{-}CH_2]_n$
    - Density: 0.95 g/cm^3

- Tyvek - A flash spun fabric made from high density polyethylene (HDPE). Since Tyvek is a woven fabric made from polyethylene, its potential for mechanical bonds with matrix material in composites is suspected to increase applicability of polyethylene materials in the FFCC as part of a polyethylene fiber reinforced epoxy layer. Tyvek is commercially used for vapor barriers in buildings; with potential use in isolating the fluid-filled core from external layers which may be sensitive to particular liquids. (An example of this is e-glass fibers microcracking with exposure to humidity/ water, and thus the susceptibility of glass-fiber reinforced epoxy composites to humidity).
    - Chemical Formula: $[CH_2\text{-}CH_2]_n$
    - Density: 0.97 g/cm^3

- Nextel Aerospace Fabric 312 – A woven fabric from 3M with extreme temperature resilience while maintaining high strength and flexibility. Generally poor shielding capabilities, but considered for structure in outermost skin layer.
    - Chemical Formula: 62.5% Al_2O_3, 24.5% SiO_2, 13% B_2O_3
    - Density: 2.7 g/cm^3

- Liquid Hydrogen - Hydrogen is the most effective shielding material currently known, though liquid hydrogen is not generally utilized due to difficulties associated with implementation of a liquid in structural applications [5].
    - Chemical Formula: H_2
    - Density: 0.07085g/cm^3

4.1. Core Layer Homogenization

Prior investigations did not consider the foam core structure of the FFCC as heterogenous. This is not necessarily an accurate assumption as MULASSIS/GEANT4 considers particle interactions on a layer-wise basis, with the order of each layer affecting the results. Layer order changes affect result values primarily by means of the secondary radiation produced in the shielding of the incident radiation. This secondary radiation can vary in form and difficulty to shield, with the subsequent layers of material seeing both the remaining primary radiation and resulting secondary radiation. As production of secondary radiation is dependent on both incident radiation type and shielding material, varied layering combinations show differing TID values. Other research has also had the difficulty of trying to model heterogenous composites, such as fiber reinforced materials, as layers of individual components in MULASSIS, and found varying results associated with layer order [18]. MULASSIS does not have a direct means of modeling nonhomogeneous materials, though a process has been presented by SPENVIS support to address this issue (see Appendix) [19]. Since the porous core layer of the FFCC is composed

of a nonhomogeneous combination of foam and liquid, several custom homogenized materials were defined with the goal of acquiring more accurate simulation results by removing potential for uncertainty. A comparison of results has been presented in Chapter 6, and an example of the homogenization process can be seen in the Appendix.

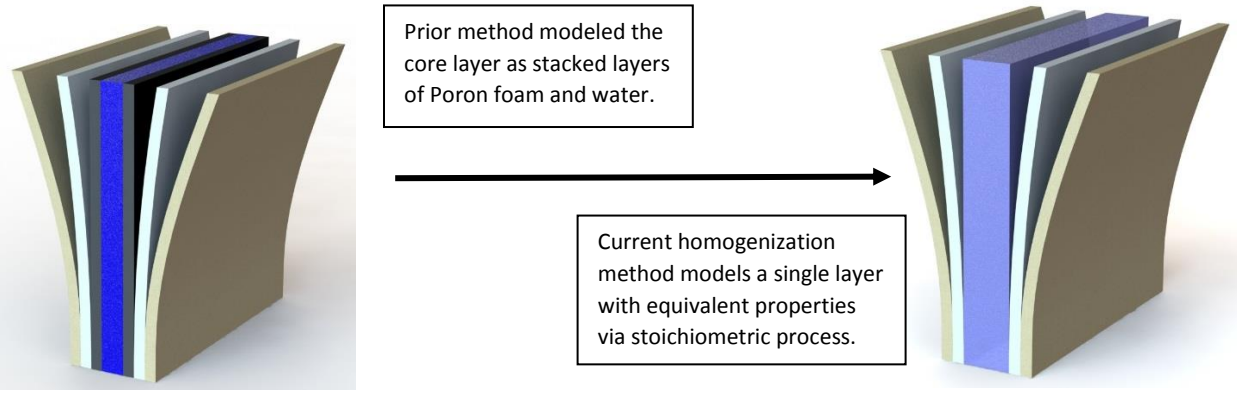

Figure 4.1. FFCC as modeled in MULASSIS, prior v. current core layer homogenization method. Example model of [Kevlar/Tyvek/(Poron/Water)]$_S$ Layered Composite

- BNWATER - is the homogenized material made to represent a solution of Boron Nitride and Water. This was made by mass percent of 11grams of BN per 1.5L (kg) of water as outlined experimentally in prior research [1].
    - Chemical Formula input in SPENVIS: B13-H4632-N13-O2316
    - Resultant Density: 1.018 g/cm^3

- PORONWATER - is the homogenized material made to represent poron foam impregnated with water. The proportion of poron to water was determined from the Poron 4701-30 Data Sheet value for water absorption via submersion of 14% weight gain [10].
    - Chemical Formula input in SPENVIS: C317-H885-N106-O284
    - Resultant Density: 0.474 g/cm^3

- BNWATERPORON - is the homogenized material made to represent a Poron foam layer impregnated with a Boron Nitride and water solution. The proportions were determined by holding the percent weight of poron constant with the PORONWATER homogenization, and dividing the remaining water portion by the percent weight of each component as determined in the BNWATER homogenization.
    - Chemical Formula input in SPENVIS: B5-N1296-C3873-H10811-O3469
    - Resultant Density: 0.476 g/cm^3

- PORONLH- is the homogenized material made to represent a Poron foam impregnated with liquid hydrogen. The proportion of poron to liquid hydrogen was held constant with the PORONWATER definition above.
    - Chemical Formula input in SPENVIS: C27-H174-N9-O18
    - Resultant Density: 0.360 g/cm^3

CHAPTER 5: MONTE CARLO ERROR ANALYSIS

5. Monte Carlo Calculation Error Analysis

In this research utilizing SPENVIS/GEANT4/MULASSIS, it is noticed that higher areal densities correspond to a greater error associated with the calculated TID value. This is expected as MULASSIS is a Monte Carlo based code where statistical methods associated with counting the interactions of (simulated) charged particles with matter are used to converge on a solution that would be difficult to obtain deterministically. This calculation error terminology does not speak to the accuracy of the output values relative to reference values (accuracy error), but with respect to the spread of calculated values around the converged solution of the Monte Carlo simulation (precision error/ uncertainty) (see Appendix for an example of Monte Carlo convergence). It is understood that the more particles the calculation is run with, error/uncertainty associated with the calculation will decrease accordingly, see Figures 5.1 and 5.2.

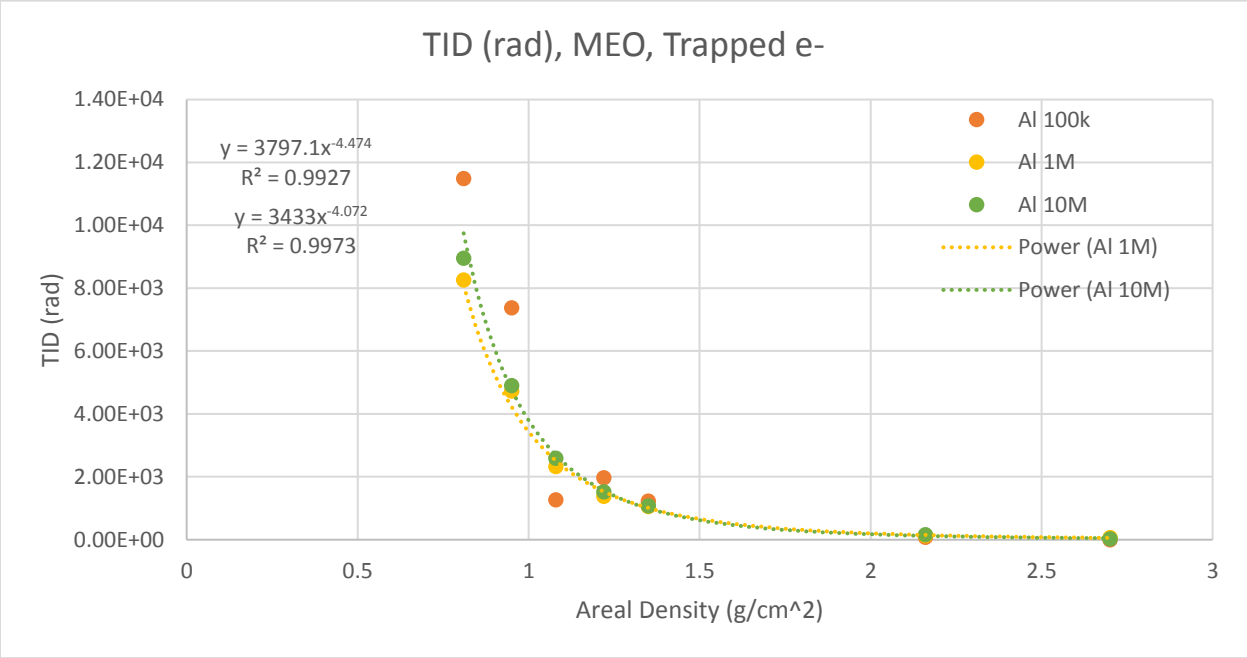

Figure 5.1. Comparison of TID vs. Areal Density for Al, with 100k, 1M, and 10M particles used in calculation

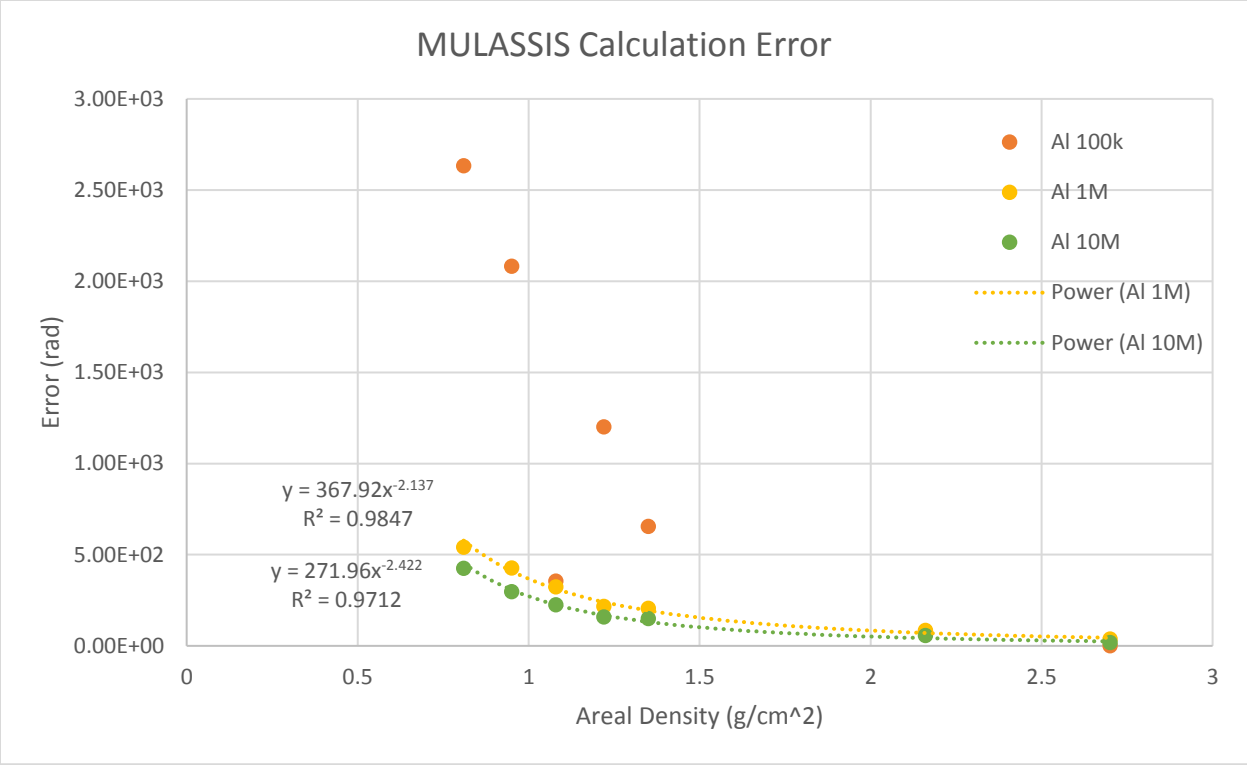

Figure 5.2. Output Error vs. Areal Density for Aluminum with 100k, 1M, and 10M particles used in the calculation

It is seen that both the TID response (Figure 5.1) and the error associated with the Monte Carlo calculation (Figure 5.2) follow a power law curve heading towards zero with increasing areal density. It is expected that the reason higher areal densities have a greater percent error in comparison to reference values is due to the fact that as the TID value decreases, the error associated with the calculation decreases at a slower rate, so the magnitude of the calculation error nears that of the TID output value resulting in a greater error relative to TID with increasing areal density (see Figure 5.3).

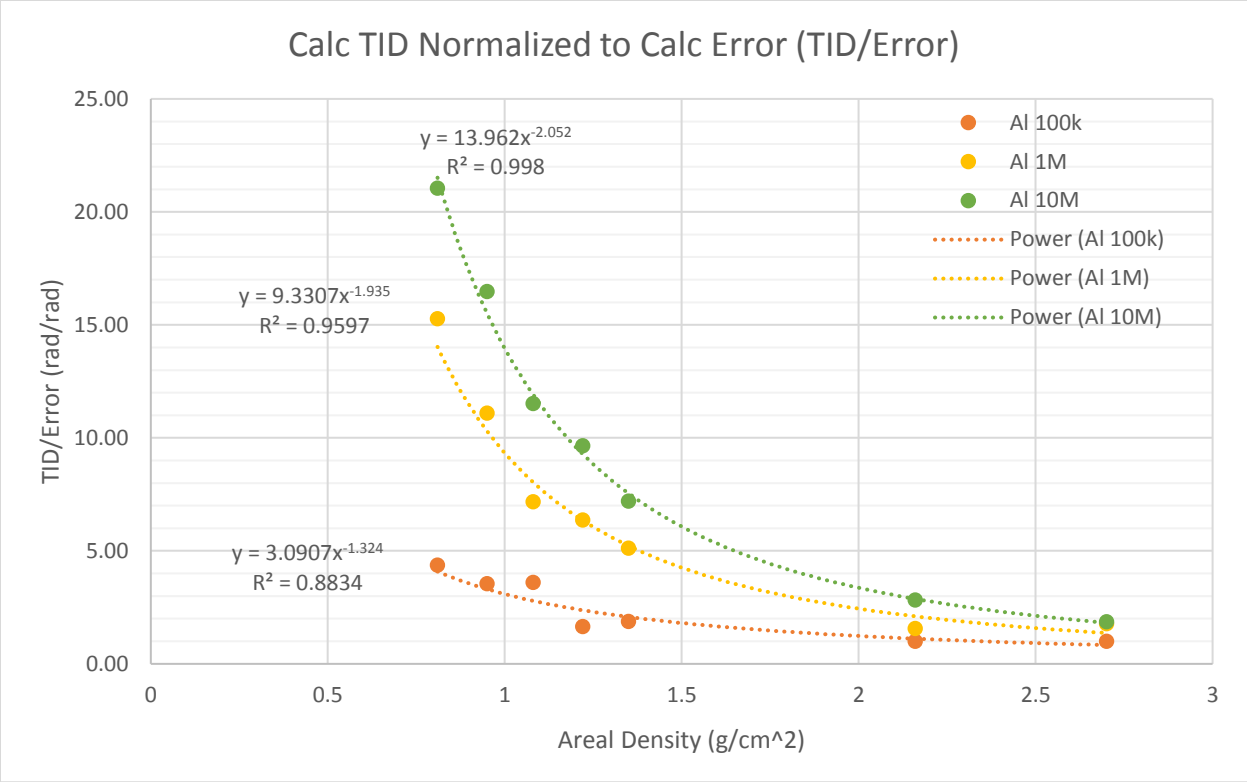

Figure 5.3. Inverse Relative Error (TID Normalized to Output Error) vs. Areal Density for Aluminum with 100k, 1M, and 10M particles used in the calculation

In Figure 5.3 it is seen that the trend of the ratio of TID/Calculation Error converges towards 1 with increased attenuation of the incident radiation, meaning that the magnitude of the error associated with the calculation is the same magnitude as the TID output value. This is not seen when the TID is much greater than the calculation error as seen at lower areal densities or in harsher radiation environments. From this it can be determined that the use of more particles does indeed decrease the calculation error, and the use of lower areal densities decreases the relative error (all else held equal). Lund et al. have shown the statistics associated with analysis of Monte Carlo simulation errors, where relative errors above 20 (in Figure 5.3) are considered quite reliable, values above 10 are reliable, while values between 10 and 5 are questionable, and values less than 5 are not reliable (keep in mind Figure 5.3 of this investigation is inverse to Lund's analysis summarized in his Table 4.6) [9]. For direct comparison to Lund's error analysis, it is useful to present the relationship seen in Figure 5.3 as Relative Error seen in Figure 5.4.

Where it can be seen that an error of less than 5 percent is very reliable, between 5 and 10 percent is reliable, between 10 and 20 percent is questionable, between 20 and 50 percent is less reliable, and relative error above 50 percent is unreliable (M. Lund Table 4.6) [9].

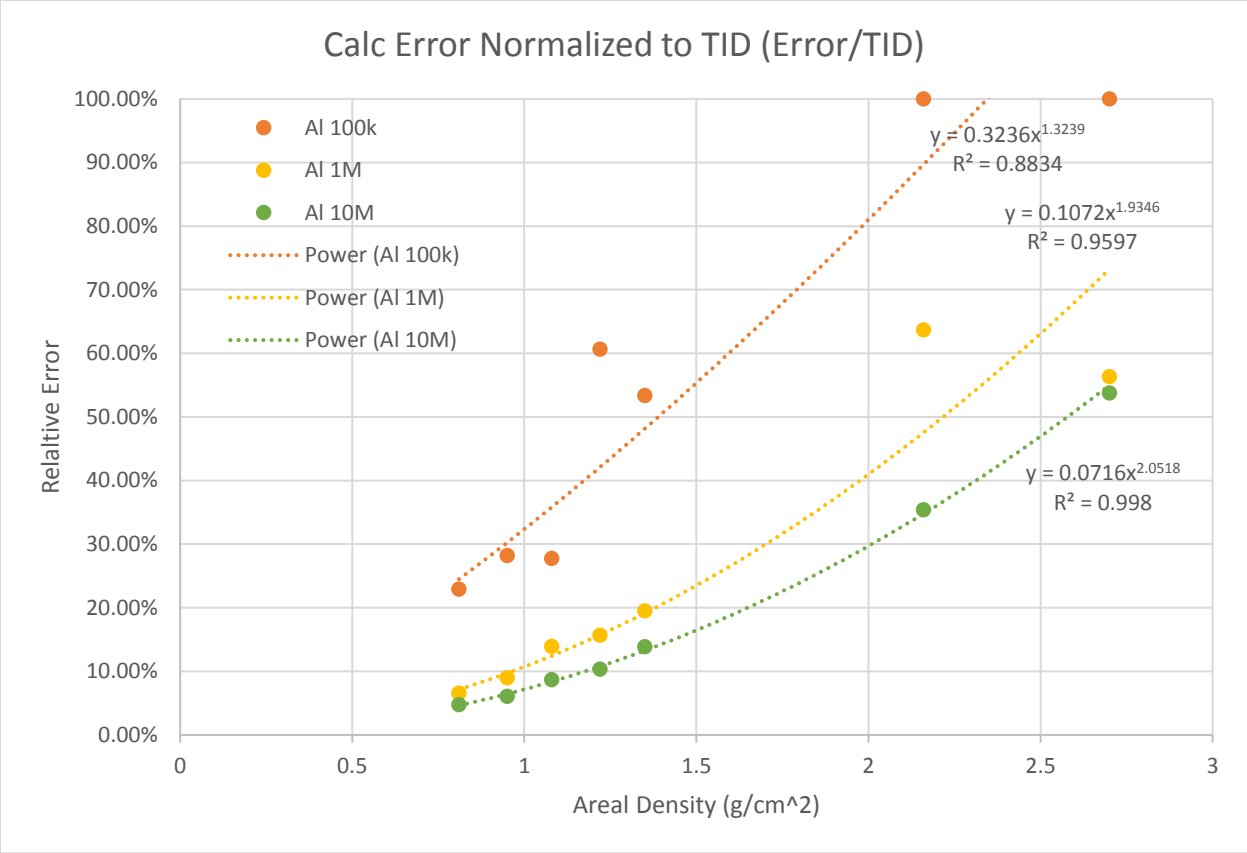

Figure 5.4. Relative Error (Calc Error/ TID) vs. Areal Density for Aluminum with 100k, 1M, and 10M particles used in the calculation

The trend seen in Figures 5.3 and 5.4 is then used to understand that the relative error will increase as TID decreases, so while this example at 10 million particles shows 5% relative error at 0.81g/cm^2, this increases to 53% error at 2.7g/cm^2. As this increased relative error is dependent on TID value (and indirectly dependent on areal density), a high relative error value is not necessarily of primary concern at low TID values. That is, a 100% relative error at a TID of 1.0E4rad spans four orders of magnitude, while 100% relative error at a TID of 1.0E0rad is comparatively miniscule at 2.0rad. Although, high relative error is expected at low TID values, the magnitude of this error fluctuated TID is still greatly diminished.

So, relative error is primarily a function of TID magnitude and number of particles used. This trend is inherent to Monte Carlo methodology and all materials investigated follow suit. Aluminum in MEO subject to trapped electrons was used for this example because aluminum is used as a reference material for this research, and the MEO radiation environment is more variable than the interplanetary environment (see 1AU results).

As the number of particles used in the simulation is the primary factor in decreasing relative error, the maximum number of particles (10 million) was used for the majority of the simulations in this research. Data points for results that lie above the 20% relative error reliability cutoff are still included in the results of this investigation as this information still has value in understanding the trend towards complete radiation attenuation.

CHAPTER 6: SIMULATION RESULTS FOR MEDIUM EARTH ORBIT

6. Results Part I: Medium Earth Orbit

6.1. SPENVIS/GEANT4/MULASSIS calculated TID values (rad) vs. Areal Density (g/cm^2)

TID After Shielding (rad)- Individual Materials and Layered Composites, MEO, AE8, Trapped Electron									
Trial #	Materials	Areal Density (g/cm^2)							# Particles
		0.81	0.95	1.08	1.22	1.35	2.16	2.7	
1	Kevlar	10414.7	5146.8	3043.1	2051.4	906.4	224.1	254.1	10,000,000
2	B-N	14534.4	7997.0	4711.6	2890.8	1500.0	384.4	229.9	10,000,000
3	Poron	8821.6	4528.3	2533.0	1528.6	957.9	249.8	199.8	10,000,000
4	Nextel	10920.6	5507.5	3058.1	1981.8	830.8	79.6	172.4	10,000,000
5	Tyvek	7789.5	4163.8	1925.0	1257.8	727.5	296.1	263.0	10,000,000
6	Polyethylene	9031.0	4580.5	2235.4	1531.2	863.9	157.7	368.6	10,000,000
7	Water	7852.3	4032.8	1995.4	1346.0	711.2	190.7	59.7	10,000,000
8	Ta	1789.8	880.0	605.8	474.1	200.1	139.3	102.0	10,000,000
9	Al	8952.0	4905.6	2591.6	1531.0	1080.7	161.6	34.4	10,000,000
10	Lunamer	7146.5	4067.4	1973.0	1197.8	563.7	30.9	26.4	10,000,000
11	LiquidHydrogen	737.2	455.1	436.8	376.3	341.9	352.5	258.3	10,000,000
12	BNWATER	8099.5	3871.9	1971.7	1325.4	850.4	174.7	114.2	10,000,000
13	PORONWATER	8922.4	4356.7	2286.8	1567.3	965.4	184.4	247.0	10,000,000
14	BNWATERPORON	9014.3	3885.9	2591.0	1324.9	970.3	169.2	153.2	10,000,000
15	PORONLH	6261.4	3126.7	1859.5	859.1	504.6	285.1	92.9	10,000,000
16	1/2 Al Ta	3302.2	1400.4	878.7	299.0	379.8	62.5	16.2	1,000,000
17	1/2 Al Pb	3060.9	1287.3	554.1	207.5	130.8	53.3	69.8	10,000,000
18	1/2 Nextel BN	13548.9	7316.2	4477.4	2533.3	1246.2	280.1	211.5	1,000,000
19	1/3 Nextel Poron Nextel	9863.8	5902.9	3101.9	1390.5	802.2	277.5	60.6	1,000,000
20	1/3 Kevlar Poron Kevlar	9331.5	6141.7	2924.4	1493.3	891.1	329.5	251.9	1,000,000
21	1/3 Nextel Tyvek Nextel	9810.2	4884.5	2629.2	1570.4	962.0	110.1	200.9	1,000,000
22	1/5 Nexteb Poron Water Poron Nextel	9680.3	4654.4	2935.7	1301.1	1313.3	109.9	187.4	1,000,000
23	1/5 Nextel Water Poron Water Nextel	8991.7	5731.5	2669.9	1425.6	888.1	239.6	281.7	1,000,000
24	1/5 Kevlar Poron Water Poron Kevlar	9567.7	5785.8	3071.4	1558.9	1245.5	207.2	65.8	1,000,000
25	1/5 Kevlar Nextel Water Nextel Kevlar	10851.0	4709.3	3462.0	1552.1	882.6	125.9	101.6	10,000,000
26	1/5 Kevlar Poron Nextel Poron Kevlar	10081.2	4876.1	2975.9	1312.3	648.1	114.3	39.6	1,000,000
27	1/5 Nextel Kevlar Poron Kevlar Nextel	10393.0	6319.4	3202.5	1836.5	968.9	112.8	242.5	1,000,000
28	1/5 Kevlar Tyvek Nextel Tyvek Kevlar	9748.4	5196.7	2628.5	1659.5	1077.7	64.4	263.1	10,000,000

29	1/5 Nextelb Tyvek Nextel Tyvek Nextelb	9129.4	4941.0	2808.1	1283.8	939.7	246.3	148.1	1,000,000
30	1/5 Kevlar BN Water BN Kevlar	11807.0	6804.1	3303.7	2200.3	2052.4	210.9	81.4	1,000,000
31	1/5 Kevlar Water BN Water Kevlar	11478.7	5858.7	3381.7	1751.8	812.0	263.6	158.8	1,000,000
32	1/5 Tyvek BN Water BN Tyvek	10909.9	5735.7	2764.8	2158.2	985.9	311.2	53.3	1,000,000
33	1/5 Tyvek Water BN Water Tyvek	9752.8	5150.4	2737.6	1681.6	942.1	172.0	15.8	1,000,000
34	1/6 Nextel 1/6 Poron 1/3 Water 1/6 Poron 1/6 Nextel	9723.2	5107.9	2789.7	1406.0	1301.9	169.2	189.2	10,000,000
35	1/6 Nextel 1/6 Water 1/3 Poron 1/6 Water 1/6 Nextel	10332.1	5592.3	2417.3	1185.3	1173.1	236.8	129.8	10,000,000
36	1/6 Kevlar 1/6 Poron 1/3 Water 1/6 Poron 1/6 Kevlar	10687.9	5332.6	2911.6	1396.0	921.3	208.6	277.2	10,000,000
37	1/6 Kevlar 1/6 Water 1/3 Poron 1/6 Water 1/6 Kevlar	10219.8	5561.3	2855.4	1340.2	959.9	210.2	153.1	10,000,000
38	1/6 Kevlar 1/6 Nextel 1/3 Water 1/6 Nextel 1/6 Kevlar	8761.0	5380.8	2747.5	1307.1	733.5	107.6	128.7	10,000,000
39	1/6 Kevlar 1/6 Water 1/3 Nextel 1/6 Water 1/6 Kevlar	10012.2	4608.3	2311.5	1553.9	904.4	188.2	72.7	10,000,000
40	1/3 Kevlar 1/3 PORONWATER 1/3 Kevlar	10381.8	5342.7	2991.3	1697.2	1192.7	318.7	195.9	10,000,000
41	1/3 Nextel 1/3 PORONWATER 1/3 Nextel	9941.4	5424.5	3023.7	1718.1	901.6	128.4	205.7	10,000,000
42	1/6 Kevlar 2/3 PORONWATER 1/6 Kevlar	9476.0	5160.1	2183.9	1906.5	1041.1	344.5	197.6	10,000,000
43	1/6 Nextel 2/3 PORONWATER 1/6 Nextel	8571.2	4915.6	2549.6	1494.5	1026.8	133.0	245.5	10,000,000
44	1/3 Kevlar 1/3 BNWATER 1/3 Kevlar	9015.7	4927.2	2981.6	1883.8	980.8	168.9	147.1	10,000,000
45	1/3 Nextel 1/3 BNWATER 1/3 Nextel	10180.6	5160.6	2820.4	1622.2	970.9	122.1	100.6	10,000,000
46	1/6 Kevlar 2/3 BNWATER 1/6 Kevlar	8311.5	4904.2	2765.8	1384.2	1018.1	203.2	212.6	10,000,000

47	1/6 Nextel 2/3 BNWATER 1/6 Nextel	8830.3	4592.3	2689.1	1190.7	891.1	234.0	79.9	10,000,000
48	1/3 Kevlar 1/3 BNWATERPORON 1/3 Kevlar	10169.9	4868.5	3108.2	1596.0	1349.3	303.9	232.6	10,000,000
49	1/3 Nextel 1/3 BNWATERPORON 1/3 Nextel	9799.2	4953.0	2991.6	1570.2	1085.3	67.9	317.5	10,000,000
50	1/6 Kevlar 2/3 BNWATERPORON 1/6 Kevlar	8533.7	4778.8	2387.1	1406.6	1039.2	256.8	132.5	10,000,000
51	1/6 Nextel 2/3 BNWATERPORON 1/6 Nextel	9305.0	4846.6	2571.5	1538.7	788.0	118.3	262.5	10,000,000
52	1/6 Tyvek 2/3 PORONWATER 1/6 Tyvek	8857.9	4205.8	2532.1	1162.3	667.6	288.5	152.5	10,000,000
53	1/6 Tyvek 2/3 BNWATER 1/6 Tyvek	7552.9	4237.8	1972.3	1146.3	739.7	140.4	115.0	10,000,000
54	1/6 Tyvek 2/3 BNWATERPORON 1/6 Tyvek	8538.7	4224.5	1943.3	1484.6	1005.0	232.4	224.7	10,000,000
55	1/6 Kevlar 1/6 Tyvek 1/3 PORONWATER 1/6 Tyvek 1/6 Kevlar	9042.6	4900.5	2316.0	1698.2	815.3	316.6	242.4	10,000,000
56	1/6 Kevlar 1/6 Tyvek 1/3 BNWATER 1/6 Tyvek 1/6 Kevlar	8465.4	4850.0	2956.7	1471.3	1097.8	288.7	141.4	10,000,000
57	1/6 Kevlar 1/6 Tyvek 1/3 BNWATERPORON 1/6 Tyvek 1/6 Kevlar	9297.6	4246.5	2484.5	1726.6	867.5	200.7	188.0	10,000,000
58	1/6 Tyvek 2/3 PORONLH 1/6 Tyvek	7045.9	3357.3	1897.9	887.4	881.1	216.1	317.7	10,000,000
59	1/6 Nextel 2/3 PORONLH 1/6 Nextel	7614.2	3806.3	1880.3	1297.8	613.5	95.7	126.8	10,000,000
60	1/6 Kevlar 2/3 PORONLH 1/6 Kevlar	7263.0	4186.4	2128.6	1005.6	747.4	262.7	330.3	10,000,000
61	1/6 Kevlar 1/6 Tyvek 1/3 PORONLH 1/6 Tyvek 1/6 Kevlar	8323.0	4512.9	2311.8	1537.6	973.9	247.5	255.6	10,000,000
62	1/6 Nextel 1/6 Tyvek 1/3 PORONLH 1/6 Tyvek 1/6 Nextel	8434.5	4386.5	2338.0	1150.2	941.2	204.9	284.8	10,000,000

Table 6.1. TID Response (rad) vs. Areal Density (g/cm^2), MEO, Trapped Electron Radiation

6.2. Part I: Discussion of MEO Results

For all trials, the plots are provided with both standard and log scale on the y-axis. This is because the log scale occasionally provides a view of the data that is more easily read, because the data commonly spans multiple orders of magnitude and follows a power law trend. (The x-axis is not on a log scale as it spans closely grouped points.)

This MEO analysis focuses on shielding trapped electrons, though trapped protons are also present in this GPS orbit to a much lower extent. This is because the GPS orbit sits in the outer belt of the Van Allen Belts, which is dominated by trapped electrons (in comparison to the inner belt which is dominated by trapped protons). FFCC response to trapped protons was not considered here because all areal densities necessary to shield trapped electrons will shield the proton spectrum. The incident particle fluence of the trapped protons in comparison to trapped electrons can be seen in A6.

Various compositions of the FFCC were analyzed in Medium Earth Orbit, with all settings but those associated with layer-wise materials and thicknesses remaining constant. For the purposes of this research, the composites investigated here were kept symmetric. This is primarily to simplify future analysis of the layered composites for mechanical structure. Composition of the FFCC can be designed to have desirable mechanical properties, by varying layer matrix materials, fibers, stacking order, symmetry, and orientation to obtain constitutive equations for particular Stress-Strain characteristics [20]. The consideration of FFCC mechanical properties in addition to shielding will be the focus of future research, with the goal of multifunctional optimization to specific use cases of the FFCC. In this respect, Yao Cai et al have considered two viable methods for multivariate optimization of resin matrix composites for shielding, mechanical properties, thermal properties, and mass [21].

Not considered in this analysis is the matrix material of the composite face layers. The FFCC matrix material that has been investigated in the past is an epoxy resin, which is noted as having substantial hydrogen content [22][23]. This epoxy layer was not considered in this investigation in an effort to keep the skin layers homogenous, as addition of a fiber reinforced epoxy layer would represent another heterogenous layer to consider in addition to the core layer. Omission of matrix material in this research is assumed to not have a large effect on shielding effectiveness, though will be considered in future investigations.

In a variety of the trials, there is a noticeable amount of ‘noise’ in the TID v. areal density response. This is most noticeable in the ‘blip’ at 1.22g/cm^2 in tantalum. This is likely due to two primary factors: that the code is Monte Carlo based, and the fluctuation of incident particles due to orbit through the Van Allen Belts. The value fluctuation inherent to Monte Carlo method is explained further in A4. The latter is explained simply by understanding that the Van Allen Belts, notably the outer belt (extending from 13,000 – 60,000km), is known to be quite variable in both its shape and intensity. Meaning there is likely some additional uncertainty in the calculation’s solution due to orbit through the outer belt.

6.2.1. **Comparative Baseline: TID, in MEO, Trapped Electron Radiation (Trials 6, 8, 9)**

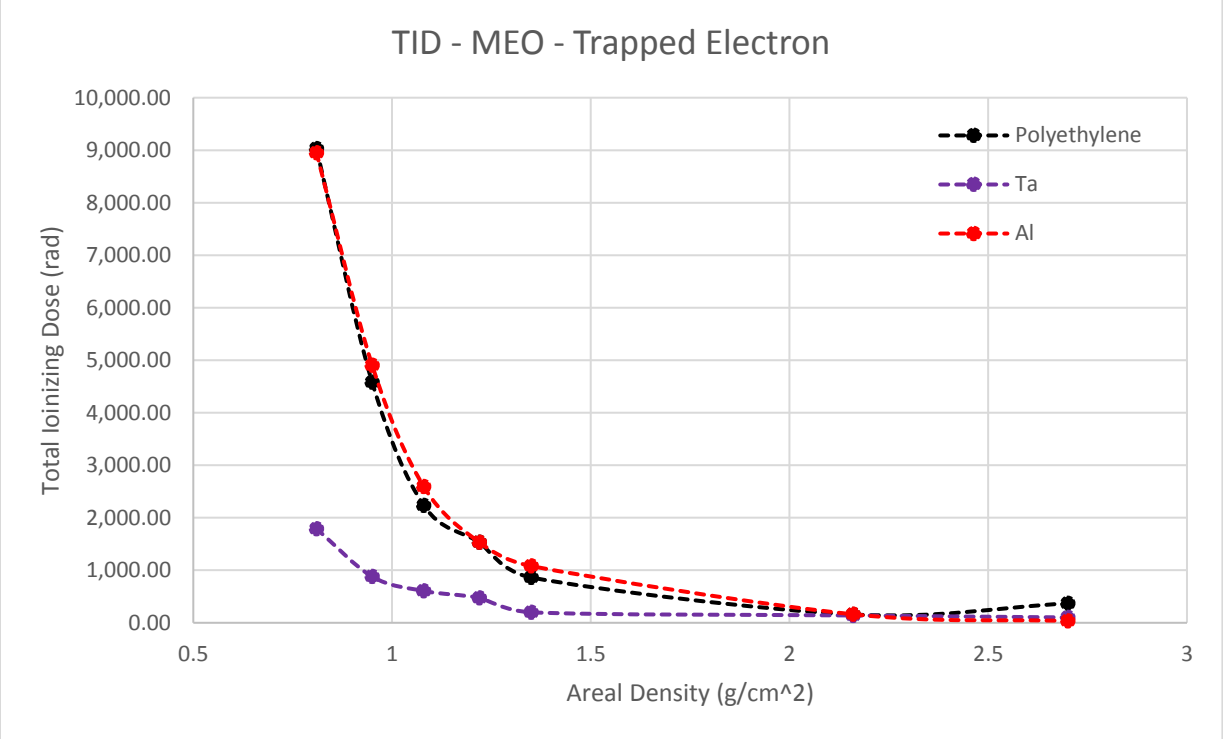

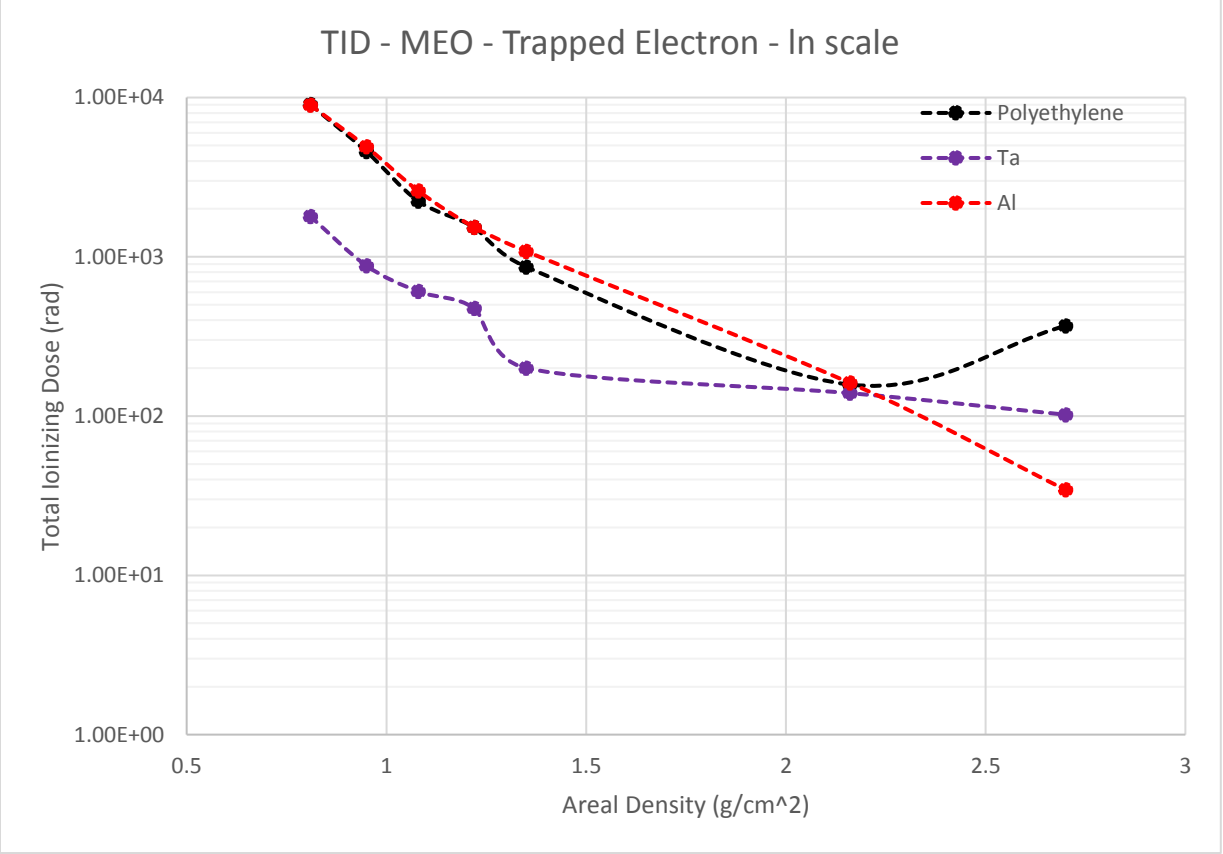

Aluminum, tantalum, and polyethylene are used as the comparative baseline for all other radiation shielding materials in a particular environment. As expected, polyethylene is the most functional shielding material of the three, with the lowest TID values, followed by aluminum and tantalum, respectively.

6.2.2. **TID, Individual Materials in MEO, Trapped Electron Radiation (Trials 1-9)**

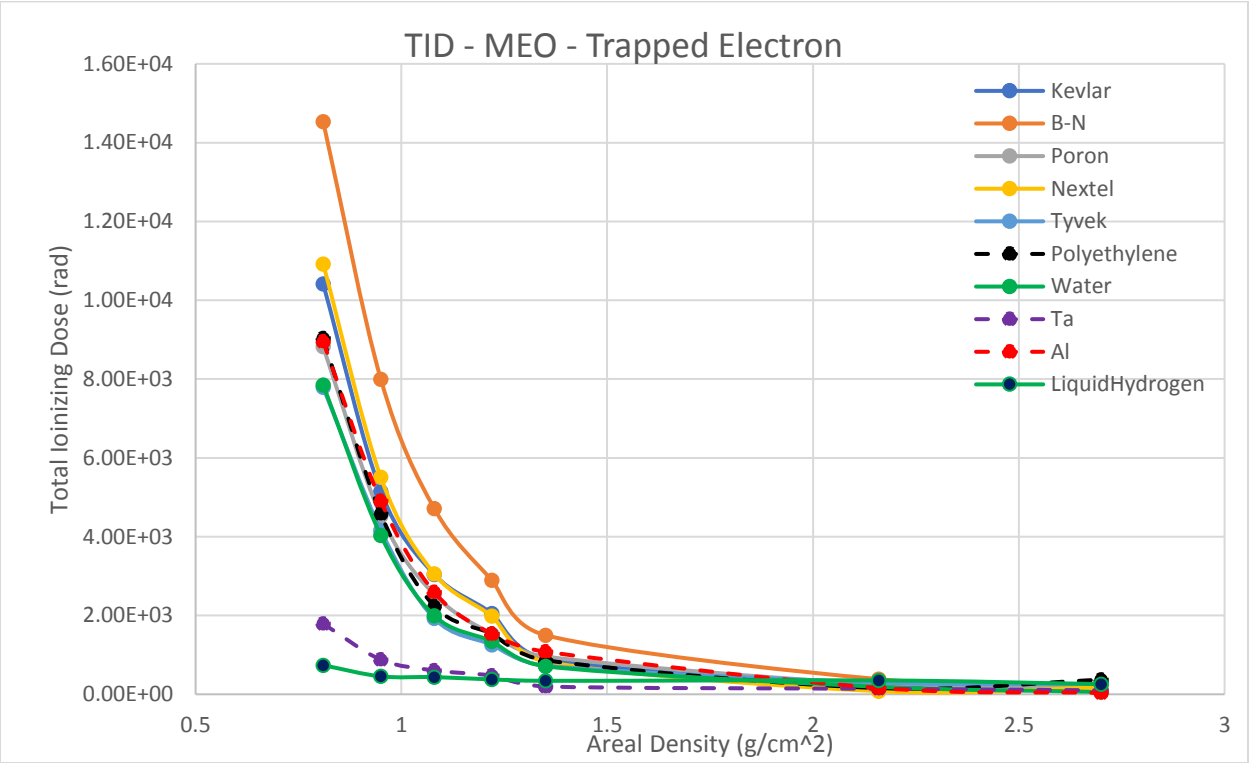

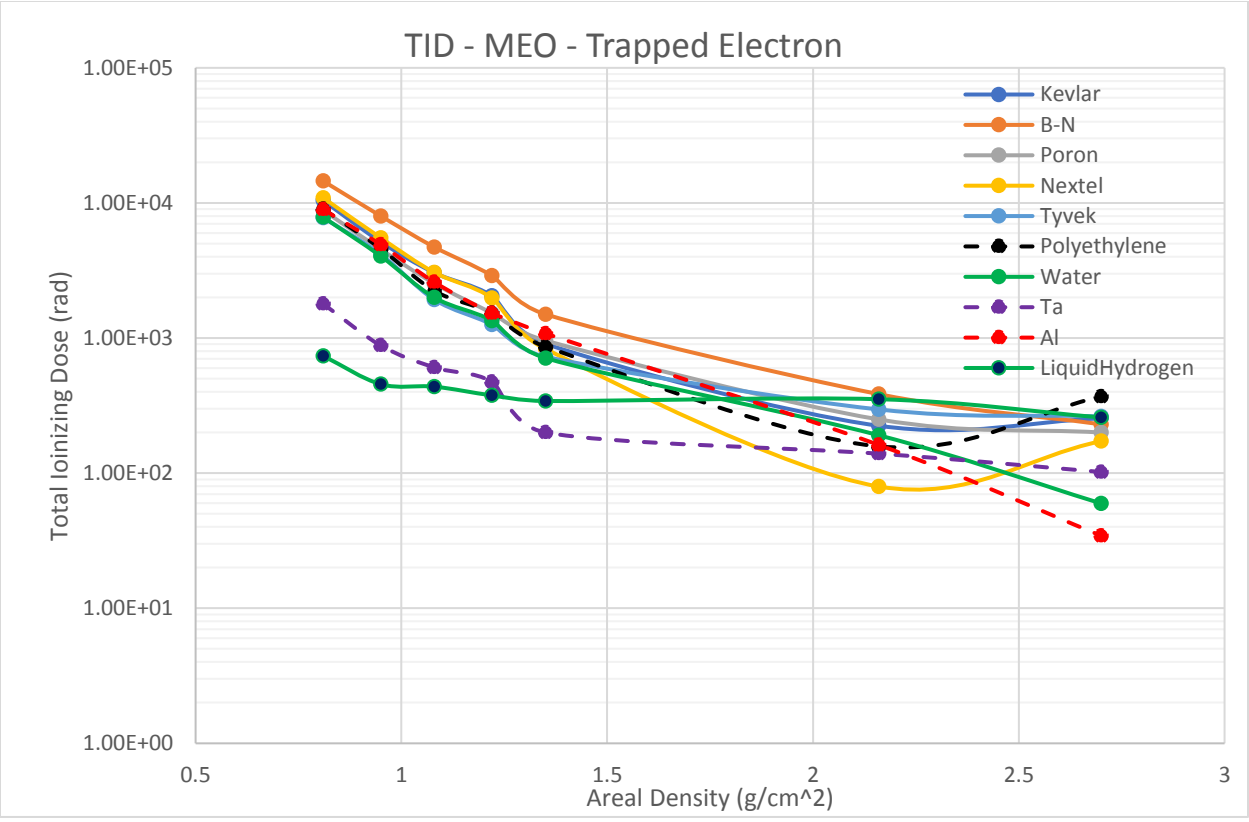

Here the individual materials considered for use in the FFCC are modeled in response to trapped electron radiation. It can be seen that Tyvek performs slightly better than polyethylene even though both have the same molecular structure. This increased attenuation is due to the slightly higher density of Tyvek over polyethylene. Interestingly, Poron, a polyurethane foam, outperforms both aluminum to have nearly the same TID as polyethylene for trapped electron radiation (within the order of the relative error). Otherwise, individual materials behave as expected, with those materials with a high hydrogen content showing improved shielding.

6.2.3. **TID, Homogenized Individual Materials in MEO, Trapped Electron Radiation (Trials 10-15)**

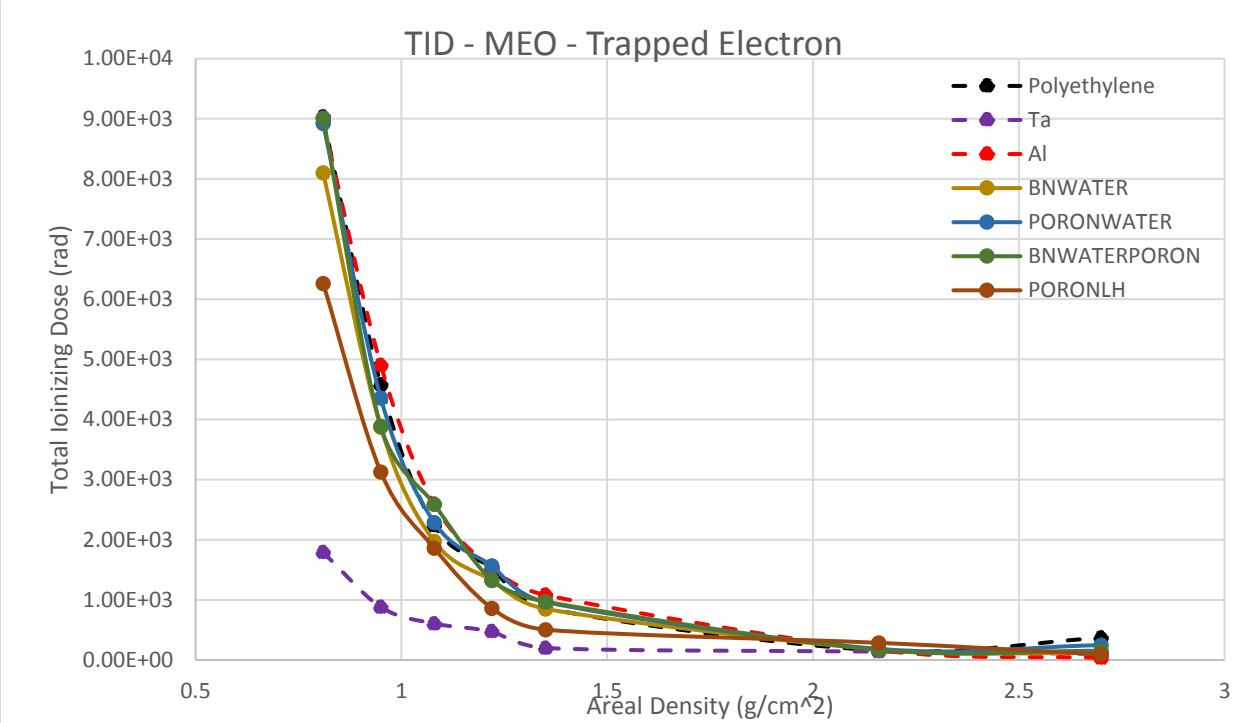

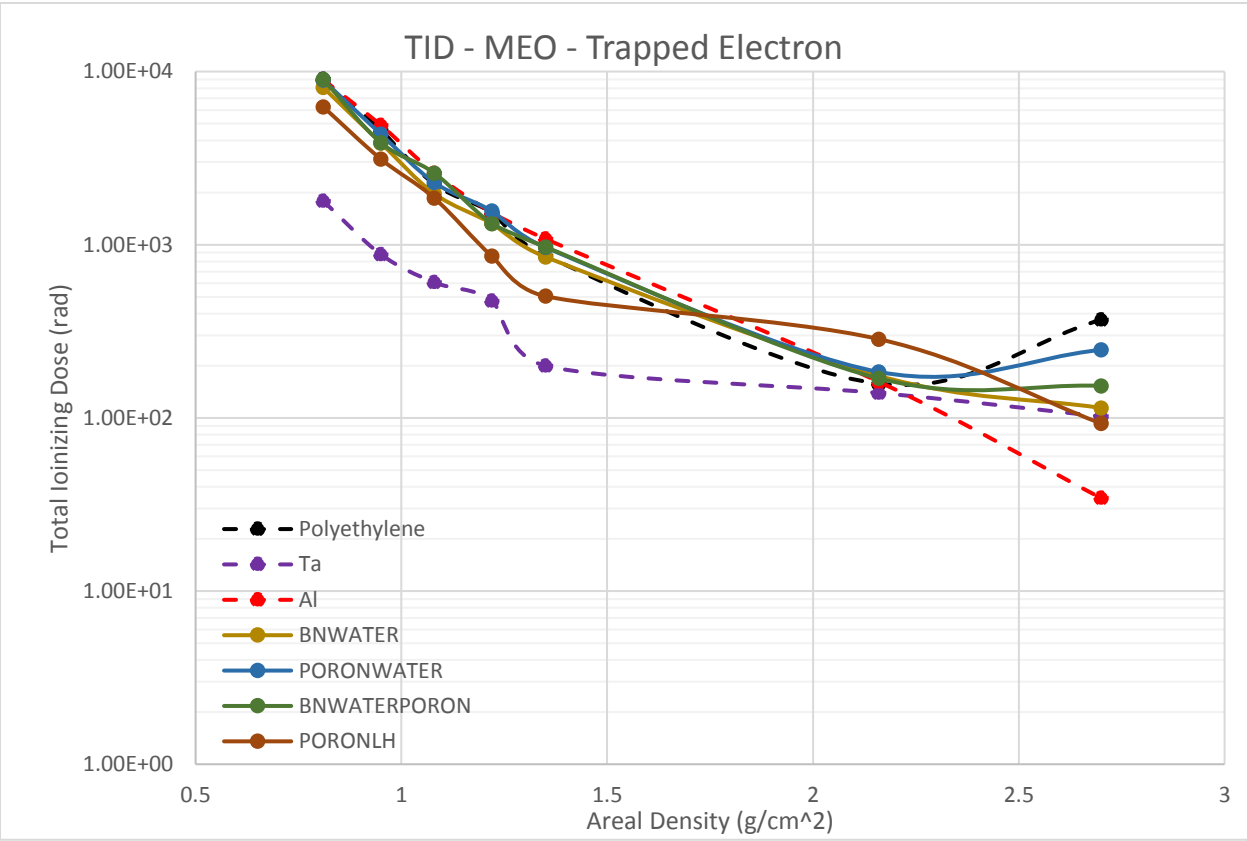

In these trials, the homogenized materials are primarily aimed at utilizing the hydrogen dense liquids (that would not be considered structural, otherwise) as an interstitial liquid in the foam core of the FFCC. Because the FFCC utilizes an interstitial liquid regardless of desired function, the use of high hydrogen density liquids is expected to benefit the FFCC for radiation shielding purposes. Liquid water is considered a consumable for manned missions with noted shielding capabilities, so storage within the FFCC is not out of the realm of possibility. In addition, liquid hydrogen has been considered as an interstitial liquid, as it is a consumable fuel for interplanetary travel, and reserves could potentially be stored in the structure's core layer. It has not yet been considered how liquid hydrogen will be stored in the foam core, though results here will determine if this is a worthwhile pursuit. Initial results here show improved shielding over that of plain water.

6.2.4. **Homogenized Materials Comparison to its Components**

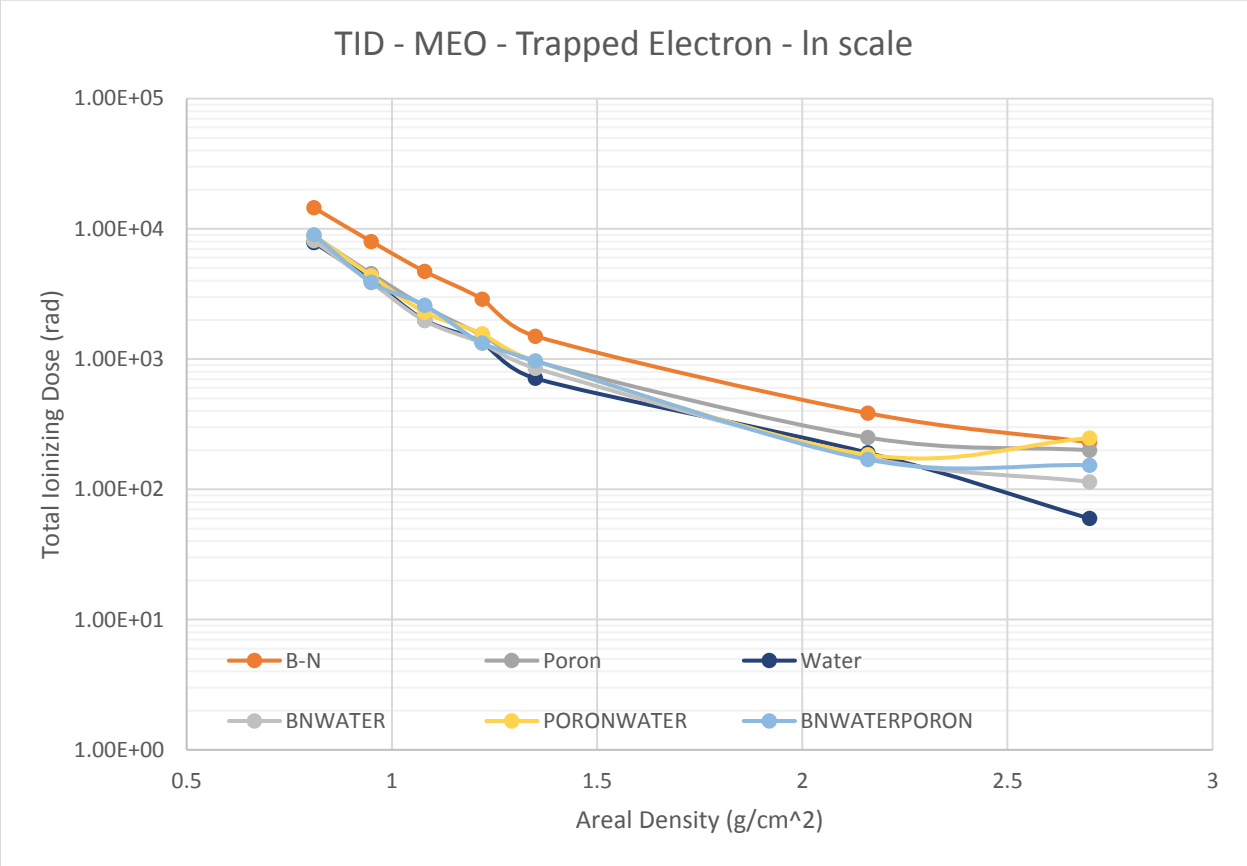

To check whether the homogenized materials behave as expected, they are compared to their individual component materials. It is expected that a custom material of poron and water for example, would have a shielding response between that of poron and water individually. Three examples are seen in the Figure above where BNWATER can be seen to fall within BN and Water individually, PORONWATER can be seen to fall between Poron and Water individually, and BNWATERPORON can be seen to fall between its components individually. It is seen that all custom homogenized materials show this behavior, with the response of each being between that of its components, and most nearing the component with the greatest content by percent mass.

6.2.5. **TID, Simplest FFCC (2, 3 Layers) in MEO, Trapped Electron Radiation (Trials 18-21)**

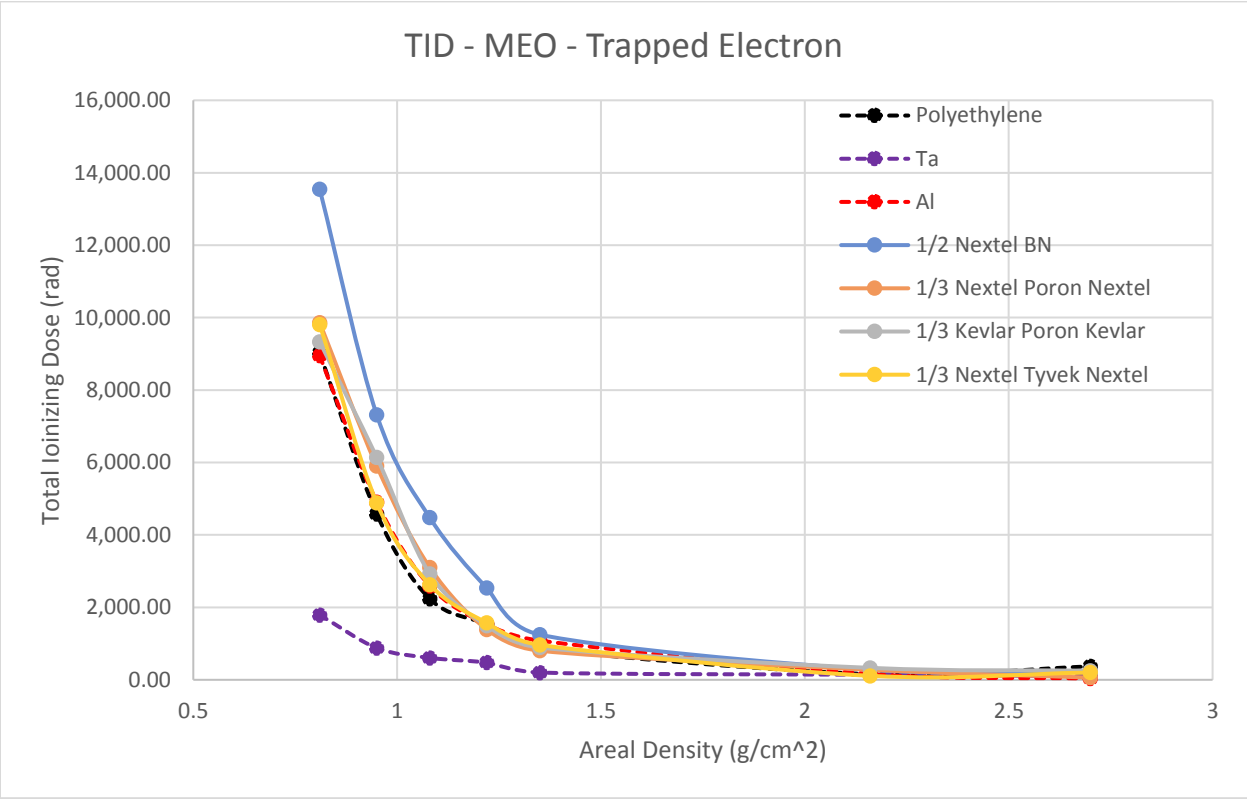

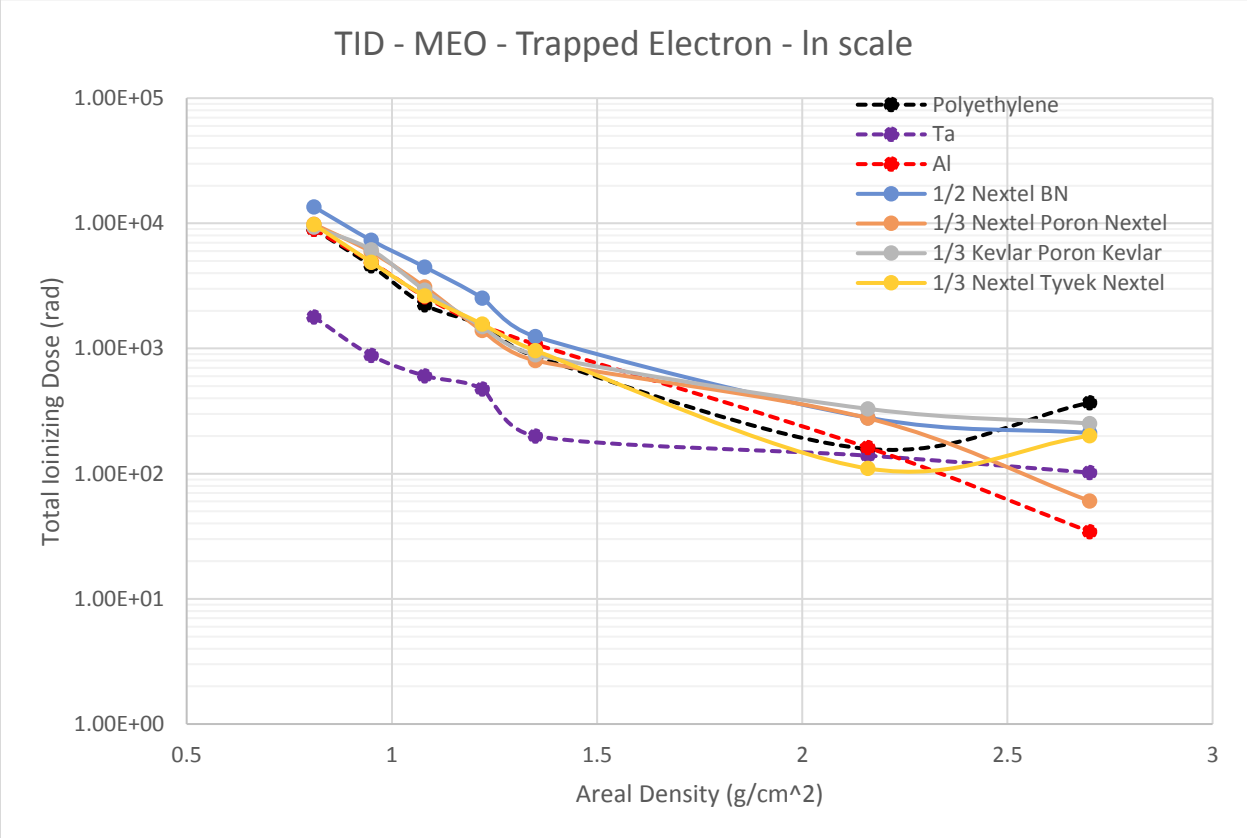

This set of trials is setup to explore the simplest model of the FFCC, a layered composite with a foam core and no liquid. This acts as a baseline for considering response of a layered material. Here, the total areal density is held constant and divided equally per layer. It is seen that no material exceeds the performance of aluminum, and more hydrogen density is necessary for satisfactory shielding response.

6.2.6. **TID, FFCC w/ Poron/Water (5 Layers) in MEO, Trapped Electron Radiation (Trials 22-25)**

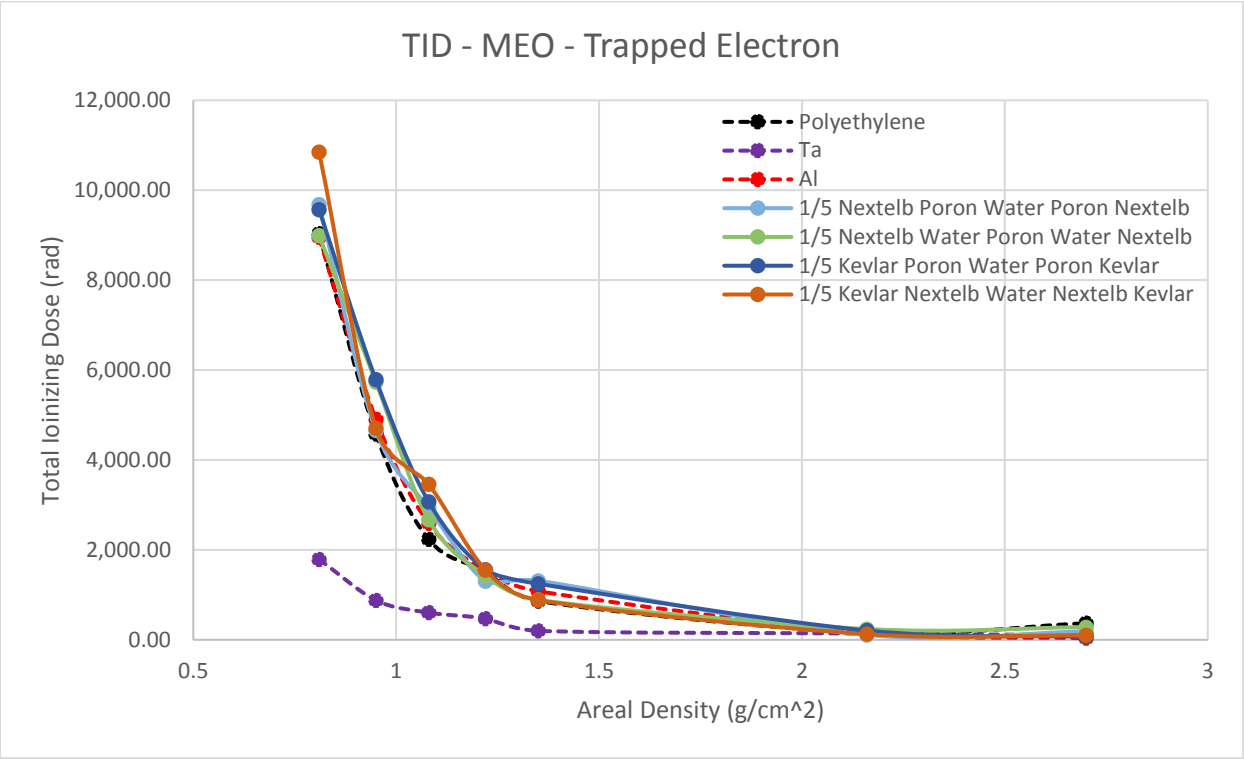

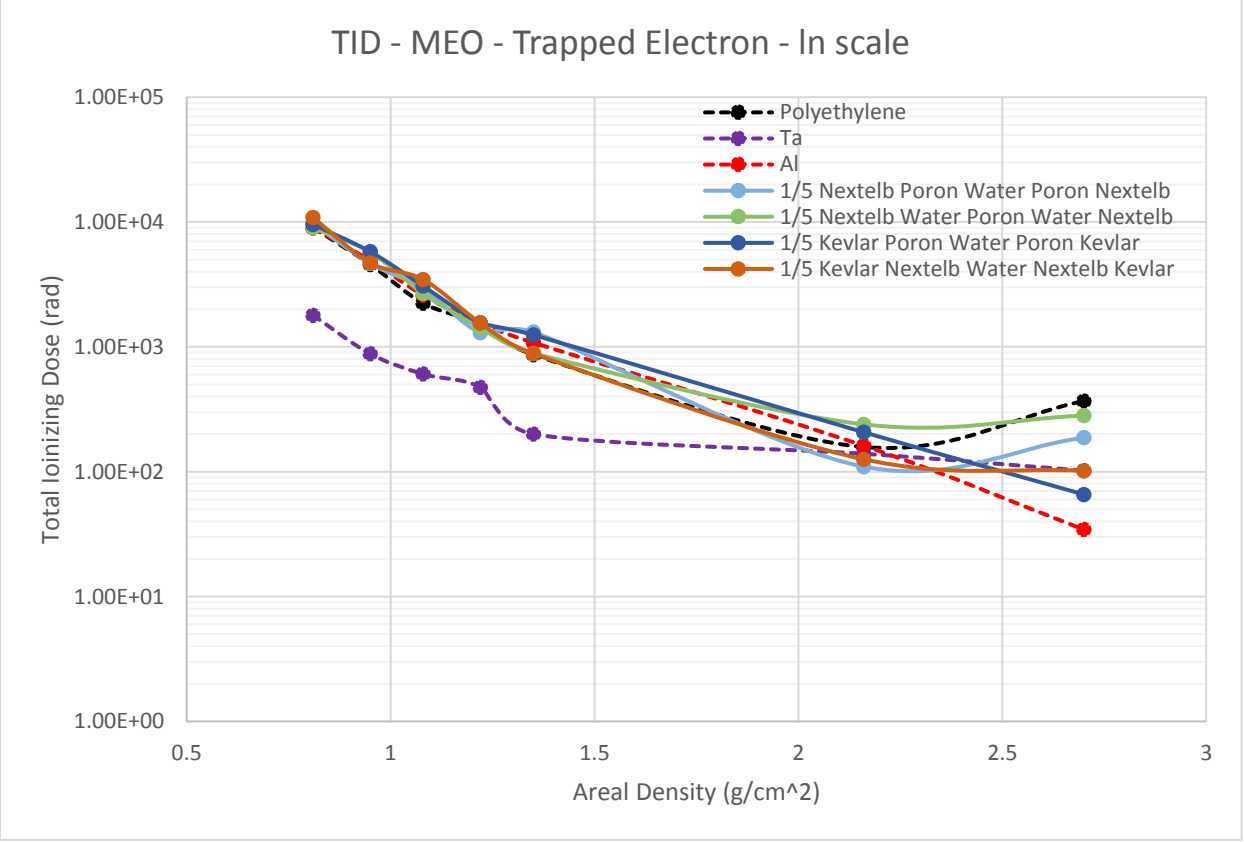

This set of trials considers a basic layered FFCC with the foam and liquid layer considered as layered materials. Each layer is one fifth of the total areal density. It can be seen that materials with the two layers of water have a lower TID response than those with two foam layers, alluding to the effects of layer order and hydrogen content on TID. Where layer order changes TID values by virtue of changing the type and amount of secondary radiation from the layer order (discussed further at the end of this section), and increased hydrogen content is expected to improve shielding response (lower TID).

6.2.7. **TID, FFCC w/ Poron (no liquid) (5 Layers) in MEO, Trapped Electron Radiation (Trials 26-29)**

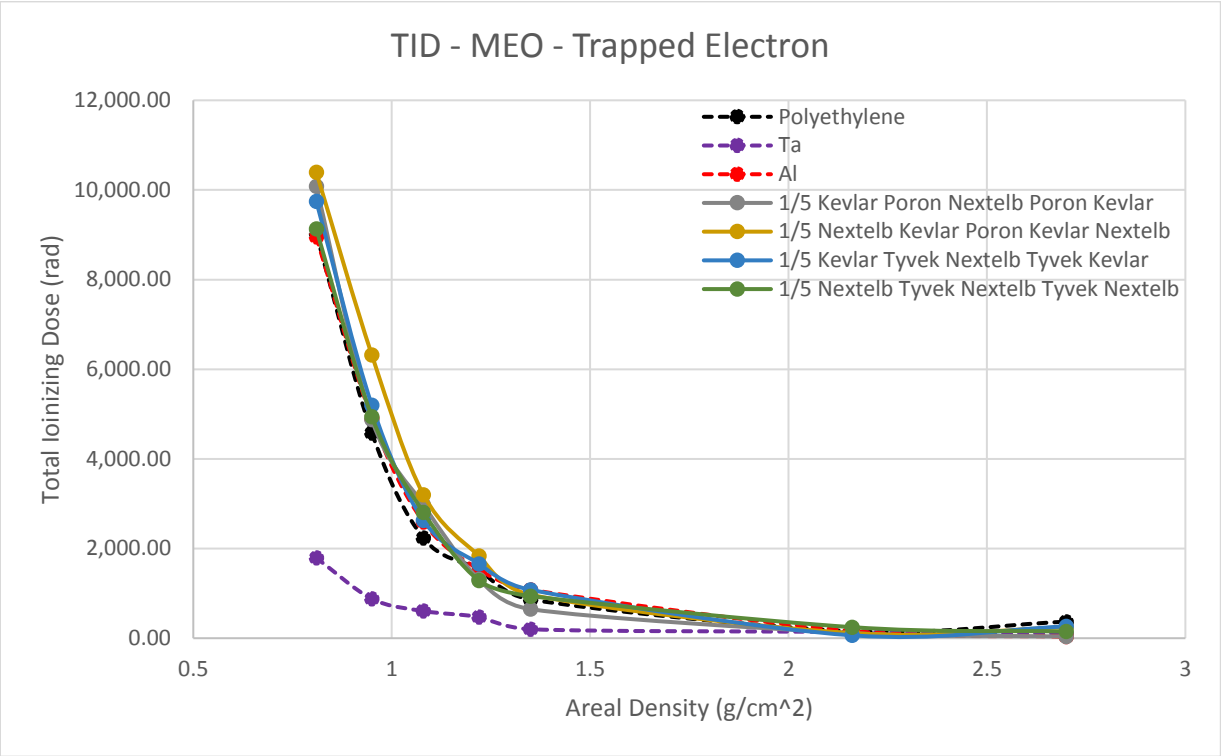

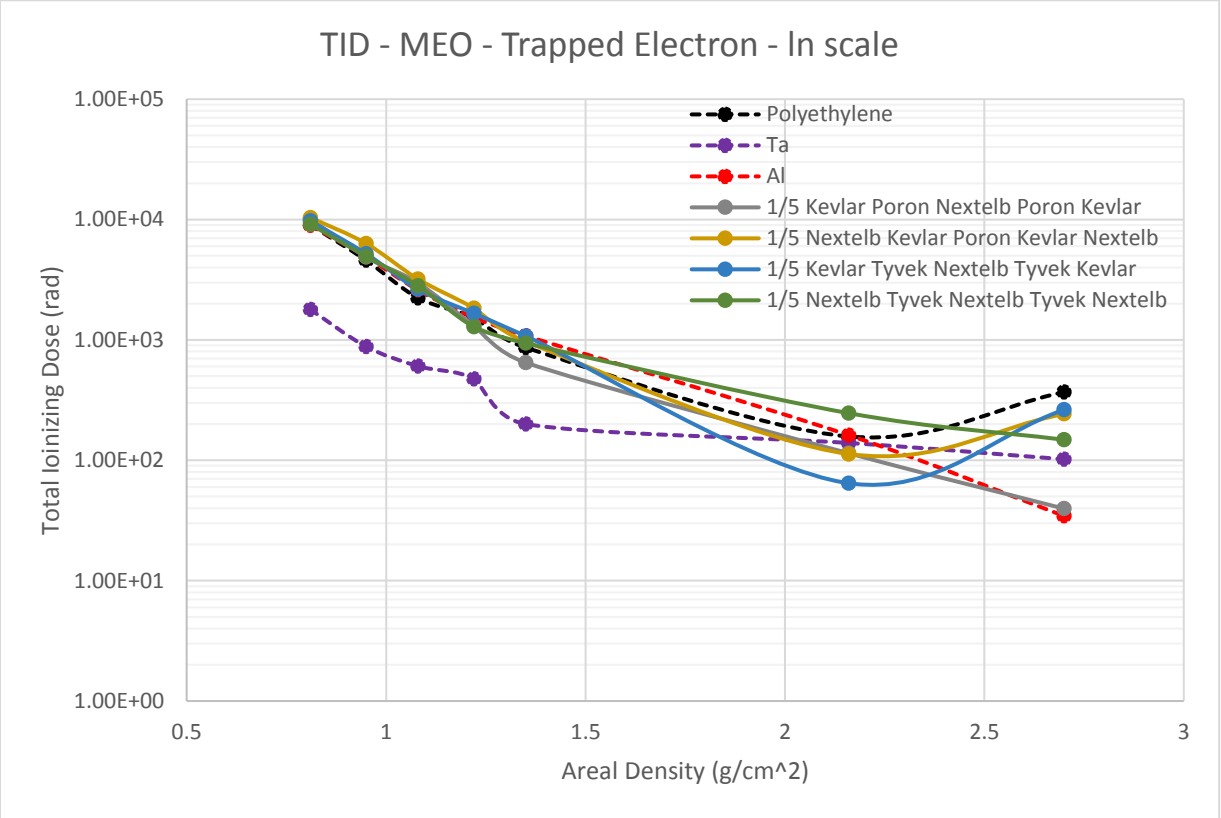

As multiple layers are seen to affect response, the liquid was removed and an additional skin layer was added in this set of trials. As expected, the trials with two layers of Tyvek had lower doses than those with materials with lower hydrogen content. No materials exceeded polyethylene in TID.

6.2.8. **TID, FFCC BN/Water, no Poron (5 Layers) in MEO, Trapped Electron Radiation (Trials 30-33)**

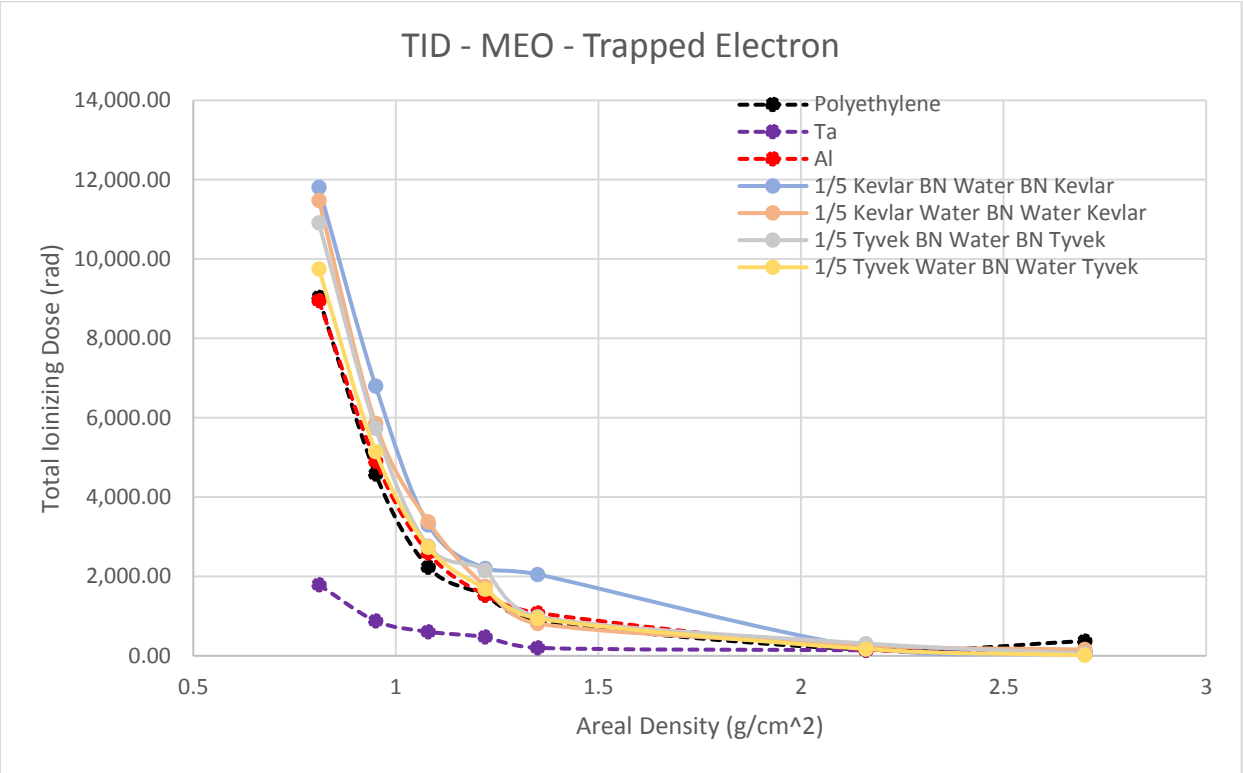

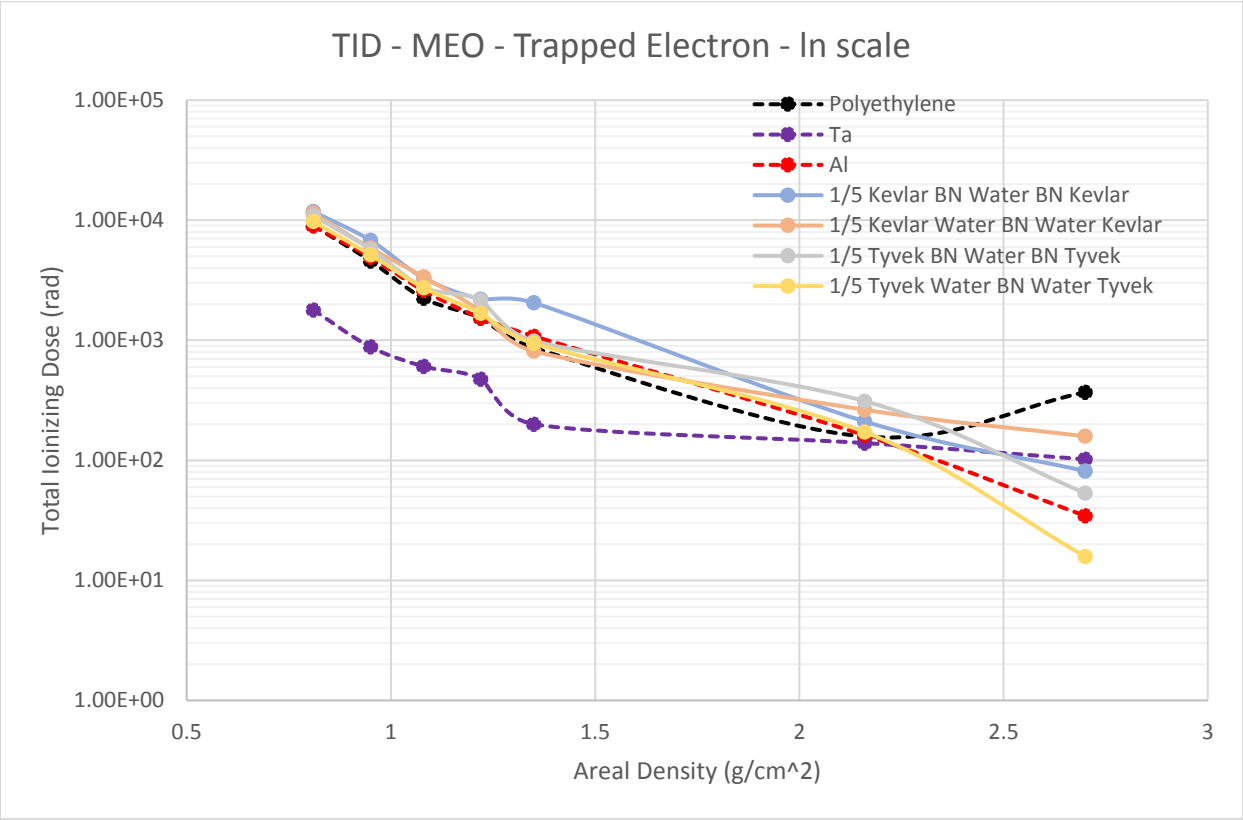

This set of trials explored the idea of including a solution of water and Boron Nitride, as initially considered in a prior investigation. Once again, all layers are divided equally from the total areal density, meaning the amount of each material is not constant for the middle material in comparison to the other materials. That is, [1/5 Kevlar BN Water BN Kevlar] has a composition of 2/5 Kevlar, 2/5 BN, and 1/5 Water by areal density. No materials exceeded polyethylene or aluminum in TID.

6.2.9. **TID, FFCC with Constant Total Areal Density, in MEO, Trapped Electron (Trials 34-37)**

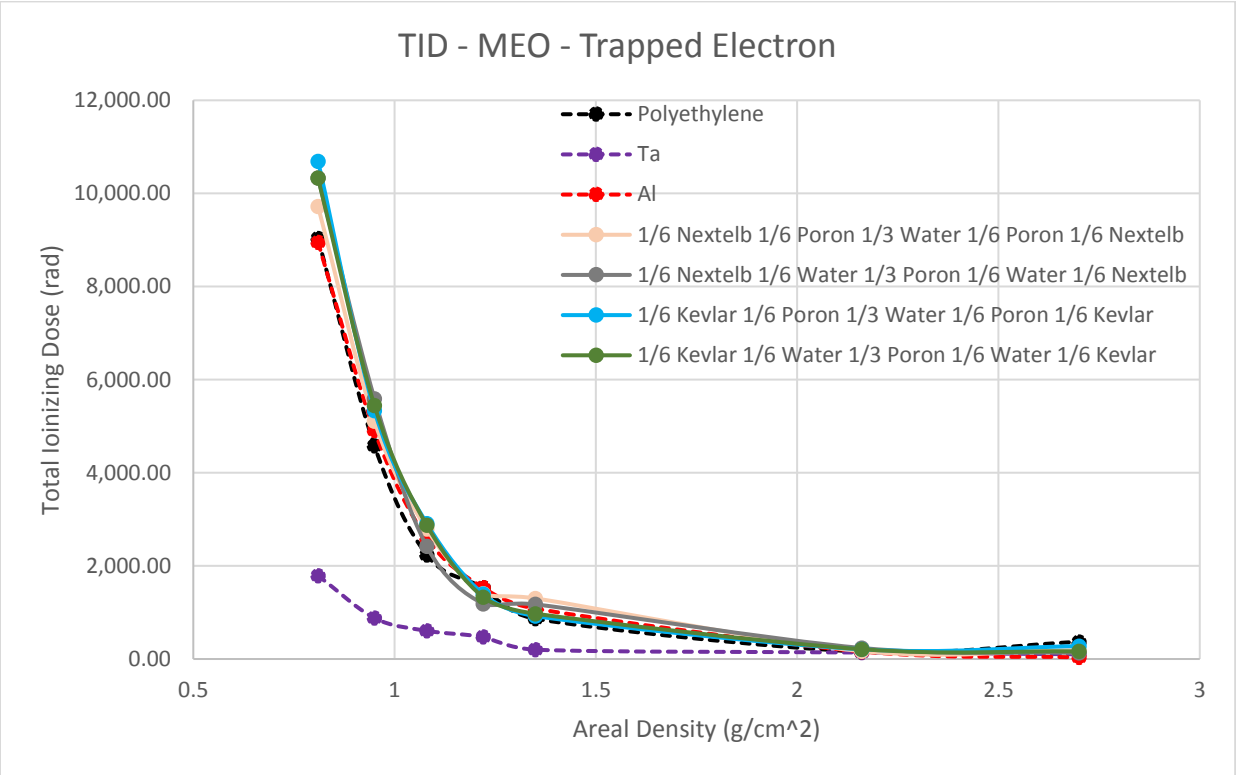

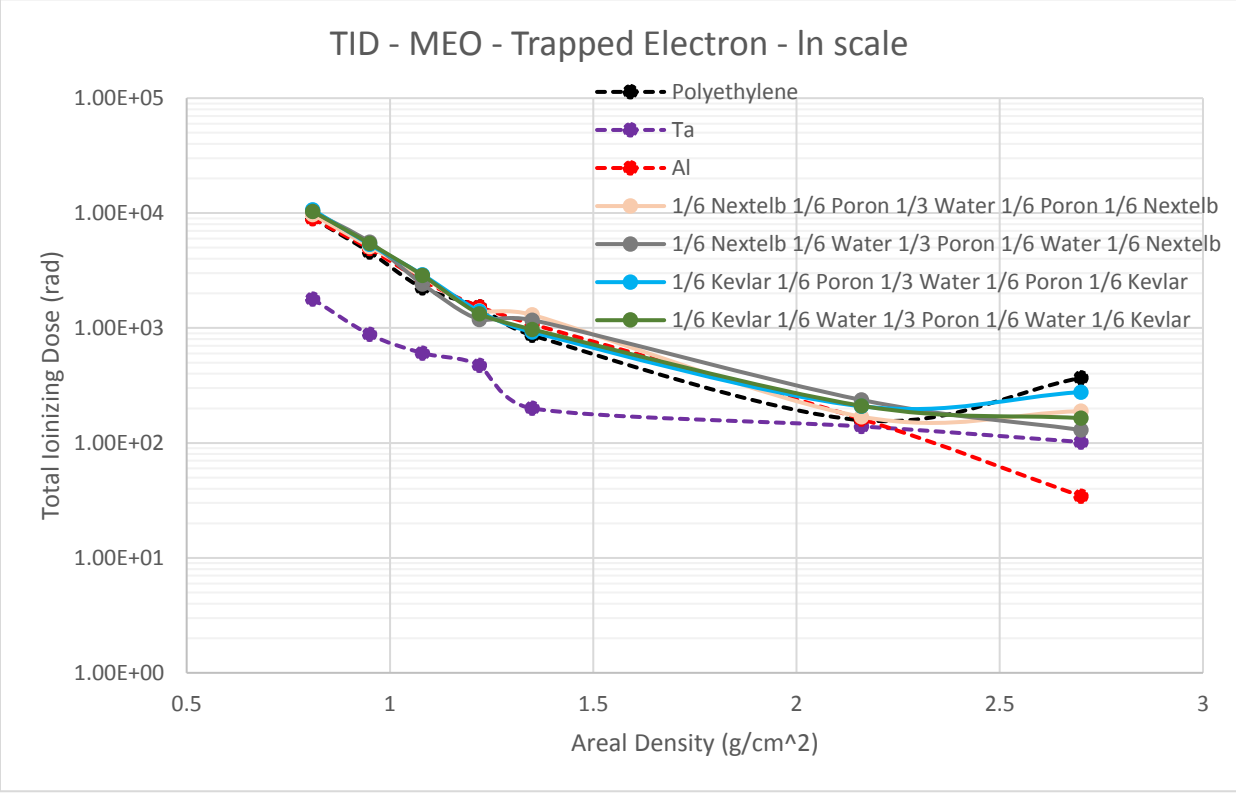

This set of trials addresses the issue of the FFCC layers not maintaining the same ratio of each material component. None of these single layer FFCC trials near TID values of aluminum or polyethylene. This set of trials shows in part the effect of layer orientation of the porous core layer. For example, in trial 34, the porous core and water layer is modeled as a split layer of poron with a solid layer of water between, in comparison to trial 35 which is the opposite (The same is true for trials 36 and 37). It can be seen that there is a difference of 200-400 rad (equating to a 6% discrepancy) between the two-layer orientations for this set of trials. This partly shows the necessity for homogenization of the heterogenous core layer, as layer orientation affects results. As a note, individual shielding capability of water and poron, respectively, is fairly close (within 1000 rad or 15%), so this layer order distinction is not as blatant as it would be for materials with a greater difference in shielding capability (as tested in the next set of trials).

6.2.10. **TID, FFCC Two Skin Layers with water core, no foam (Trials 38-39)**

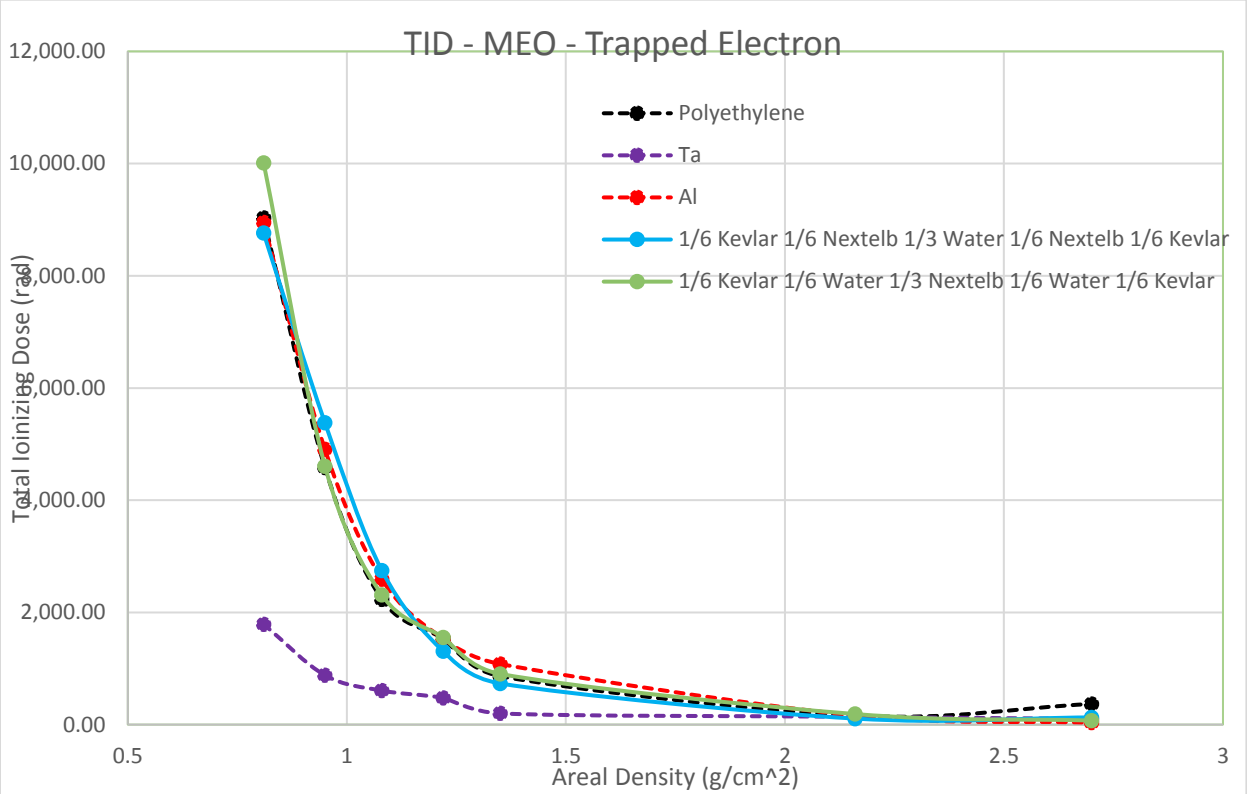

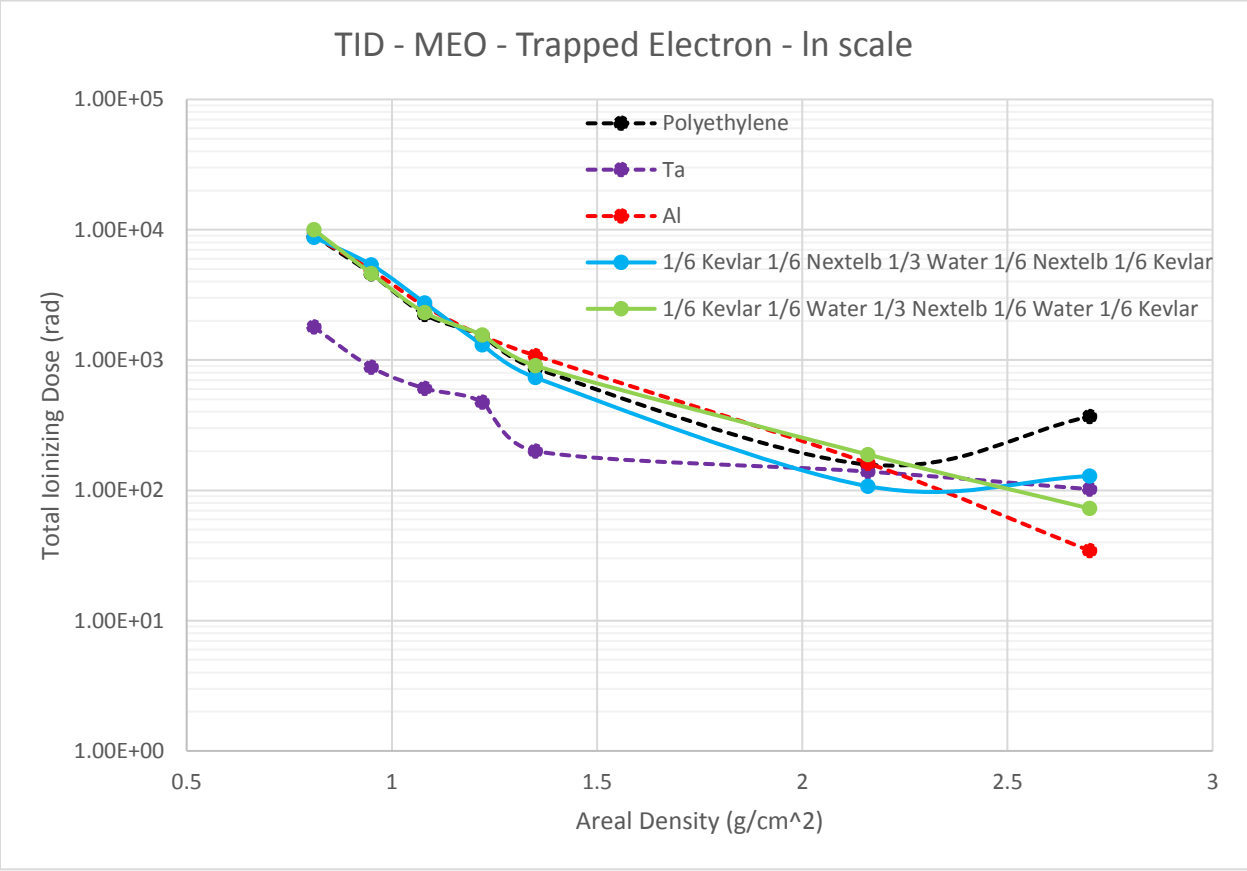

This set of trials addresses the areal density issue of the last set, but instead replaces the Poron with Nextel in the core layer of the FFCC. Here, Nextel is used to represent a material that has a shielding capacity that is more distant from that of water (roughly 27% average difference) to show more plainly the effect of layer orientation in modeling a heterogenous core as multiple individual layers. It can be seen that trial 38 outperforms both aluminum and polyethylene, while trial 39, which has the same total areal density of each component material but a different layer orientation, has a much higher dose. The difference in layer structure is the split Nextel layer around a solid water layer in trial 38, in comparison to a split water layer around a solid Nextel layer in trial 39. This shows quite blatantly that the layering method of homogenizing the FFCC core is not reliable due to layer order effects, and a true homogenization technique is necessary.

6.2.11. **TID, FFCC w/ Homogenized Poron and Water (3 Layers) in MEO, Trapped Electron Radiation (Trials 40-43)**

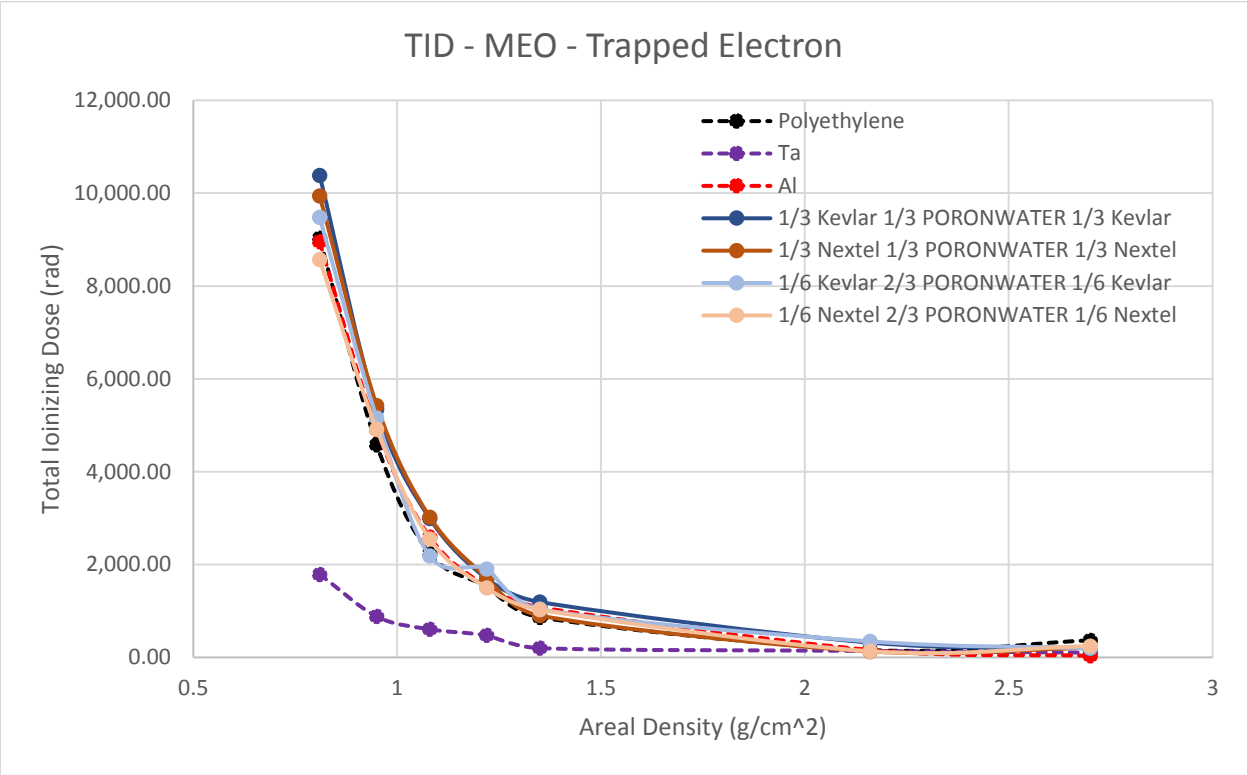

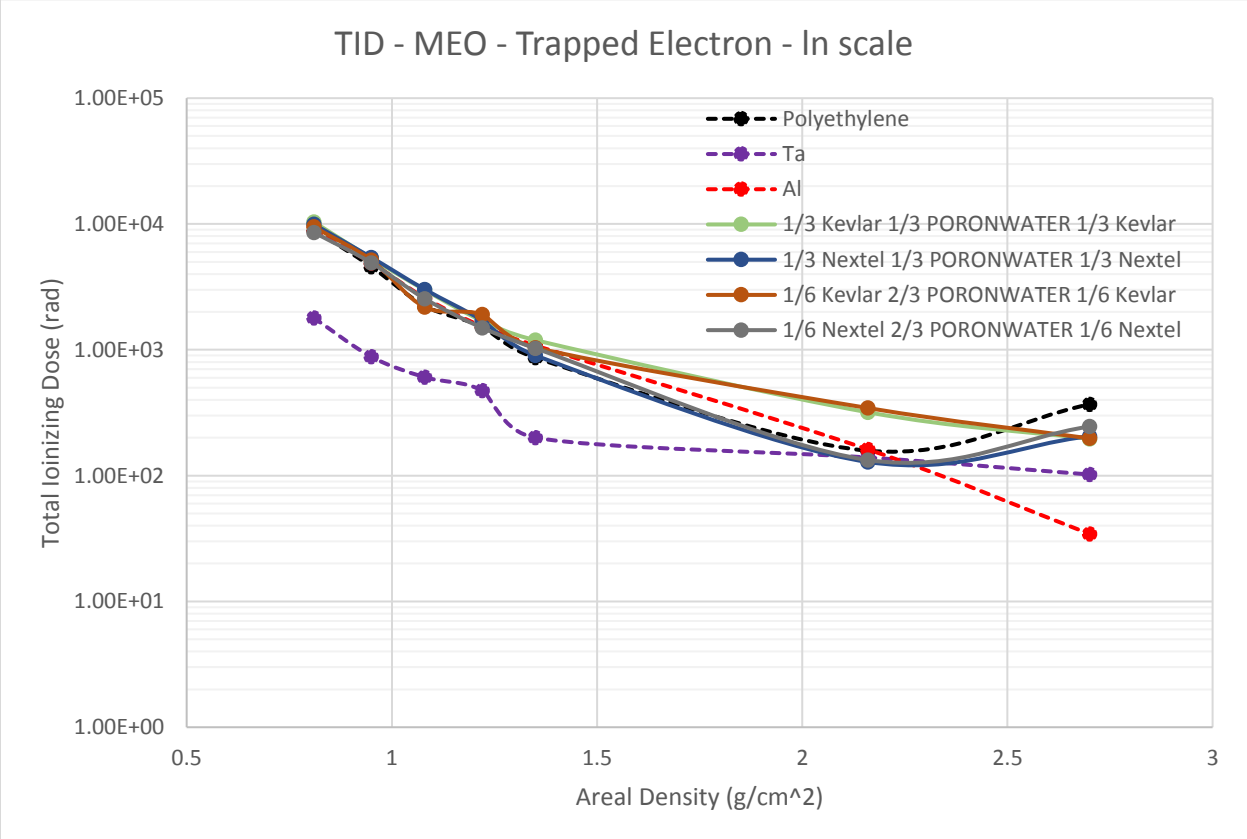

Here, the core layer of poron foam and interstitial water has been homogenized by the method outlined in Chapter 3, in an effort to model the fluid-filled core of the FFCC more accurately. In addition, the areal density distribution of the last sets of trials is carried on here, with the larger core layer being directly comparable to the layered core method of trials 34-37. It is noticed that the TID of the homogenized core trials is within the range of those with the layered core method. Additionally, it can be seen that the trials with greater core sizes, trials 42 and 43, have TID values nearing and exceeding that of aluminum and polyethylene. This is another example of shielding capability increasing with hydrogen density. For all the remaining FFCC compositions, the areal density distribution will be weighted more heavily towards the core (similar to that of trials 42 and 43), as the true FFCC is similarly proportioned.

6.2.12. **TID, FFCC w/ Homogenized BN and Water (3 Layers) in MEO, Trapped Electron Radiation (Trials 44-47)**

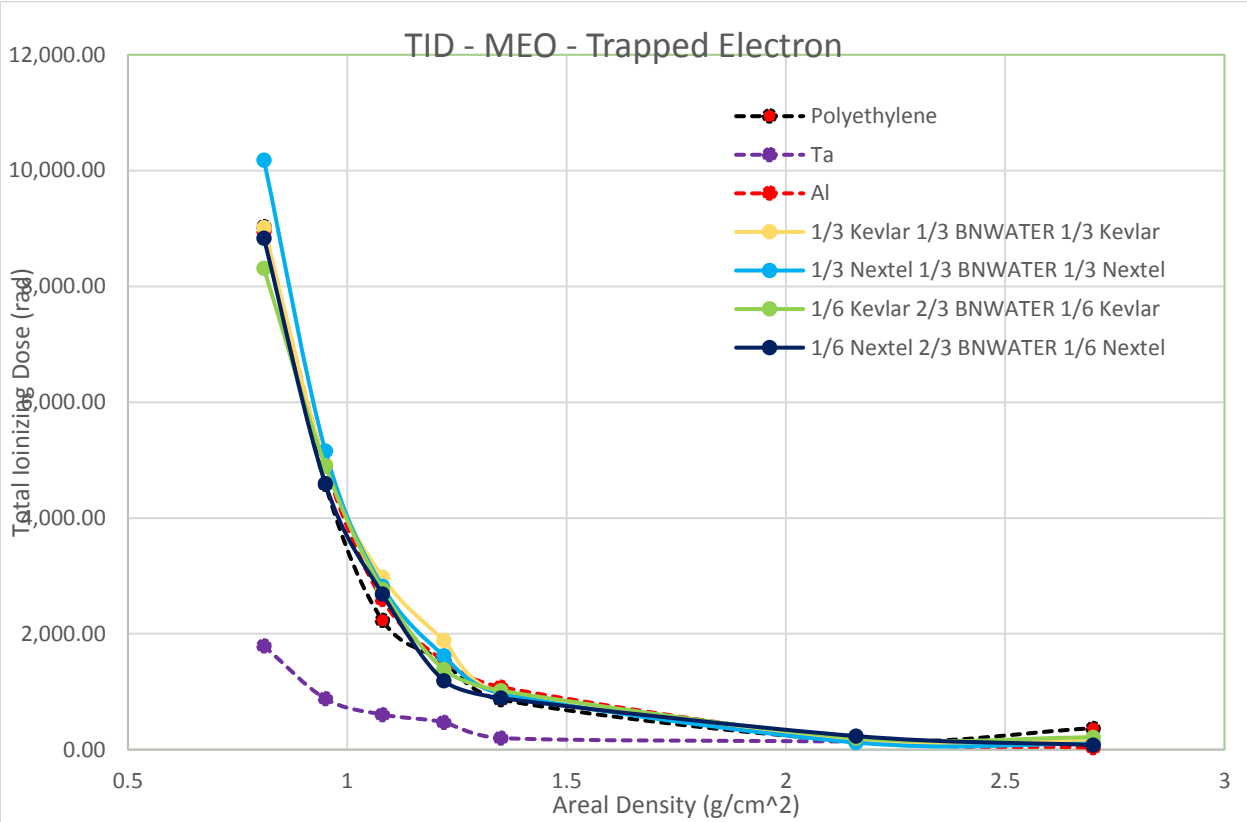

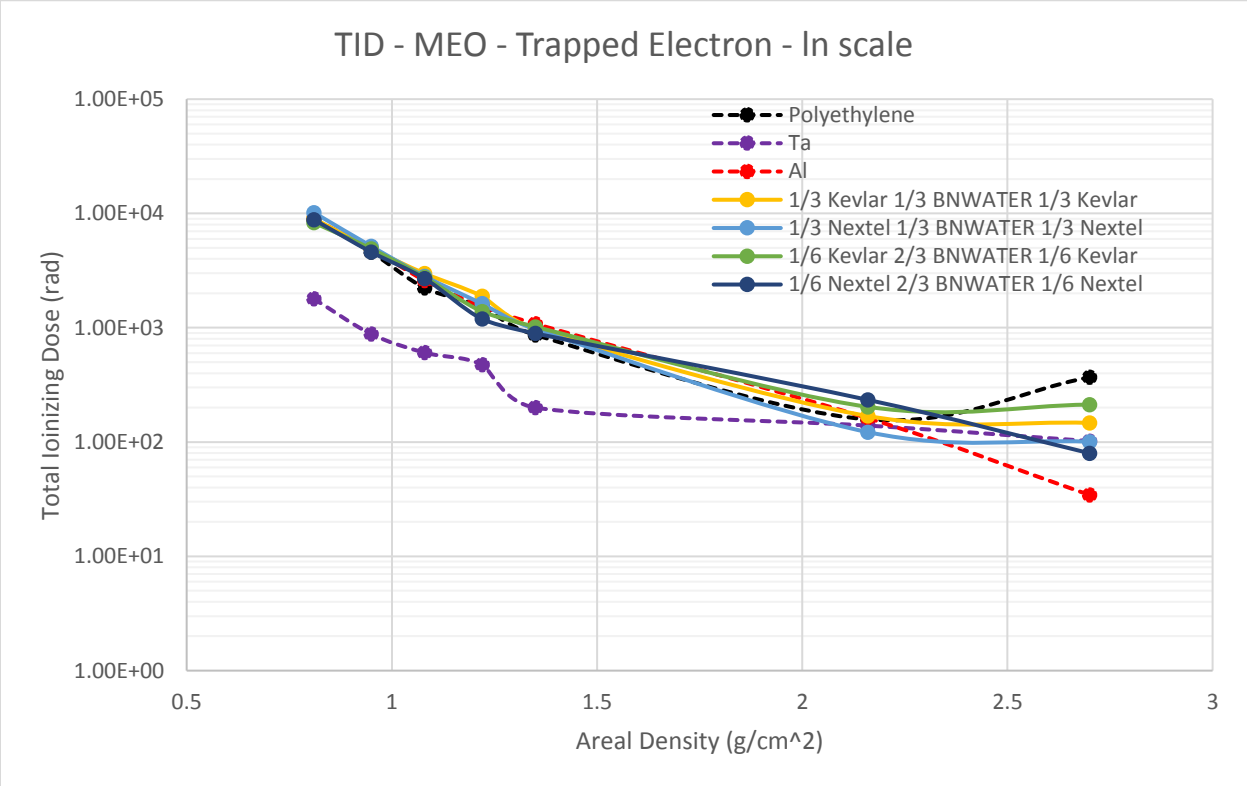

This set of trials considers the an FFCC without a foam core, but with a BN and water solution for the middle layer. This BN and water solution was initially considered in prior research, as a means of doping the interstitial fluid into better shielding performance [3]. Future investigations would benefit from doping external layer materials so as not to allow the BN's structural and thermal properties to go to waste as they do in solute. The idea here would be to dope fiber reinforced epoxies (or polymers) with the BN (or BNNTs) so as to provide additional strength and shielding to the skin layers of the FFCC. BNNT structural composites are something NASA has deemed plausible with the onset of manufactured structural BNNTs [4]. In addition, epoxies doped with either graphite powder or Boron Nitride powder (in addition to stabilizers) have been found to have improved use life in exposure to gamma radiation with a Cobalt 60 source [24]. Where Saiyad et al. [24] found that pure epoxy has a lifespan of roughly 11 years, in comparison to epoxy with BN powder which has a lifespan of 11.5 years (at 50 degrees Celsius) and epoxy with graphite powder which has a lifespan of 45 years (at 50 degrees Celsius).

In this set, it can be seen that trials 46 and 47 outperformed both aluminum and polyethylene at low areal densities. This shifts at mid areal density (around 1.22 g/cm^2) where polyethylene has the lowest TID. Both polyethylene and the trials perform similarly at high areal densities. As expected, the BN and Water trials generally outperformed the Poron and Water trials, as the amount of water present is greater without the polyurethane foam modeled in the homogenized material.

6.2.13. **TID, FFCC w/ Homogenized Poron, BN, and Water (3 Layers) in MEO, Trapped Electron Radiation (Trials 48-51)**

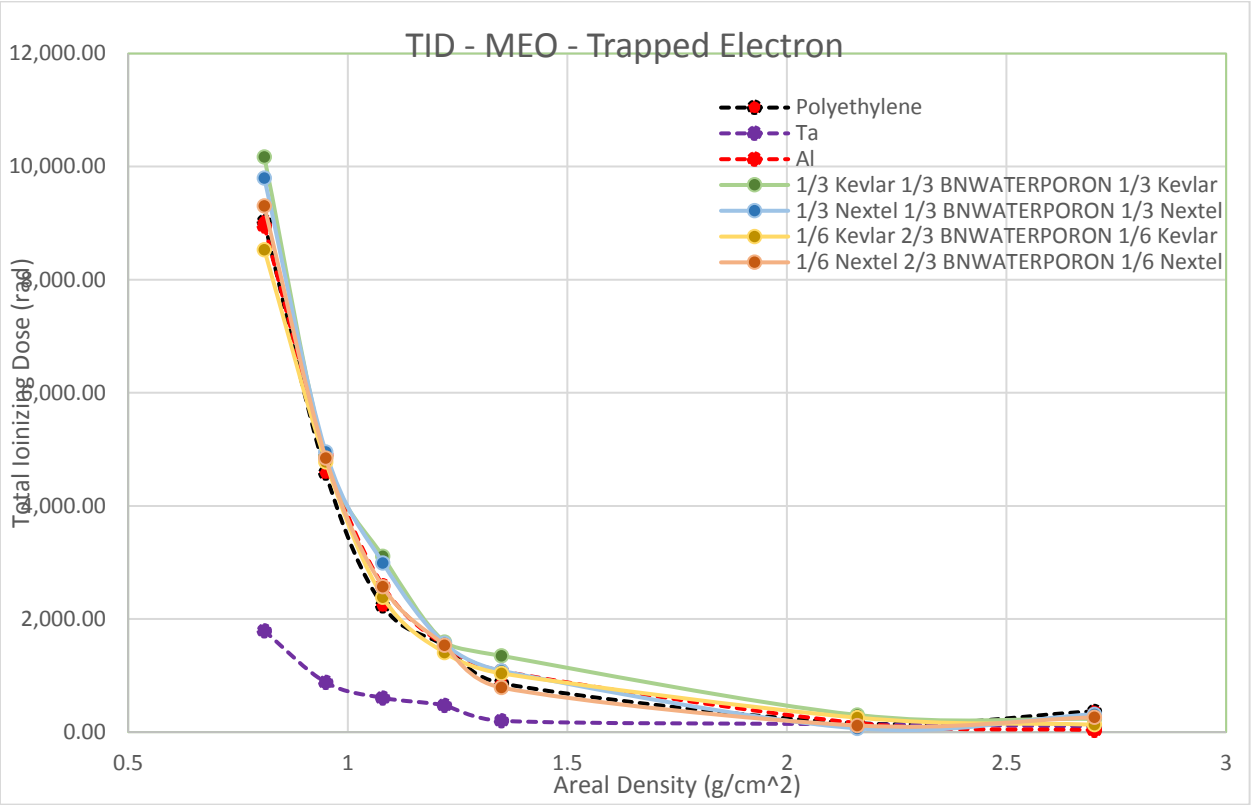

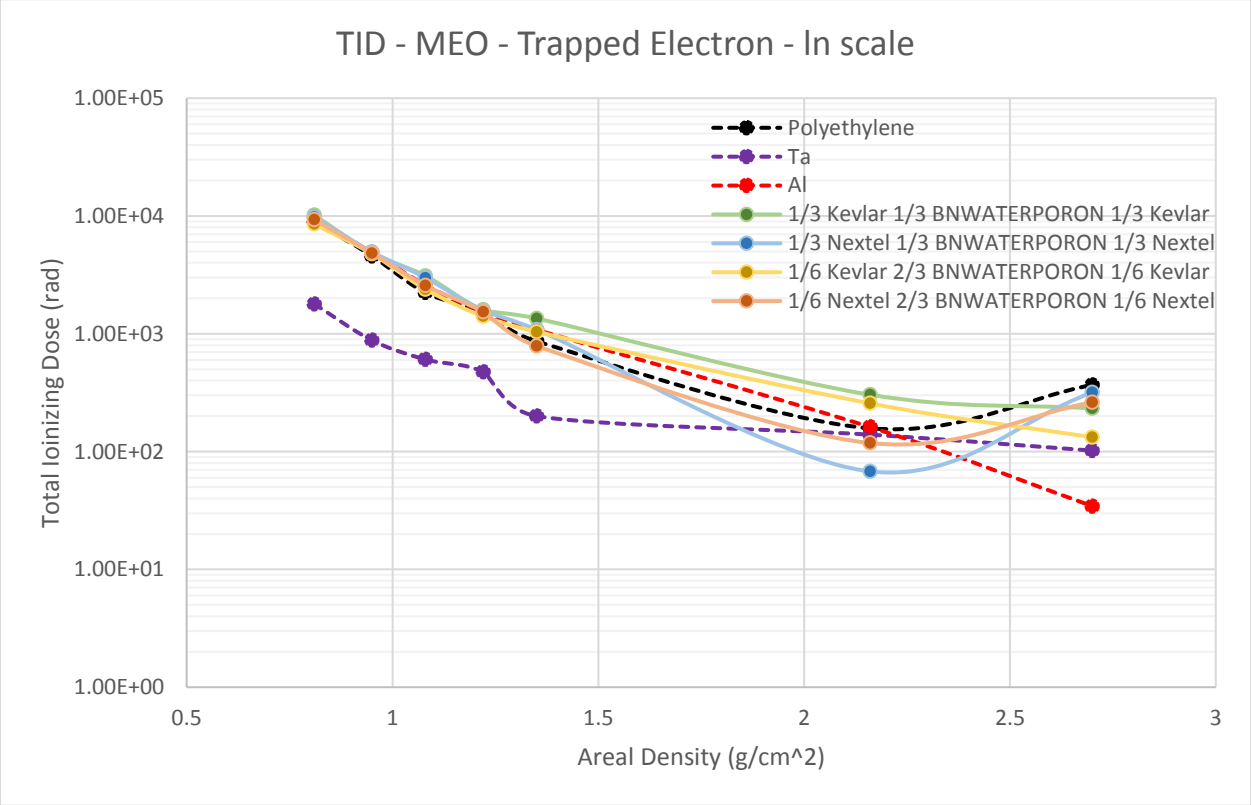

This set of trials was performed for an accurate comparison of a core with interstitial water and a core with doped interstitial water, as the last set did not include a foam core, just liquid. The difference between the homogenized PORONWATER and BNWATERPORON materials is purely in the liquid distribution. That is, BNWATERPORON has the same distribution of polyurethane foam to liquid by percent weight as the PORONWATER material, though in this case the liquid is the BNWATER solution.

In comparison to the PORONWATER set (trials 40-43), the BNWATERPORON trials have a roughly ten percent lower dose value for all four trials. This would seem to indicate additional shielding potential with the addition of BN solute interstitially.

Interestingly, the FFCC composition with Kevlar face layers (trial 50) was the trial to outperform pure aluminum and polyethylene, in comparison to the Nextel face layer composition in the PORONWATER set (trial 43) which was the trial to outperform polyethylene in that case. The magnitude of the relative error associated with the calculation convergence is up to 400 rad (at 0.81g/cm^2), which may explain the discrepancy.

6.2.14. **TID, FFCC w/ Tyvek Face Layers (3 Layers) in MEO, Trapped Electron Radiation (Trials 52-54)**

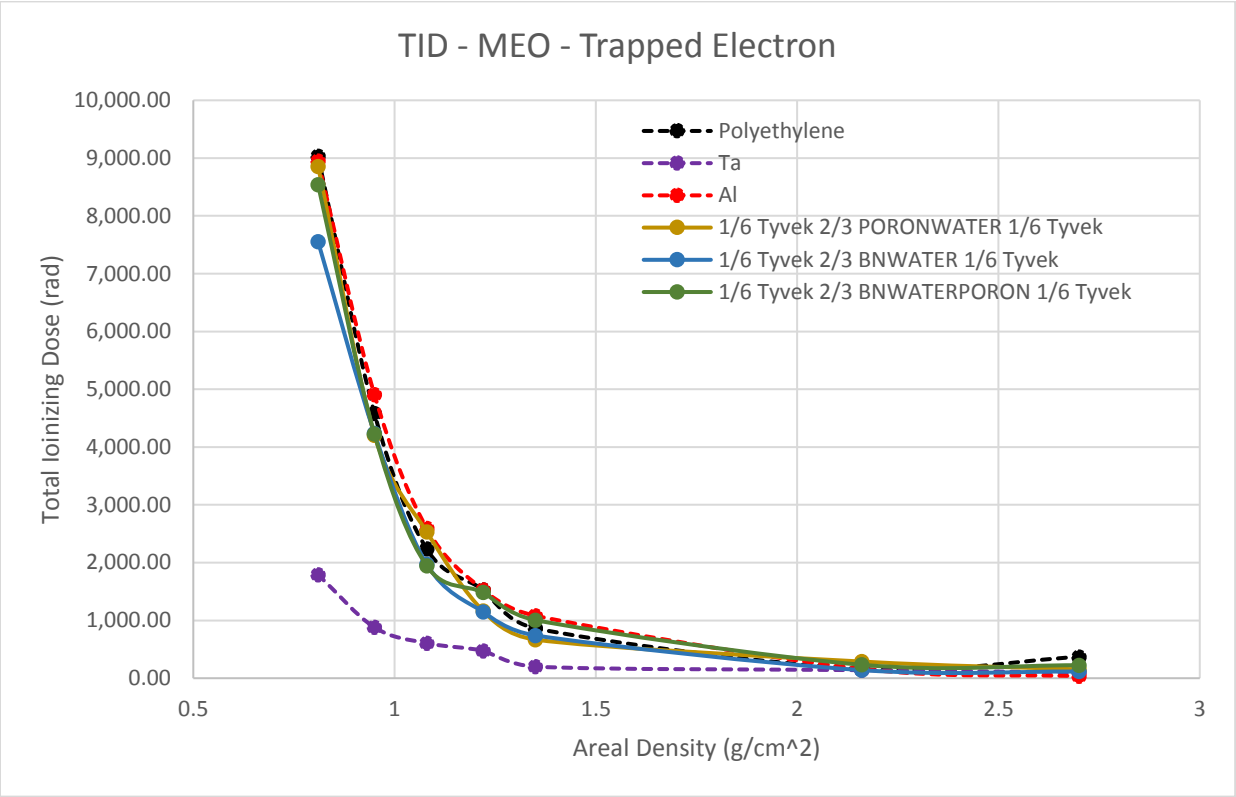

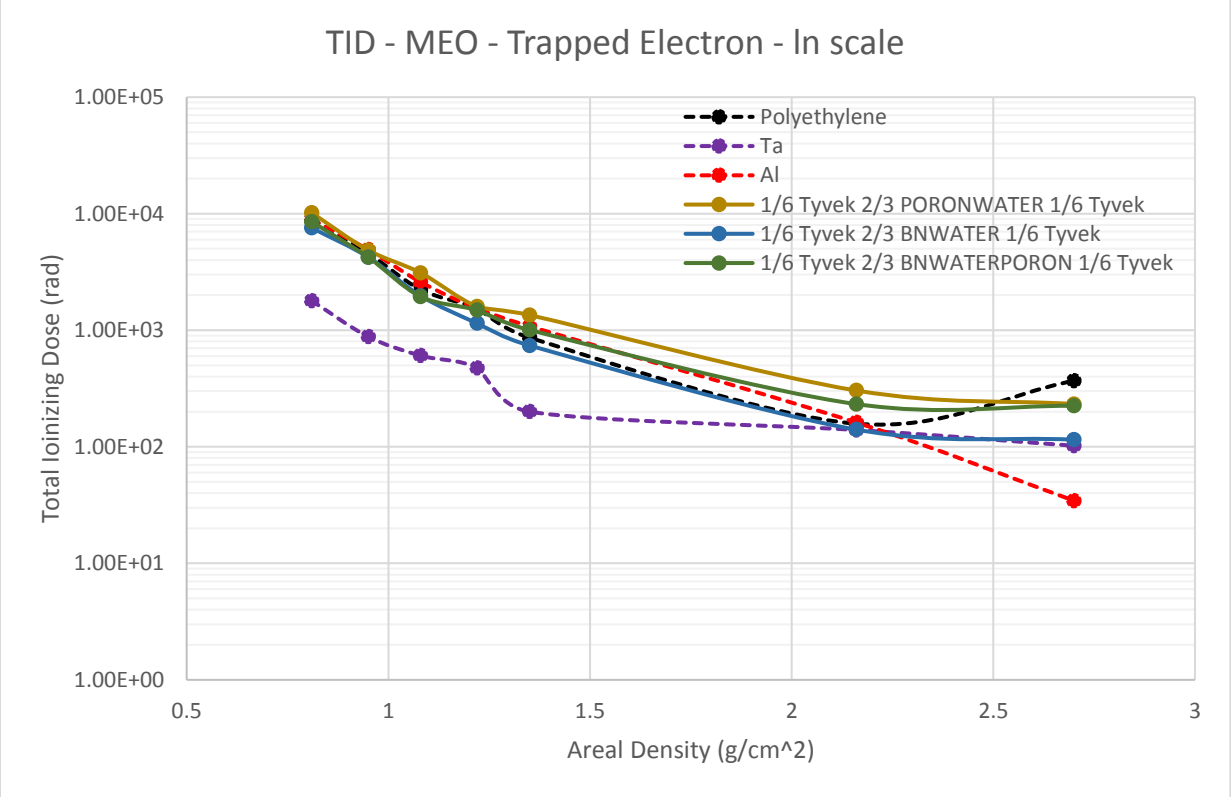

In this set of trials, Tyvek is considered as a face layer for the FFCC. Tyvek has good properties for water resistance and could make for a good layer to keep next to the various foam and liquid cores. The larger core size of the latter trials (42 and 43) was maintained. All three trials appear to outperform aluminum and polyethylene with lower TID values for most all areal densities. These trials have the highest hydrogen densities tested so far and perform as expected in that respect.

6.2.15. **TID, FFCC w/ Kevlar and Tyvek Face Layers (5 Layers) in MEO, Trapped Electron Radiation (Trials 55-57)**

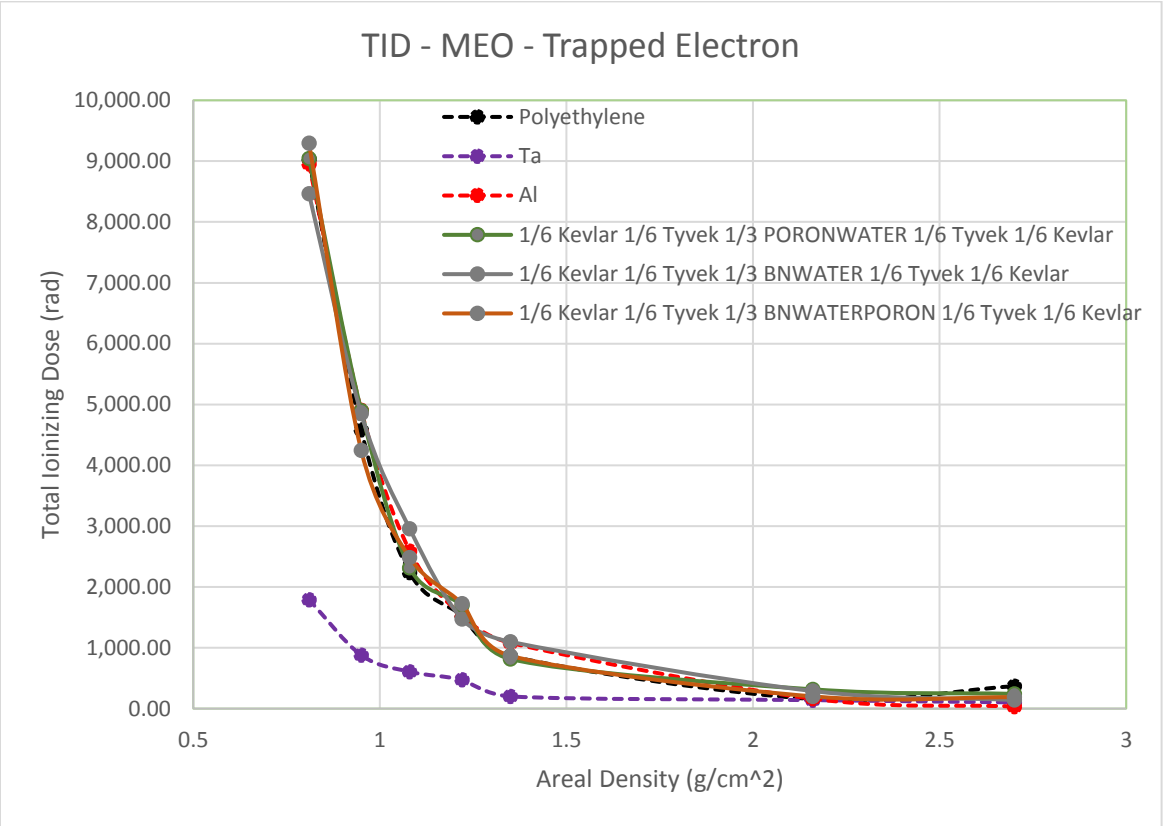

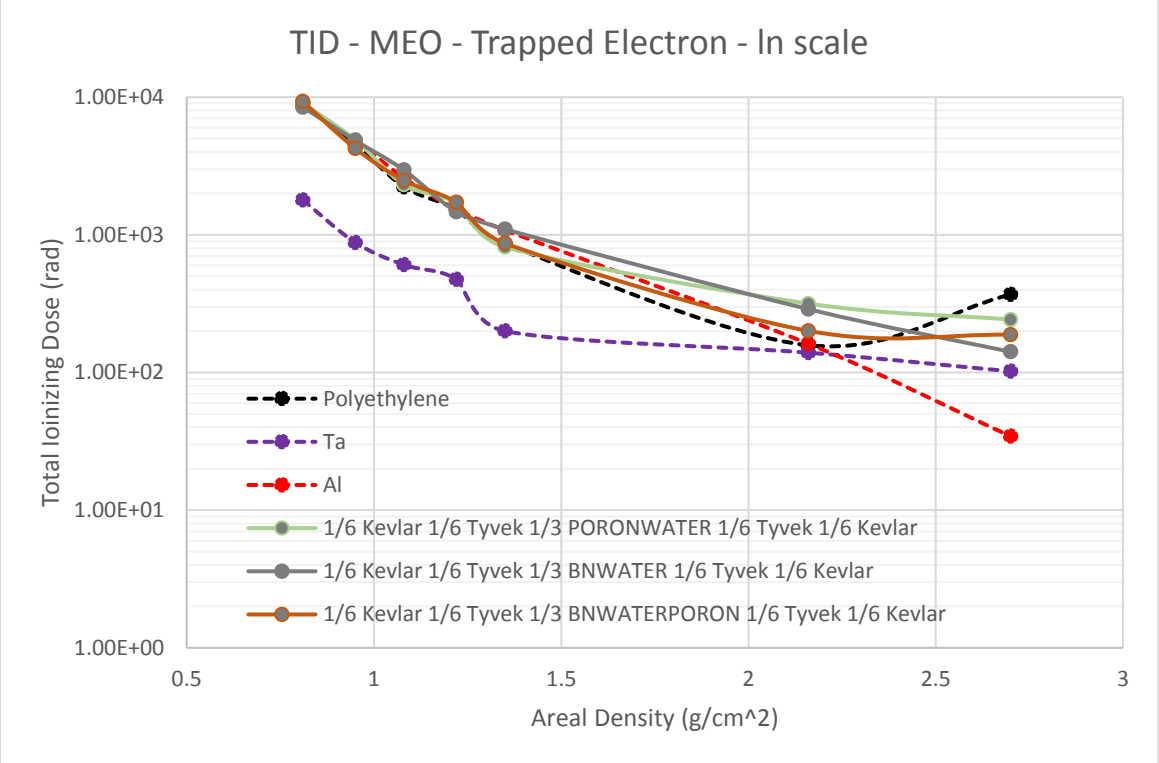

These trials are a full FFCC composition with Kevlar face layers and secondary Tyvek layers surrounding the homogenized foam and liquid core, similar to the prior set but with the additional exterior Kevlar layers for structure. As expected, these trials had decreased shielding associated with the decreased hydrogen content from the prior set of trials (52-54). Although the shielding decreased, trials 55 and 57 still performed equally and better, respectively, than aluminum and polyethylene. This is considerable as the FFCC composition for these trials is more structural than plain polyethylene and has more uses than plain aluminum.

6.2.16. **TID, FFCC w/ Homogenized Poron and Liquid Hydrogen (3 Layers) in MEO, Trapped Electron Radiation (Trials 58-60)**

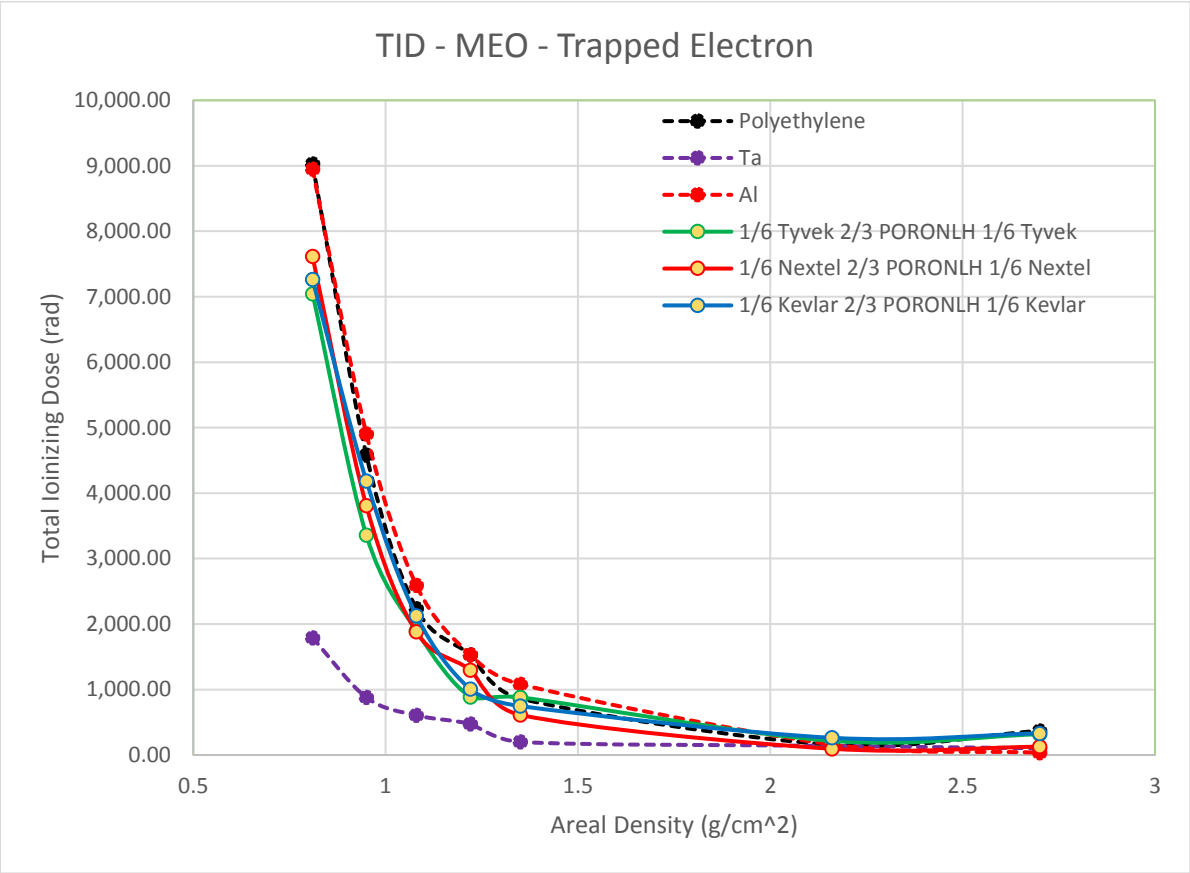

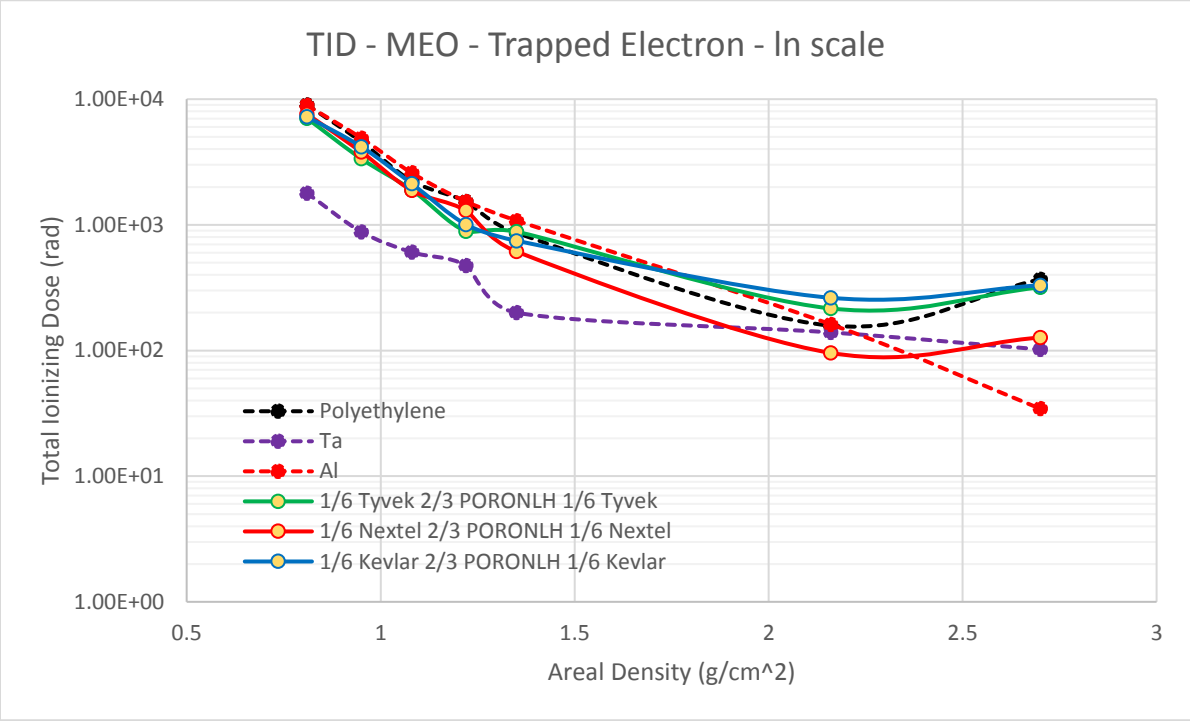

This set of trials considers a homogenized core layer of poron foam and liquid hydrogen. It is unclear at this time whether liquid hydrogen will function in the FFCC though it is considered for much the same reason as water. Of all the FFCC trials, trial 58 has performed the best. This trial has the greatest hydrogen density modeled, with Tyvek face layers and liquid hydrogen interstitially. Although exceptional in radiation shielding, it is expected that this material will not be as structural as the trials with the Nextel and Kevlar skin layers (trials 59 and 60 respectively), which also provided very good shielding.

6.2.17. **TID, FFCC w/ Kevlar and Tyvek Face Layers and Homogenized Poron and Liquid hydrogen (5 Layers) in MEO, Trapped Electron Radiation (Trials 61, 62)**

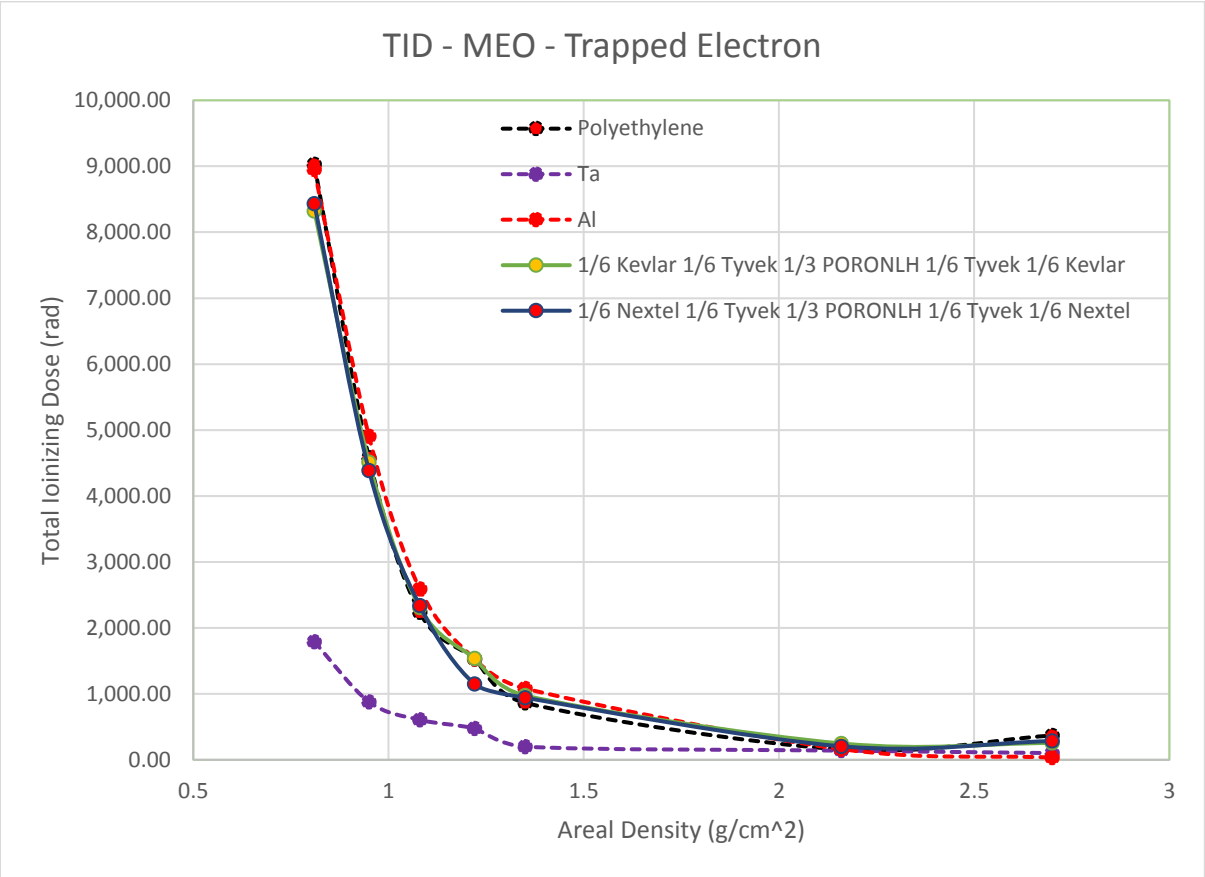

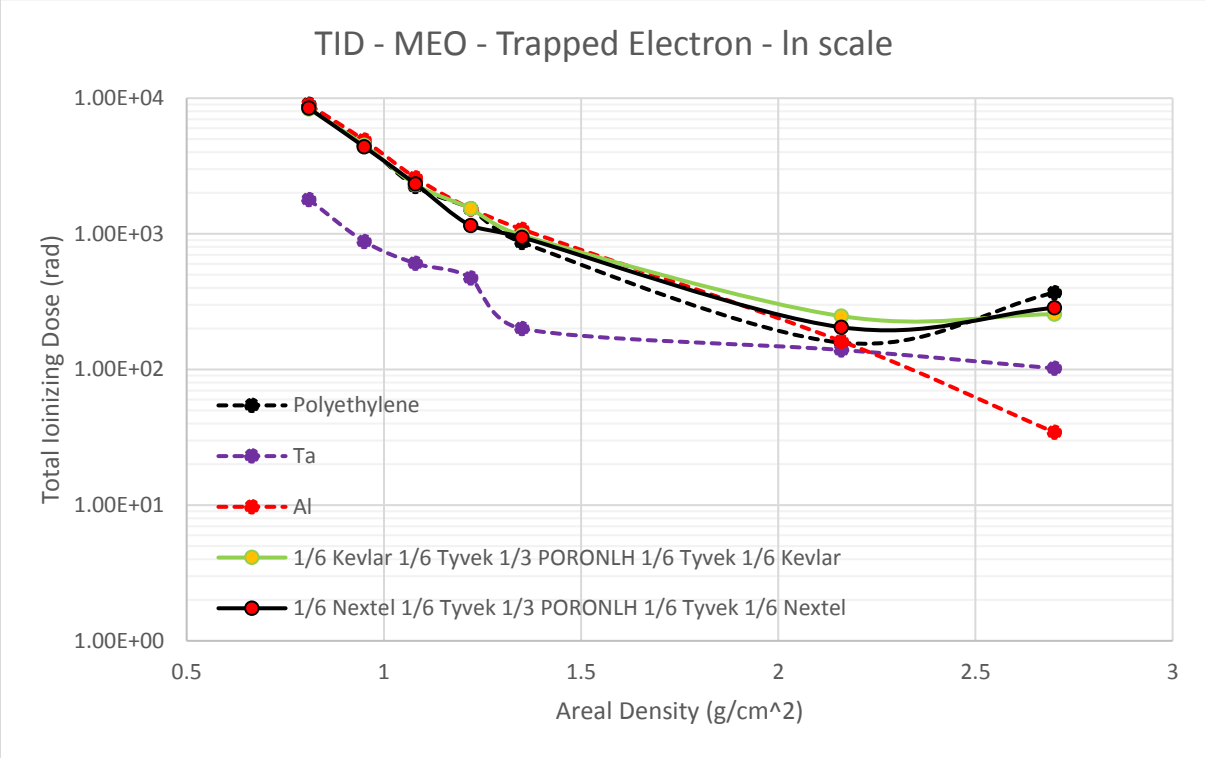

As the last set of FFCC trials were successful in shielding but not as functional for structure, this final set considers a double skin layer FFCC with homogenized poron and liquid hydrogen core. The goal here being that the foam core can be enclosed with Tyvek as both a liquid barrier material, and a more structural polyethylene for use in a fiber reinforced epoxy matrix. The primary face layer will remain either Nextel or Kevlar, to maintain the primary structure of the FFCC. Both trials outperformed aluminum and polyethylene by a margin of up to seven percent in shielding alone, though at higher areal densities the difference subsides.

6.2.18. **A Closer look at the Core Homogenization**

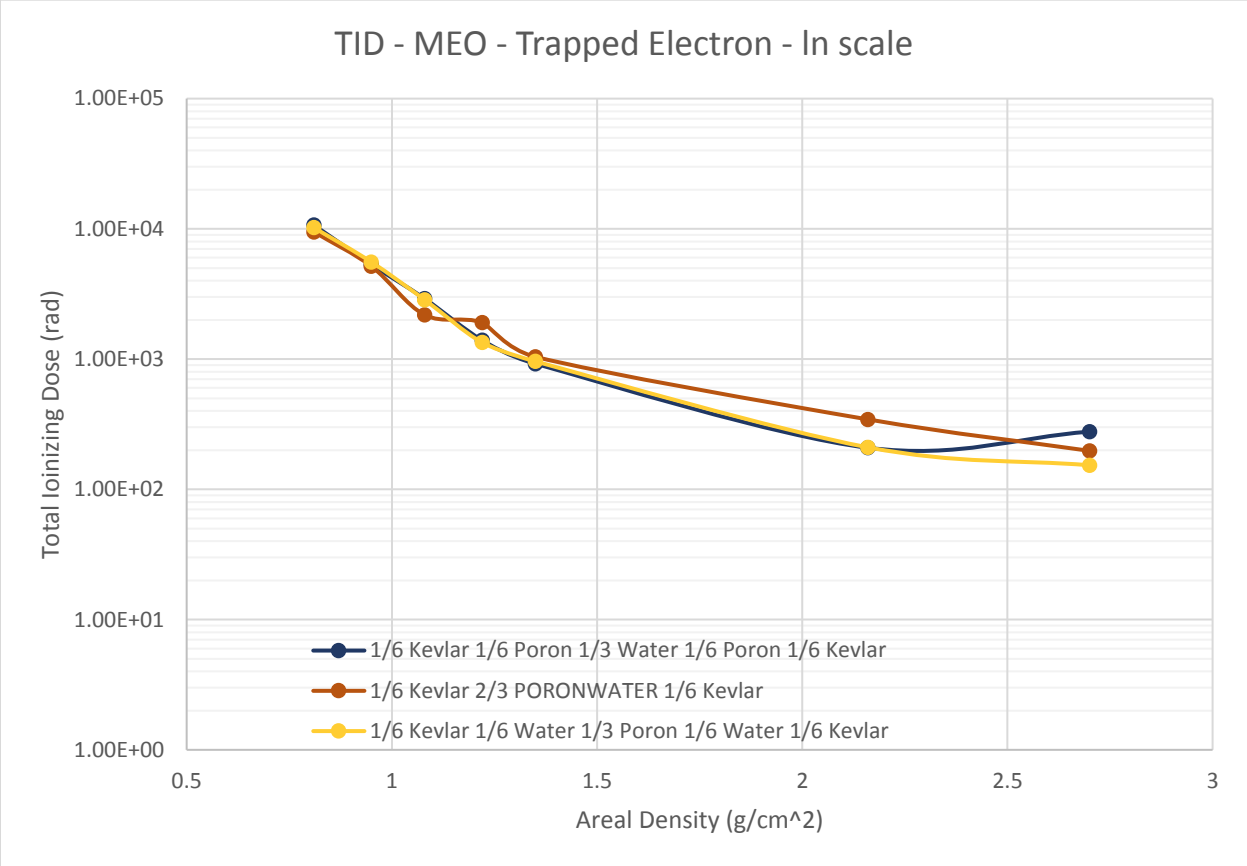

In an effort to understand layer order effect in modeling of the FFCC's core layer, the example of the Figure above is selected. It can be seen that the FFCC with the poron and water core has a 4-5% difference in TID value due to layer order effects in stacking the core rather than using the homogenization method from SPENVIS. Ultimately, this is a small effect that falls within the bounds of relative error discussed earlier. This small change in TID output value is due to the similar shielding response of the layered materials, where poron and water have individual responses that are within (an average of) 17% of eachother. It is expected that the greater the difference in individual shielding capability, the greater this layer order discrepency will be. It is seen that the FFCC with the homogenized core provides a consistent TID value, while the layered core method allows for error stacking of the layering error with the relative error.

CHAPTER 7. SIMULATION RESULTS FOR INTERPLANETARY SPACE

For the analysis in interplanetary space, all calculations were performed with 10,000,000 particles. To reduce total computation time, only the FFCC compositions that are viable for consideration are carried over from the MEO environment. This means that trials such as those comparing layer order effect are not included as a determination has been made in that respect. Individual materials are presented in an effort to form a database of comparative shielding response, and FFCC trials are used primarily to determine if those compositions that were most applicable in MEO have a commensurate shielding response in interplanetary space.

7. Results Part II:

7.1. 1AU Interplanetary, GCR Protons, TID v. Areal Density

TID After Shielding (rad) - Interplanetary 1AU, GCR, CRÈME-96, Proton (1-H)										
Trial #	**Materials**	**Areal Density (g/cm^2)**								
		0.81	**1.08**	**1.35**	**1.89**	**2.43**	**3.24**	**4.05**	**5.13**	**6.75**
64	Kevlar	1.86	1.91	1.92	1.97	1.98	2.00	2.04	2.08	2.09
65	B-N	1.87	1.89	1.92	1.96	1.98	2.00	2.06	2.05	2.10
66	Poron	1.86	1.89	1.92	1.95	1.94	2.00	2.04	2.07	2.11
67	Nextel	1.88	1.93	1.94	1.96	2.02	2.06	2.06	2.12	2.15
68	Tyvek	1.87	1.89	1.91	1.92	1.96	2.00	2.01	2.03	2.08
69	Polyethylene	1.86	1.89	1.90	1.93	1.96	2.00	2.02	2.04	2.08
70	Water	1.87	1.88	1.92	1.95	2.00	2.01	2.03	2.07	2.10
71	Ta	1.99	2.04	2.06	2.11	2.18	2.24	2.29	2.35	2.41
72	Al	1.91	1.93	1.97	1.99	2.03	2.08	2.10	2.14	2.23
73	Lunamer	0.01	0.01	0.01	0.01	0.01	0.02	0.02	0.02	0.02
74	LiquidHydrogen	1.84	1.84	1.84	1.91	1.89	1.91	1.96	2.01	1.97
75	BNWATER	1.87	1.90	1.90	1.97	2.01	2.02	2.01	2.05	2.11
76	PORONWATER	1.87	1.91	1.90	1.93	1.99	1.99	2.04	2.05	2.12
77	BNWATERPORON	1.87	1.89	1.93	1.95	1.99	2.01	2.04	2.09	2.07
78	PORONLH	1.85	1.89	1.92	1.94	1.96	1.97	2.02	2.05	2.05

7.2. 1AU Interplanetary, SPE Protons, TID v. Areal Density

TID After Shielding (rad) - Interplanetary 1AU, SPE, Rosenquist 97.7%, Proton (1-H)										
Trial #	**Materials**	**Areal Density (g/cm^2)**								
		0.81	**1.08**	**1.35**	**1.89**	**2.43**	**3.24**	**4.05**	**5.13**	**6.75**
79	Kevlar	3072.3	1968.4	1309.7	651.3	384.1	196.8	110.8	59.4	26.3
80	B-N	3486.7	2328.1	1566.6	800.5	469.3	241.0	140.7	75.0	34.0
81	Poron	2954.1	1861.4	1213.4	616.0	351.1	179.1	102.3	55.1	24.6
82	Nextel	3777.3	2598.1	1764.0	916.5	532.1	279.7	163.9	86.3	40.3
83	Tyvek	2592.0	1587.1	1036.9	516.6	294.3	146.9	79.3	40.8	18.9
84	Polyethylene	**2614.9**	1596.7	1030.0	516.2	295.2	149.0	83.9	43.2	19.4
85	Water	2944.1	1843.5	1199.5	610.8	346.5	174.1	100.5	54.3	23.8
86	Ta	7090.9	5456.4	4376.9	2856.3	1845.6	1027.0	636.6	373.8	192.5

87	Al	4160.6	2959.1	2056.5	1078.5	637.1	340.2	198.9	106.8	50.4
88	Lunamer	3922.8	2712.7	1859.3	962.1	572.6	298.6	173.6	94.3	44.1
89	LiquidHydrogen	704.5	380.1	234.4	98.0	51.3	21.3	11.5	5.2	1.8
90	BNWATER	2838.7	1771.6	1167.3	585.4	334.9	169.5	97.1	51.7	23.6
91	PORONWATER	2932.7	1871.4	1215.4	621.0	355.8	183.3	102.9	57.7	24.6
92	BNWATERPORON	2940.9	1863.1	1212.3	607.9	350.5	183.2	101.4	53.5	23.9
93	PORONLH	2429.9	1462.7	930.5	459.2	262.3	132.6	70.7	37.1	15.7
94	1/3 Kevlar 1/3 PORONWATER 1/3 Kevlar	3018.6	1934.3	1284.7	637.6	377.3	190.2	108.2	58.5	26.0
95	1/3 Nextel 1/3 PORONWATER 1/3 Nextel	3505.3	2325.2	1559.6	791.5	467.7	240.9	140.7	74.5	34.1
96	1/6 Kevlar 2/3 PORONWATER 1/6 Kevlar	2992.9	1893.9	1245.6	615.2	362.2	184.2	107.2	57.9	26.5
97	1/6 Nextel 2/3 PORONWATER 1/6 Nextel	3232.9	2075.3	1383.4	704.7	412.3	208.8	117.1	64.4	28.6
98	1/3 Kevlar 1/3 BNWATERPORON 1/3 Kevlar	3036.8	1934.6	1281.1	636.3	374.5	190.7	106.1	58.0	27.6
99	1/3 Nextel 1/3 BNWATERPORON 1/3 Nextel	3499.6	2326.1	1555.1	793.3	466.9	240.9	139.3	74.3	33.6
100	1/6 Kevlar 2/3 BNWATERPORON 1/6 Kevlar	2998.8	1888.9	1246.2	620.9	362.2	184.2	105.0	55.2	25.2
101	1/6 Nextel 2/3 BNWATERPORON 1/6 Nextel	3215.1	2084.9	1396.4	692.2	405.3	206.4	119.4	62.5	29.0
102	1/6 Tyvek 2/3 PORONWATER 1/6 Tyvek	2813.8	1757.2	1141.8	574.3	329.0	163.7	97.8	47.9	21.1
103	1/6 Tyvek 2/3 BNWATERPORON 1/6 Tyvek	2823.9	1754.0	1142.2	576.1	328.2	165.6	95.4	49.7	22.3
104	1/6 Tyvek 2/3 PORONLH 1/6 Tyvek	2473.4	1500.9	959.7	475.7	269.6	133.5	74.4	36.8	17.6
105	1/6 Nextel 2/3 PORONLH 1/6 Nextel	2829.6	1746.9	1156.0	576.2	329.9	166.4	93.6	48.7	22.3
106	1/6 Kevlar 2/3 PORONLH 1/6 Kevlar	2634.2	1587.7	1032.8	514.8	294.2	149.0	83.3	42.8	19.1
107	1/6 Kevlar 1/6 Tyvek 1/3 PORONWATER 1/6 Tyvek 1/6 Kevlar	2867.6	1805.7	1175.5	591.3	341.7	171.3	96.7	51.9	23.7
108	1/6 Kevlar 1/6 Tyvek 1/3 BNWATERPORON 1/6 Tyvek 1/6 Kevlar	2867.0	1799.4	1172.8	585.7	337.5	172.1	97.9	51.5	23.4
109	1/6 Kevlar 1/6 Tyvek 1/3 PORONLH 1/6 Tyvek 1/6 Kevlar	2688.4	1657.1	1076.1	531.6	304.7	153.5	87.0	44.3	20.8
110	1/6 Nextel 1/6 Tyvek 1/3 PORONLH 1/6 Tyvek 1/6 Nextel	2892.3	1804.9	1184.0	592.5	344.8	172.1	97.6	50.7	23.3

7.3. 1AU Interplanetary, SPE, Helium Nuclei, TID v. Areal Density

TID After Shielding (rad) - Interplanetary 1AU, SPE, ESP-PSYCHIC (total fluence) 97.7%, 4-He										
Trial #	Materials	Areal Density (g/cm^2)								
		0.81	1.08	1.35	1.89	2.43	3.24	4.05	5.13	6.75
111	Kevlar	201.65	123.97	80.81	42.55	25.52	13.06	8.22	4.68	2.03
112	B-N	235.17	144.41	97.55	53.01	31.49	16.87	10.11	5.98	2.81
113	Poron	189.07	113.02	75.84	40.22	23.67	12.55	7.58	4.30	1.69
114	Nextel	264.35	161.66	109.66	58.34	34.28	19.52	11.72	7.10	3.44
115	Tyvek	160.56	96.23	63.12	32.64	19.11	10.68	6.55	3.28	1.52
116	Polyethylene	163.70	95.60	63.23	32.55	18.99	10.78	6.74	3.55	1.37
117	Water	185.61	113.20	75.27	38.11	22.67	12.11	7.23	4.28	2.01
118	Ta	726.55	472.72	328.34	184.15	117.30	65.69	42.21	26.25	13.55
119	Al	303.66	186.41	127.27	67.26	39.86	22.62	13.48	8.19	4.44
120	LunarRegolith	555.38	422.16	333.18	229.40	170.02	118.10	87.24	62.26	41.58
121	LiquidHydrogen	45.36	25.52	15.68	7.72	4.56	1.81	0.82	0.44	0.13
122	BNWATER	181.04	110.34	71.86	37.12	22.81	12.07	7.63	4.42	1.80
123	PORONWATER	185.09	115.12	76.28	38.87	23.53	12.09	7.50	4.52	1.61
124	BNWATERPORON	185.56	111.14	73.57	39.55	23.01	12.04	7.54	3.80	1.64
125	PORONLH	150.46	91.60	60.23	30.18	17.91	9.36	5.15	2.84	1.33
126	1/3 Kevlar 1/3 PORONWATER 1/3 Kevlar	198.41	120.16	79.14	40.61	24.98	13.22	8.03	4.55	2.03
127	1/3 Nextel 1/3 PORONWATER 1/3 Nextel	233.83	142.65	96.73	50.32	29.85	16.83	10.06	5.78	2.75
128	1/6 Kevlar 2/3 PORONWATER 1/6 Kevlar	194.55	118.58	77.96	40.42	23.91	12.98	8.13	4.32	1.97
129	1/6 Nextel 2/3 PORONWATER 1/6 Nextel	212.73	125.57	83.95	43.23	26.09	13.90	8.63	4.67	2.41
130	1/3 Kevlar 1/3 BNWATERPORON 1/3 Kevlar	198.69	122.56	79.20	40.87	24.74	13.13	7.90	4.89	2.06
131	1/3 Nextel 1/3 BNWATERPORON 1/3 Nextel	231.55	144.44	97.28	51.72	29.82	16.60	10.29	5.88	2.79
132	1/6 Kevlar 2/3 BNWATERPORON 1/6 Kevlar	194.00	117.59	78.28	40.13	24.11	12.78	8.10	4.40	1.96
133	1/6 Nextel 2/3 BNWATERPORON 1/6 Nextel	211.52	127.44	83.18	44.51	25.99	14.37	8.66	4.98	2.43
134	1/6 Tyvek 2/3 PORONWATER 1/6 Tyvek	176.85	104.88	70.85	35.87	22.26	11.94	6.77	4.09	1.73
135	1/6 Tyvek 2/3 BNWATERPORON 1/6 Tyvek	179.33	108.04	71.52	37.44	22.48	12.14	7.07	3.59	1.66
136	1/6 Tyvek 2/3 PORONLH 1/6 Tyvek	153.06	95.50	59.77	32.01	18.01	9.59	5.92	2.89	1.29

137	1/6 Nextel 2/3 PORONLH 1/6 Nextel	174.75	106.63	68.96	35.89	21.96	11.84	6.87	3.91	1.62
138	1/6 Kevlar 2/3 PORONLH 1/6 Kevlar	165.63	98.80	65.50	34.29	20.10	10.54	6.44	3.74	1.30
139	1/6 Kevlar 1/6 Tyvek 1/3 PORONWATER 1/6 Tyvek 1/6 Kevlar	181.81	108.11	73.25	37.23	23.42	12.02	7.37	4.29	1.78
140	1/6 Kevlar 1/6 Tyvek 1/3 BNWATERPORON 1/6 Tyvek 1/6 Kevlar	184.81	109.16	74.24	36.83	23.70	11.94	7.61	4.21	1.73
141	1/6 Kevlar 1/6 Tyvek 1/3 PORONLH 1/6 Tyvek 1/6 Kevlar	167.66	102.59	67.85	35.07	20.64	10.54	7.59	3.76	1.59
142	1/6 Nextel 1/6 Tyvek 1/3 PORONLH 1/6 Tyvek 1/6 Nextel	181.02	110.38	75.34	38.25	22.60	12.12	7.16	4.04	1.62

7.4. Part II: Discussion

Part two of this research is concerned with FFCC analysis in interplanetary space. The primary two radiation sources being SPE and GCR. The harsh radiation environment necessitated the use of greater thicknesses of shielding materials to attenuate the high energy incident particles. Additional data points were added in an effort to portray a clear trend towards complete attenuation with fewer "blips" than seen in the MEO environment. All Monte Carlo simulations for this environment were conducted with the maximum number of particles (10,000,000). This high particle count increases computation time, though the number of areal density data points that are reasonable to analyze in the harsher environment is increased to nine, in comparison to the seven data points used in the MEO environment.

7.5. Discussion: 1AU Interplanetary, GCR, CREME96, 1-H

7.5.1. Comparative Baseline: TID, 1AU Interplanetary, GCR, Proton (Trials 69, 71, 72)

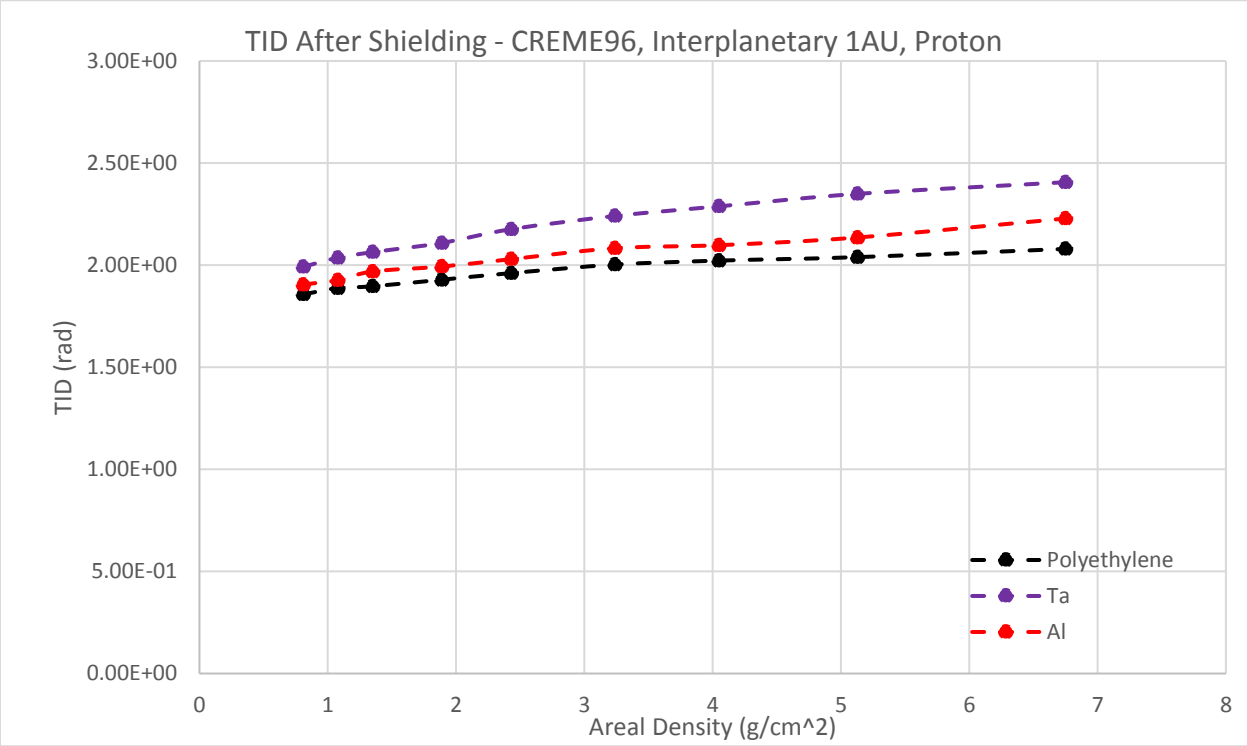

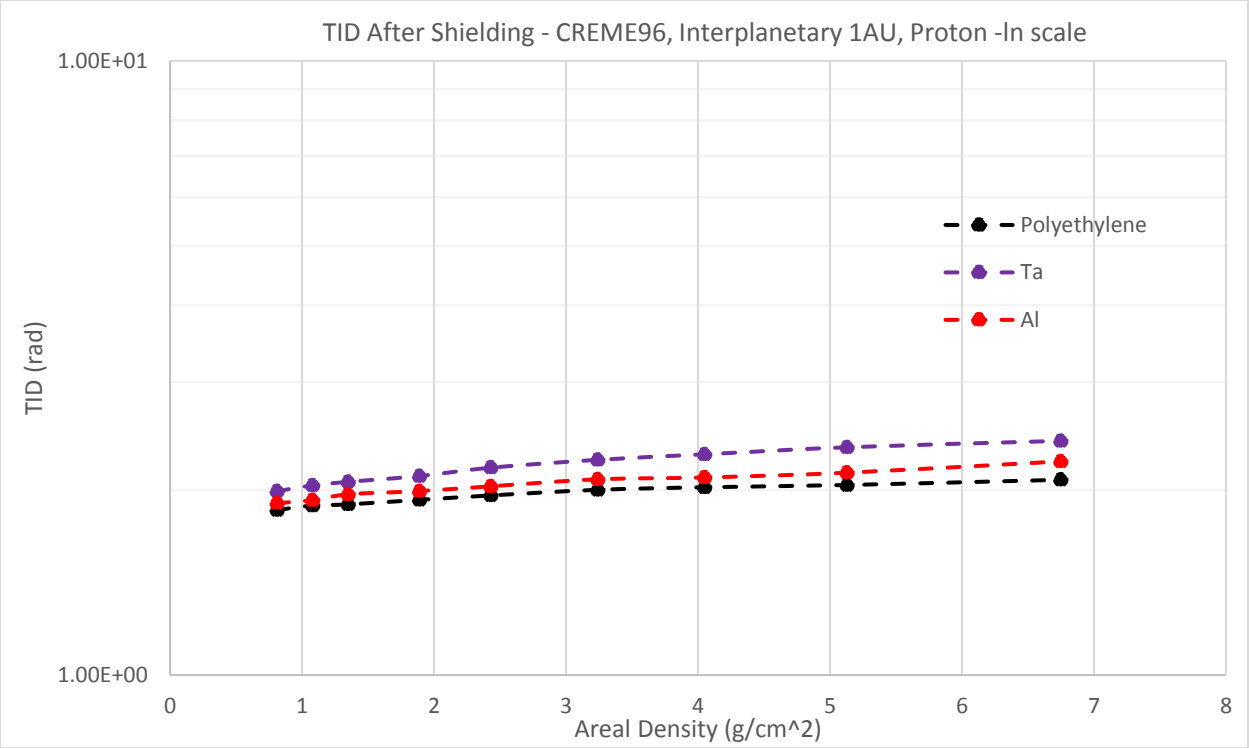

Aluminum, tantalum, and polyethylene are used as the comparative baseline for all other radiation shielding materials in a particular environment. As expected, polyethylene is the most functional shielding material of the three, with the lowest TID values, followed by aluminum. The TID after shielding for GCR is very low in comparison to the SPE, which is something that can be inferred from the radiation spectrum plot comparing GCR and SPE (Figure 3.2). For this reason, the analysis of the FFCC response to GCR protons is only conducted for individual material components of the FFCC, because all FFCC compositions that will shield SPE will shield GCR. This is seen by the TID after shielding for SPE being three orders of magnitude larger than that for GCR at the lowest areal density (0.81 g/cm^2).

7.5.2. **TID, Individual Materials at 1AU Interplanetary, GCR, Proton (Trials 64-72)**

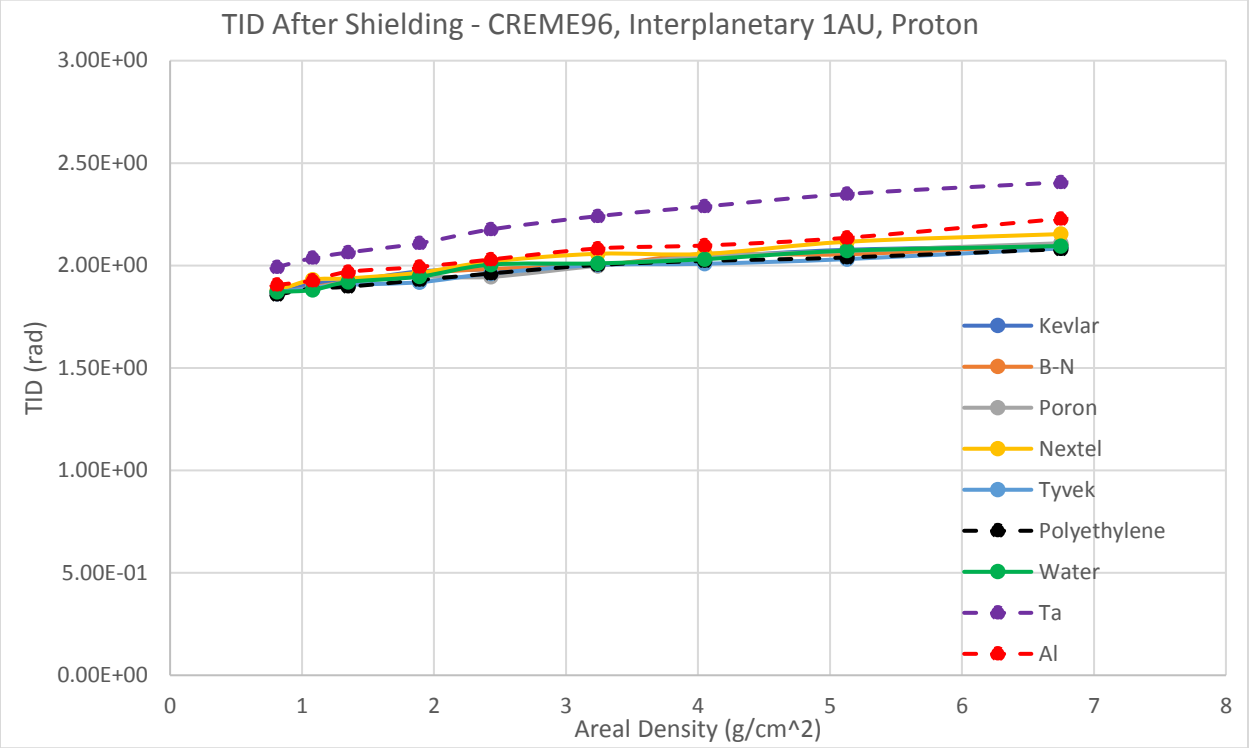

Of all the materials tested, both polyethylene and Tyvek showed the lowest absorbed dose of GCR protons in the detector. This is a similar result to that seen for trapped electrons in MEO. It can also be seen that all materials outperformed aluminum and tantalum in shielding of incident protons, which is likely due to the formation of secondary radiation inherent to high Z materials. This set of data shows an upward trend in TID as a function of areal density, this is not unsurprising as the median TID value is 2 rad, meaning a fluctuation in shielding of 0.125 rad is not outside the bounds of relative error as discussed in Chapter 5. That is, it can be seen that the GCR protons have been attenuated nearly completely by all areal densities tested, so the whole of the standard trend of decreasing TID v. Areal Density is not seen in the areal density range simulated. What is presented is seen to be representative of the tail of the standard TID v. Areal density trend, where the TID value has low enough magnitude that the magnitude of uncertainty (as discussed in the Error Analysis section) nears that of the TID and results in a trend that appears to be upward. In actuality, the trend of decreasing TID with areal density is expected to continue until 0 rad (complete attenuation), though the 'nearly' complete attenuation (at 2 rad) of the Monte Carlo simulation is effectively complete attenuation.

7.5.3. **TID, Custom Materials at 1AU Interplanetary, GCR, Proton (Trials 73-78)**

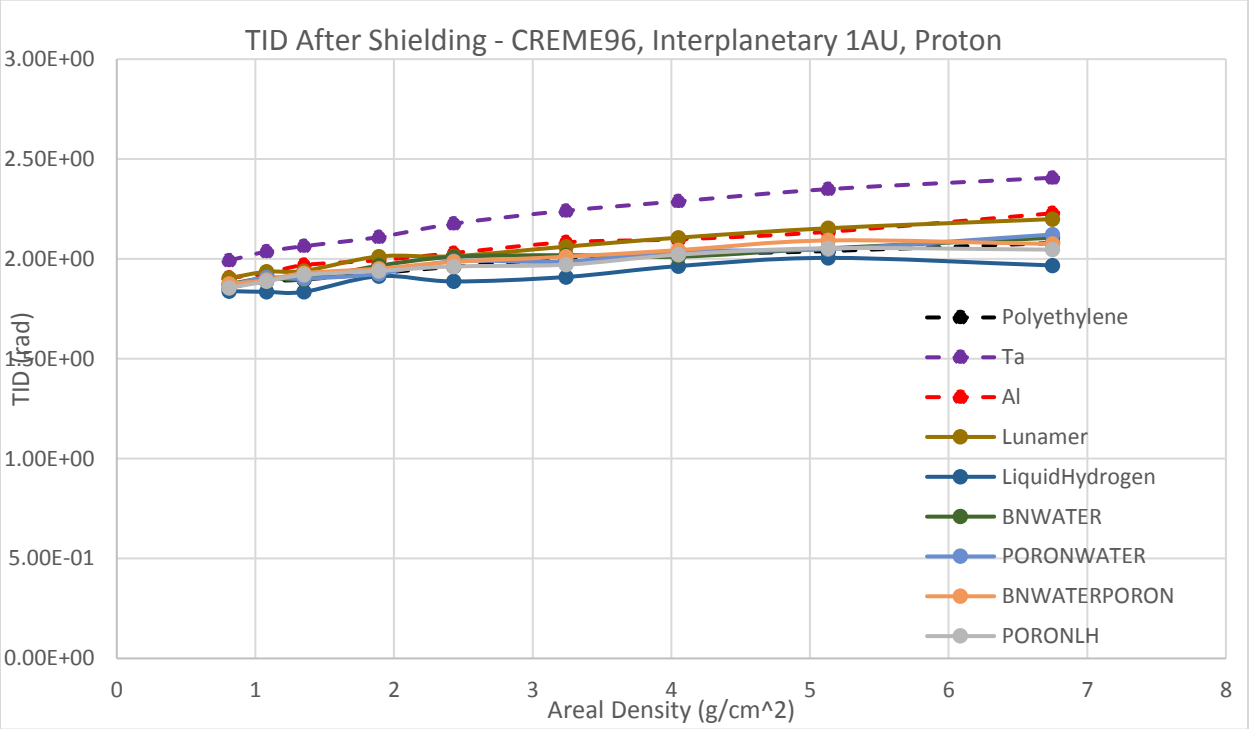

The custom materials all perform as expected in comparison to the MEO environment. The two most interesting observations are that PORONLH performs nearly the same as polyethylene, and PORONWATER outperforms both of these. Interestingly, the Lunamer material has an equivalent performance to aluminum, something not expected from its atomic composition of many different Z. This is discussed further in Chapter 8.

7.6. Discussion: 1AU Interplanetary, SPE, Rosenquist 97.7%, 1-H

7.6.1. Comparative Baseline: TID, 1AU Interplanetary, SPE, Proton (Trials 84, 86, 87)

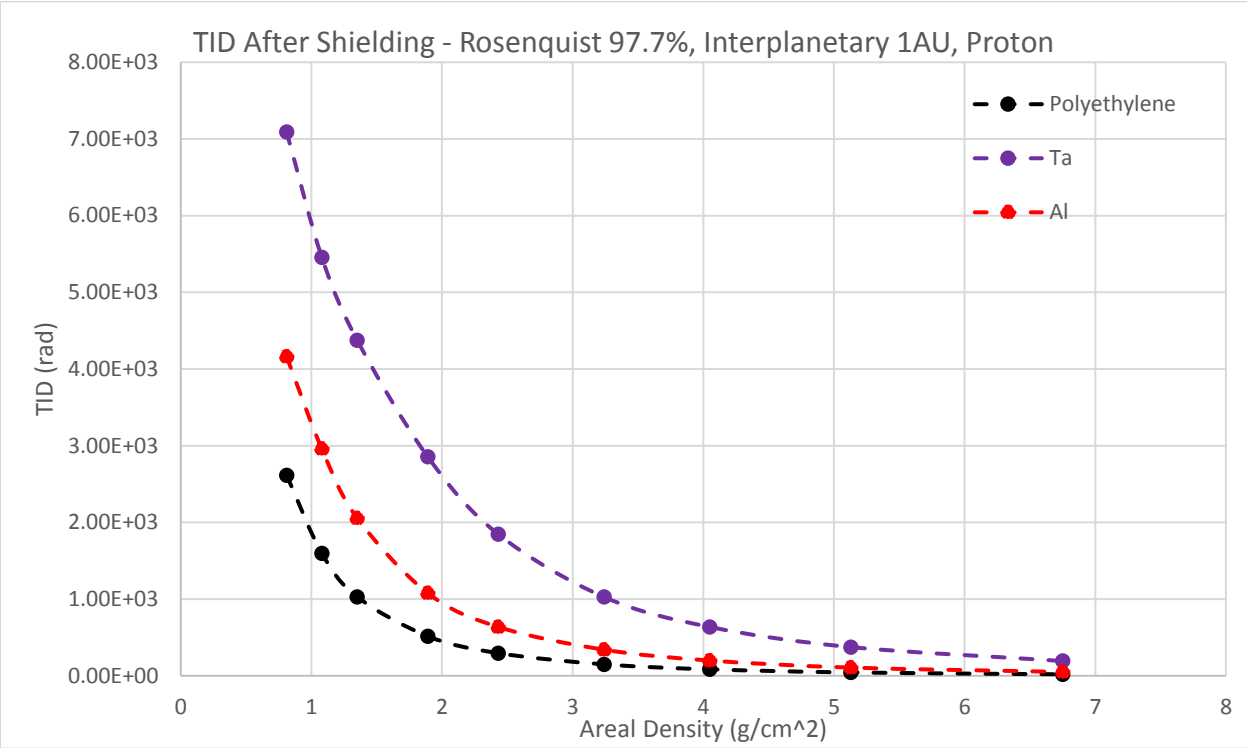

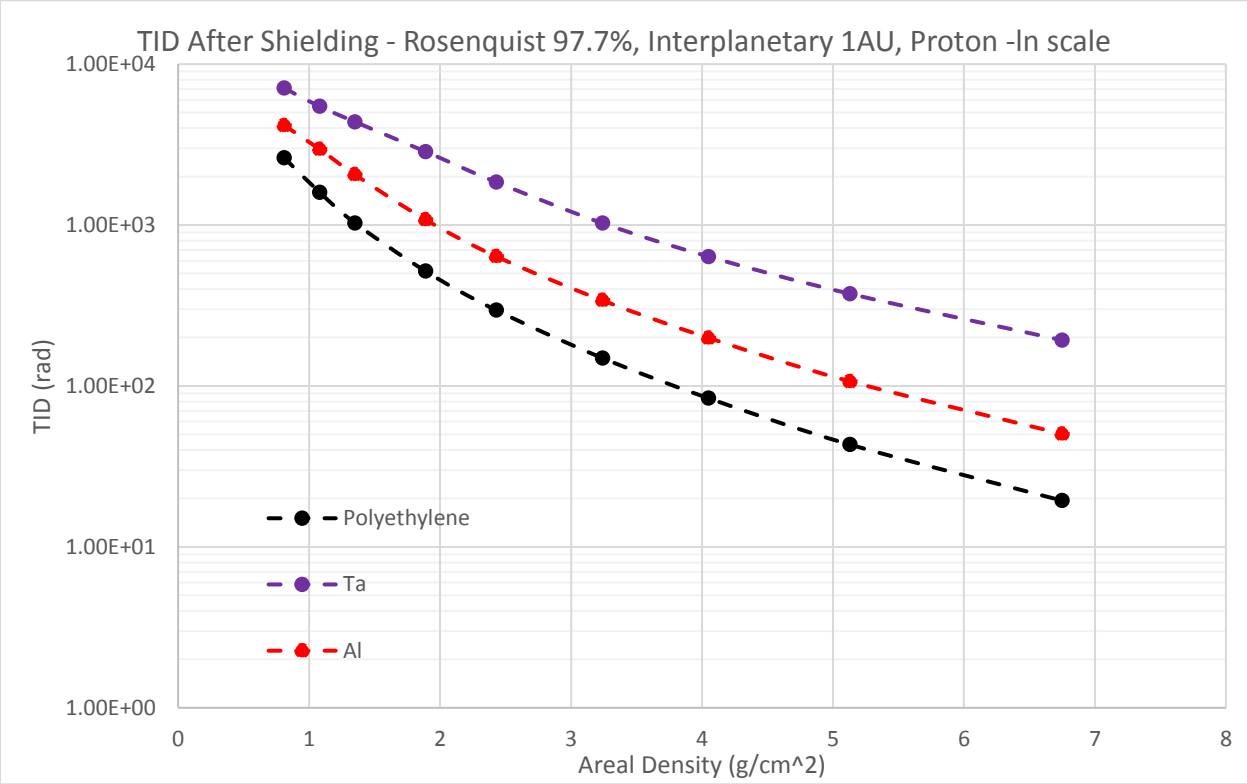

Aluminum, tantalum, and polyethylene are used as the comparative baseline for all other radiation shielding materials in a particular environment. As expected, polyethylene is observed to provide the most shielding, followed by aluminum and tantalum respectively. In similar respect to GCR protons, the metals start to show decreased shielding capability due to secondary radiation associated with the shielding of solar protons. It can be seen that the TID after shielding for solar protons of the SPE environment is much higher than those seen for the GCR environment, and represents the worst-case scenario for a the FFCC as a shielding material. This is predicted by the radiation spectrum plot of Figure 3.2. It is also observed that the general trend of the radiation attenuation is smoother than that seen in the MEO environment. This is likely due to the fluctuation of trapped electron fields in MEO in comparison to the consistent ejection of protons (and other ions) in SPE and GCR.

7.6.2. **TID, Individual Materials at 1AU Interplanetary, SPE, Proton (Trials 79-87)**

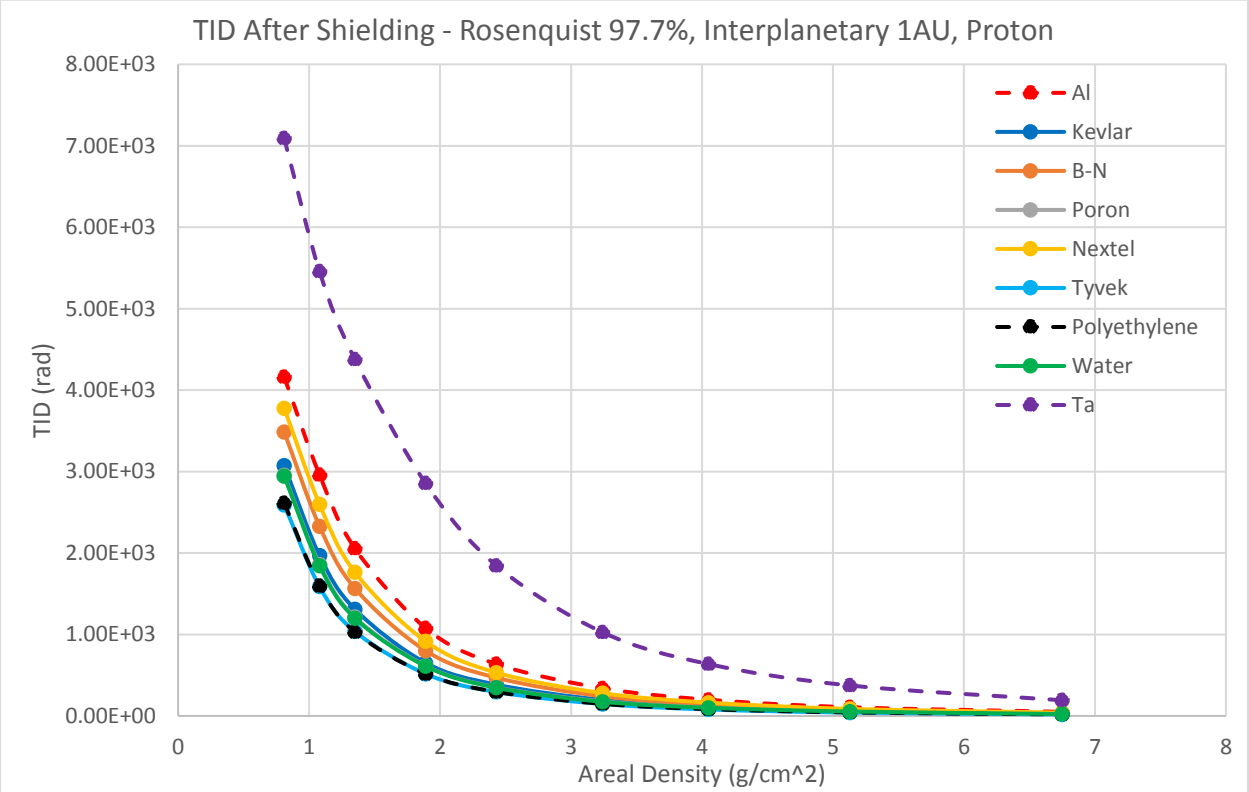

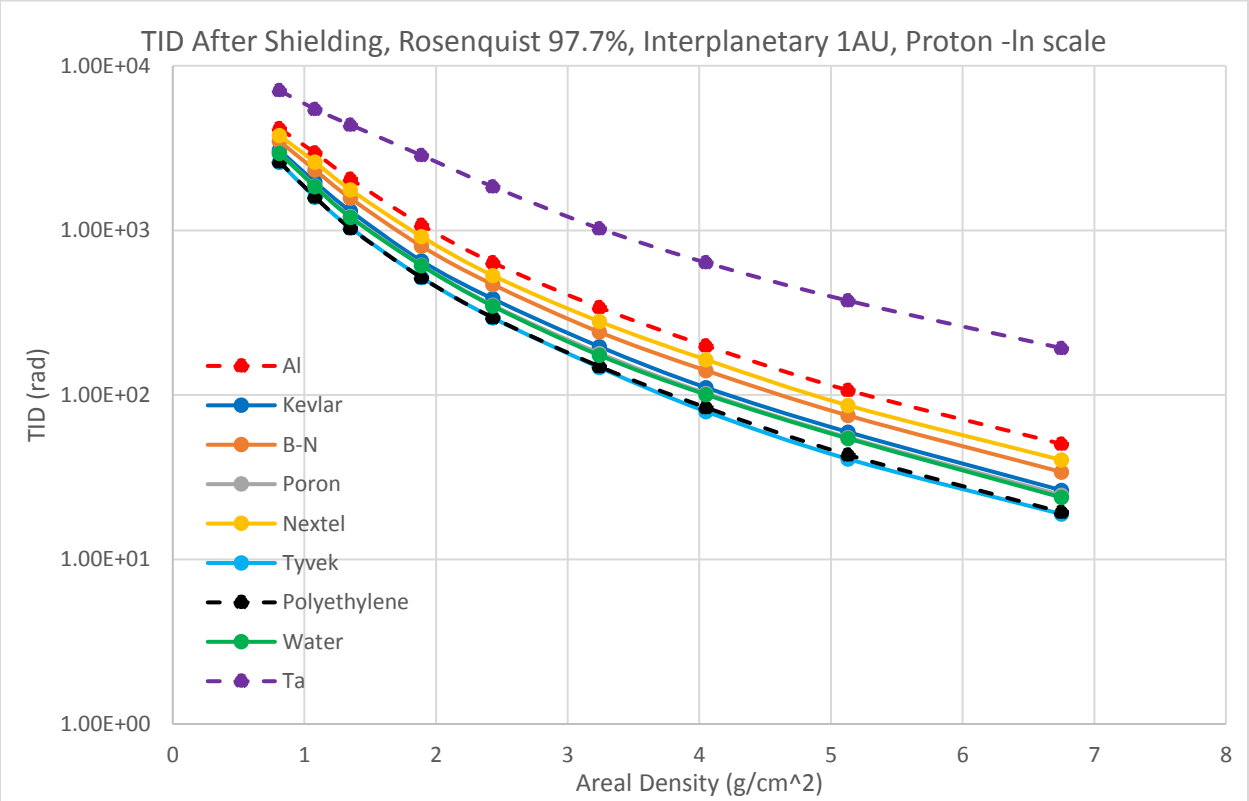

All individual materials behave slightly better than expected, as the simulation results predict that all materials will outperform the traditional shielding metals in attenuation of solar protons, in comparison to the response of the same materials to trapped electrons. In MEO, the materials had a shielding attenuation varying around that of aluminum, while the harsher environment of SPE predicts a decrease in the performance of the metals. This is likely due to an increase in secondary radiation generation due to the high energy protons from SPE in comparison to the low energy electrons of MEO. Although trapped electrons are of ionizing energy levels and can thus create secondary radiation upon interaction with shielding materials, the type of secondary radiation is less harsh and at lower energy than those created in interaction with solar protons. In SPE and GCR the known risk of metals and other high Z materials creating dangerous secondary radiation is realized.

7.6.3. **TID, Custom Materials at 1AU Interplanetary, SPE, Proton (Trials 88-93)**

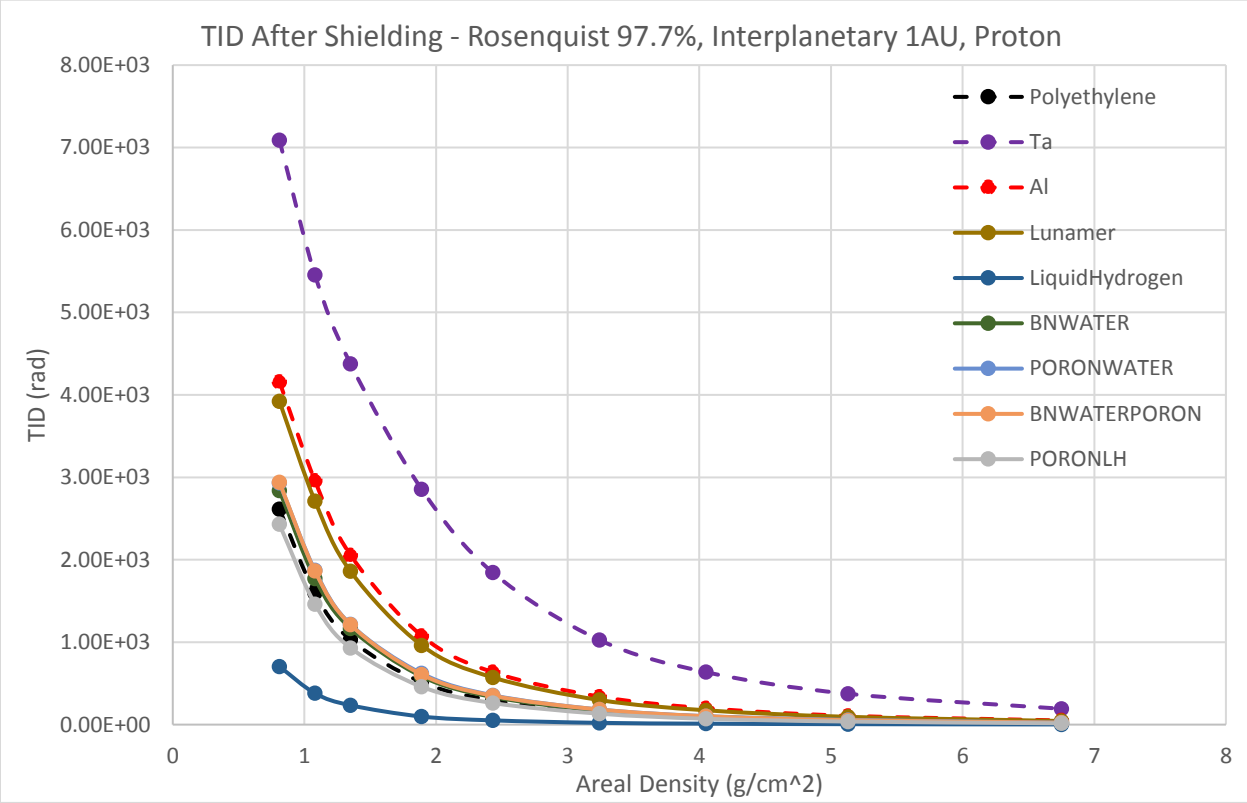

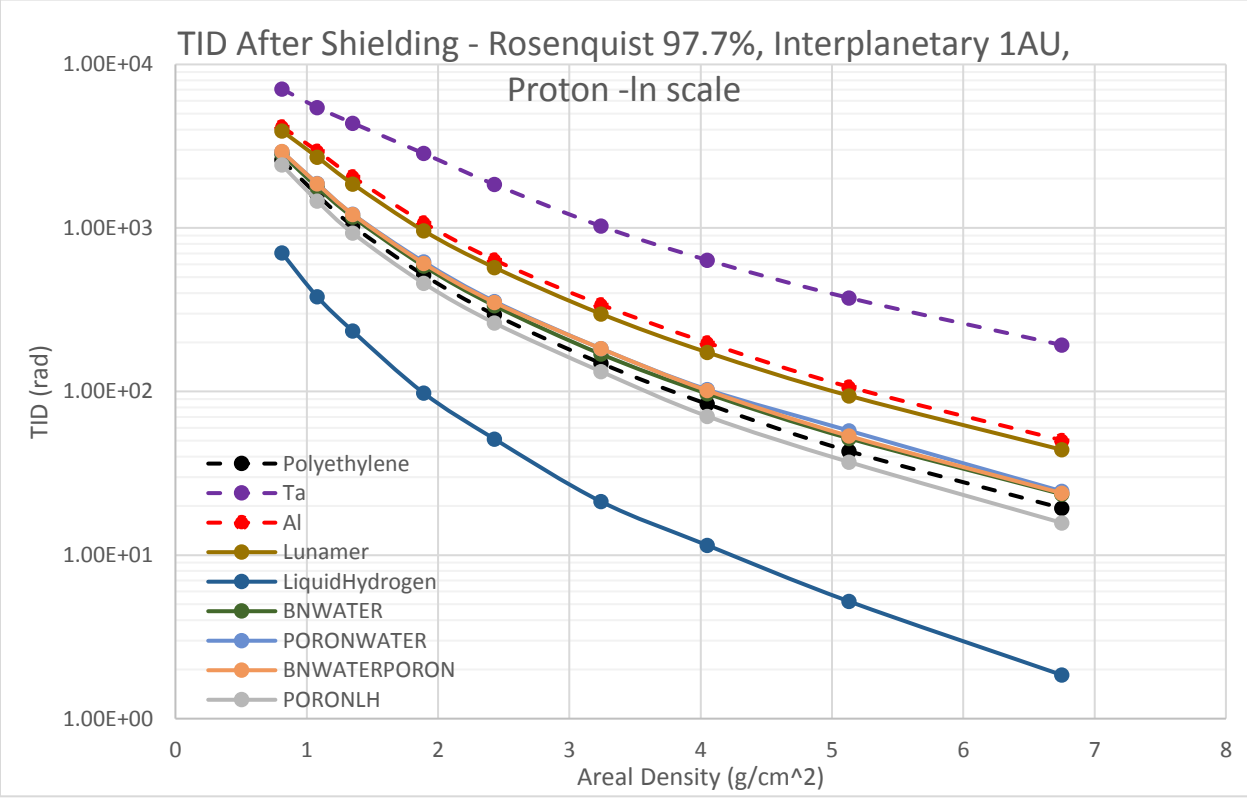

The custom materials also generally behave as expected from the trends associated with the MEO and interplanetary GCR environments. Once again, all the homogenized core layers with water perform nearly identically to pure polyethylene. The effect of adding BN to the interstitial water is not fully noticed in this respect, though may be realized in analysis with high Z incident particles. Liquid hydrogen also outperforms all materials in shielding solar protons, which is expected considering the mass of the hydrogen atoms of the incident particles are the same as the impacted atoms. This means that the PORONLH homogenized core is able to decrease the dose in a silicon detector to an extent that is slightly greater than that of pure polyethylene (at an average of 12% lower TID). This speaks to the goal of creating an FFCC with the greatest amount of hydrogen possible for improving shielding characteristics.

7.6.4. **TID, FFCC w/ Homogenized Poron and Water (3 Layers) in 1AU Interplanetary, SPE, Proton (Trials 94-97, 102)**

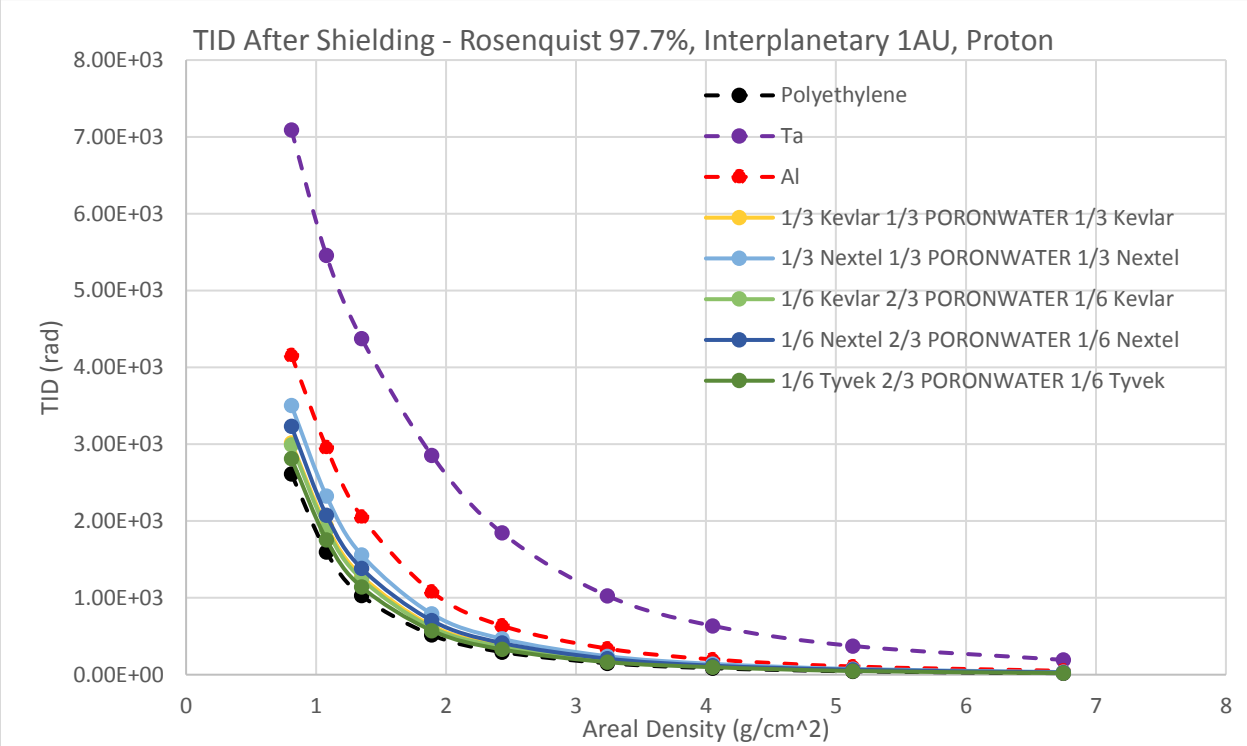

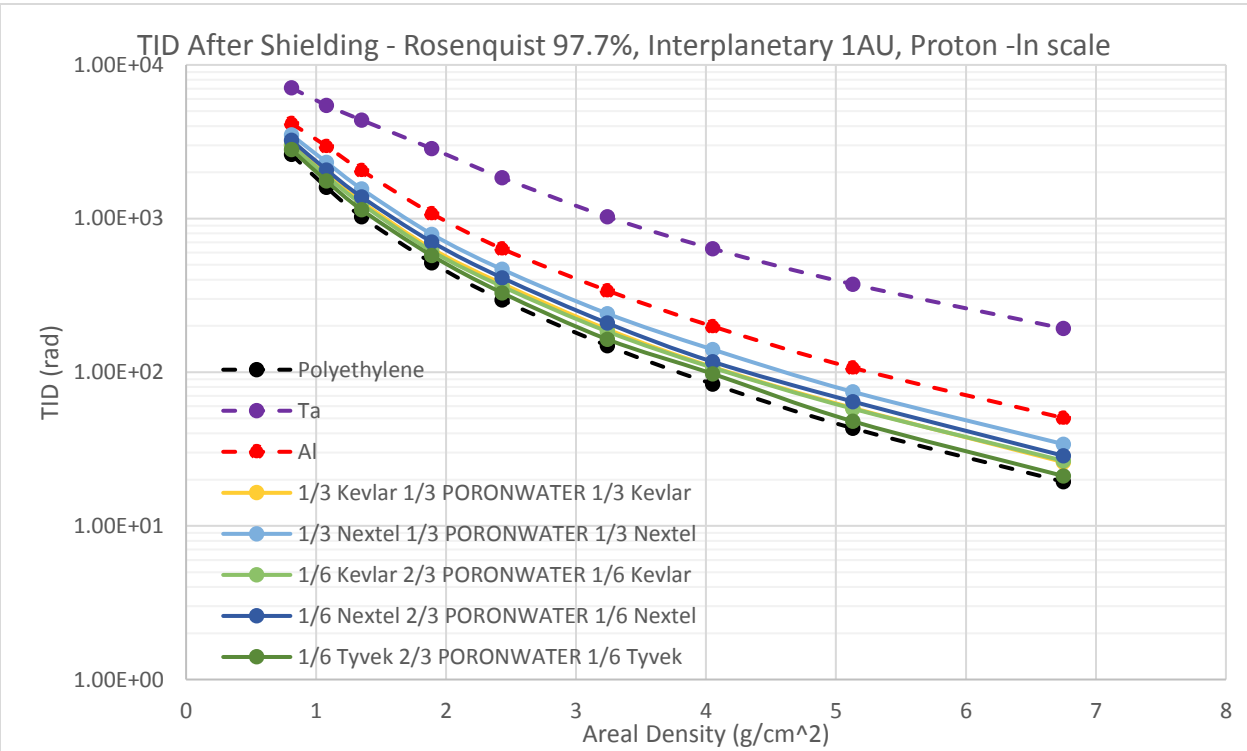

As discussed earlier, this set of trials represents a simplified FFCC composition with a singular skin layer on each side of a fluid-filled core. The three primary skin layers are Kevlar, Nextel, and Tyvek. The ratio of areal density for each layer was kept constant with those defined in the MEO environment, though with different total areal densities. That is, the core layers are defined as having 2/3 of the total areal density as the largest layer in the FFCC. Of these trials, the FFCC with the Tyvek face shows the greatest shielding capability for solar protons, and represents the highest hydrogen density of this set of trials. Interestingly, the trials that have equally distributed areal densities for each layer (94 and 95) do not have vastly decreased shielding in comparison to the trials with the larger core layer, though they do have slightly decreased shielding. Overall, all materials outperform aluminum, though only trial 102 shows a TID nearing polyethylene (within an average of 9%).

7.6.5. **TID, FFCC w/ Homogenized BN, Poron, and Water (3 Layers) in 1AU Interplanetary, SPE, Proton (Trials 98-101, 103)**

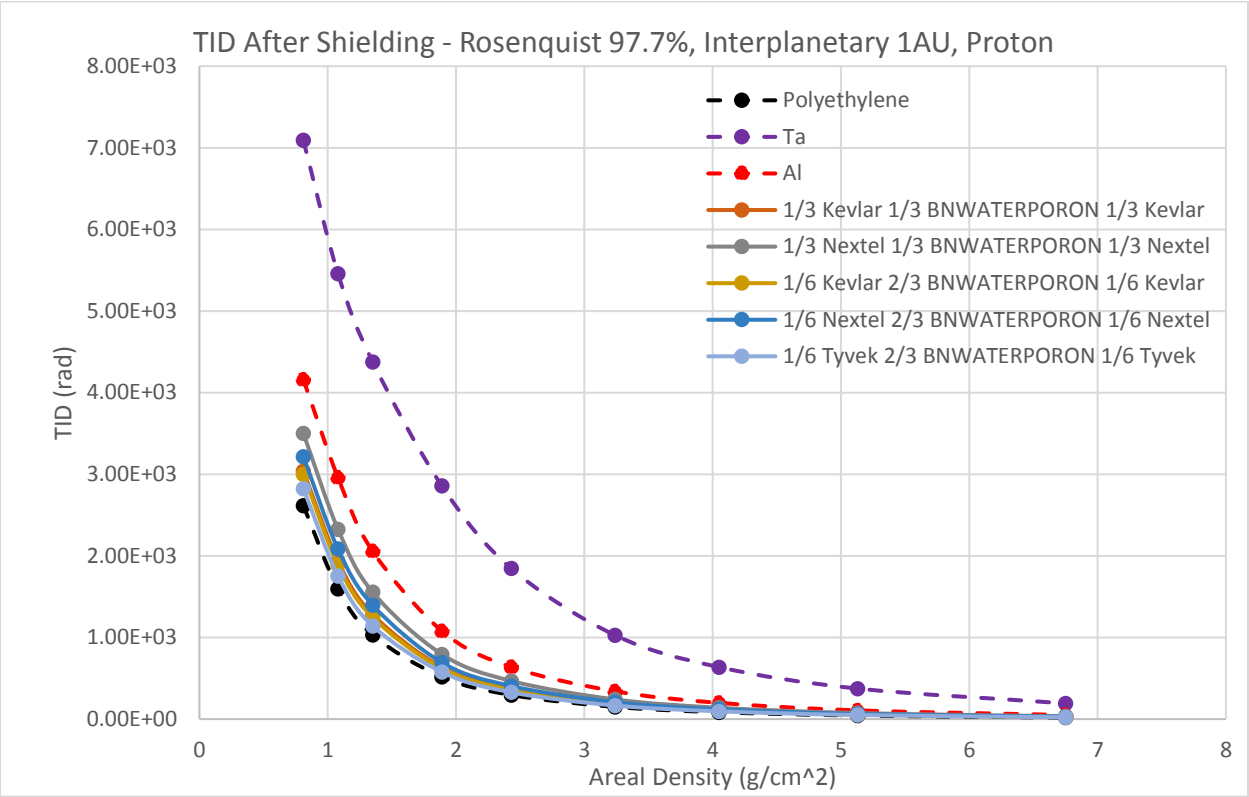

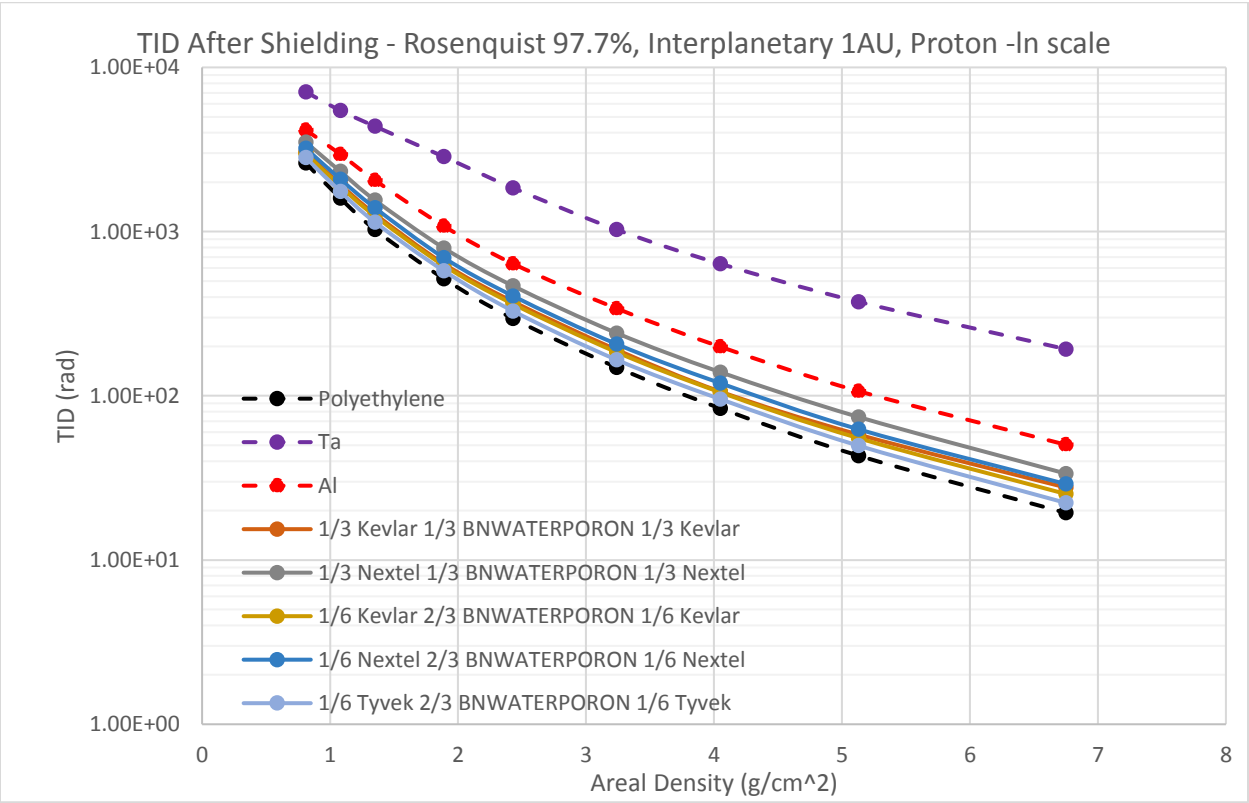

This set of trials represents a simplified FFCC composition of three layers with a single skin layer surrounding a porous core layer filled with a solution of cubic BN and water. The addition of BN in this set of trials is a direct comparison to the last set which did not have the BN. It can be seen that the effect of including BN is not fully realized in shielding of solar protons, as the trends of each trial mirrors those of the last set. As discussed earlier in this investigation, the merit of BN is primarily in shielding of neutrons. Because proton radiation is a single proton as a nucleus, the merit of BN is likely to be realized in shielding higher Z neutrons present in GCR and SPE. Because shielding capability is not harmed by the inclusion of BN, the other characteristics associated with improved thermal and chemical stability are enough to merit its inclusion in the matrix material of the skin layer, as discussed for MEO.

7.6.6. **TID, FFCC w/ Homogenized Poron and Liquid Hydrogen Core (3 Layers) in 1AU Interplanetary, SPE, Proton (Trials 104-106)**

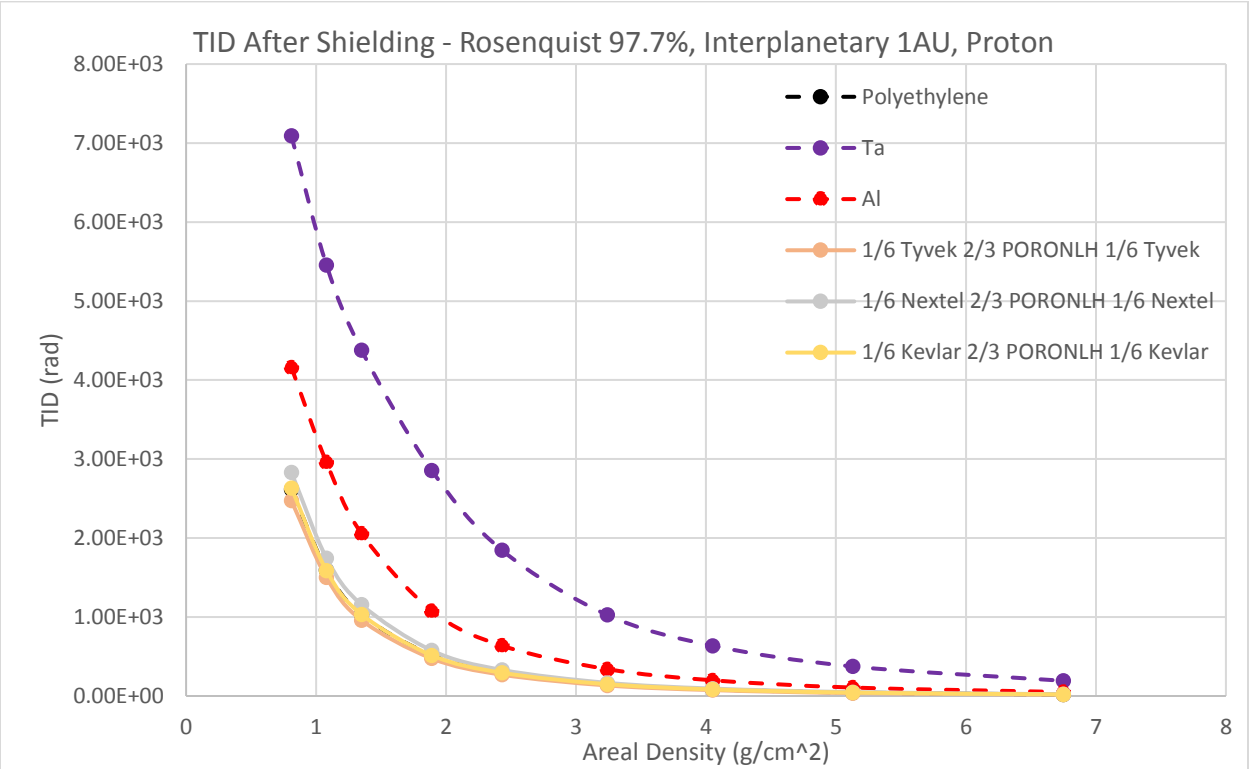

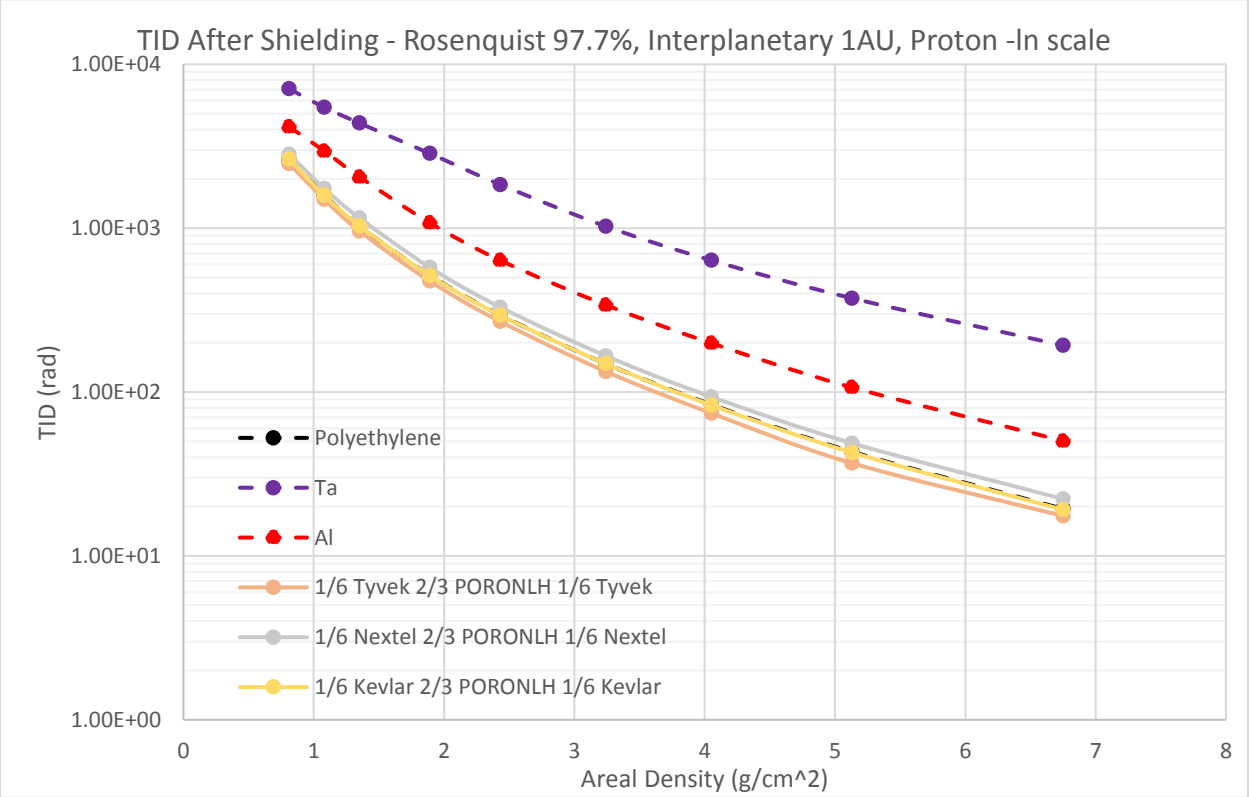

This set of trials represents the simple three-layer FFCC whose porous core is filled with liquid hydrogen instead of water. Once again, it is unclear if this is physically possible given the difficulty associated with storing liquid hydrogen, though the shielding response to solar protons is enough to merit further investigation. That is, all FFCC compositions with the liquid hydrogen filled core predict a dose after shielding commensurate with that of pure polyethylene. The trial with the Tyvek face layer slightly exceeds the shielding capability of polyethylene (by about 9% on average), which is understandable when considering this trial has the highest hydrogen content of any FFCC simulated.

7.6.7. **TID, FFCC w/ Dual Skin Layers and Homogenized Poron and Liquid Hydrogen Core (5 Layers) in 1AU Interplanetary, SPE, Proton (Trials 107-110)**

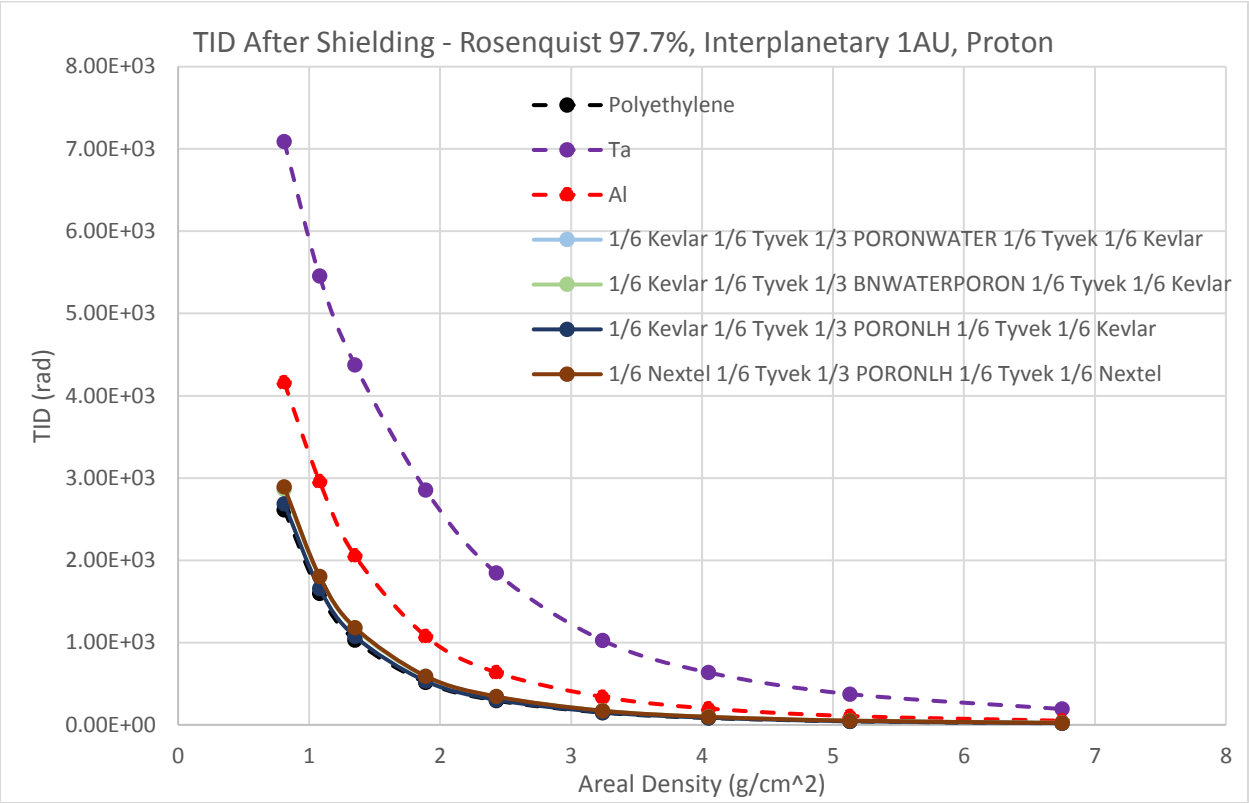

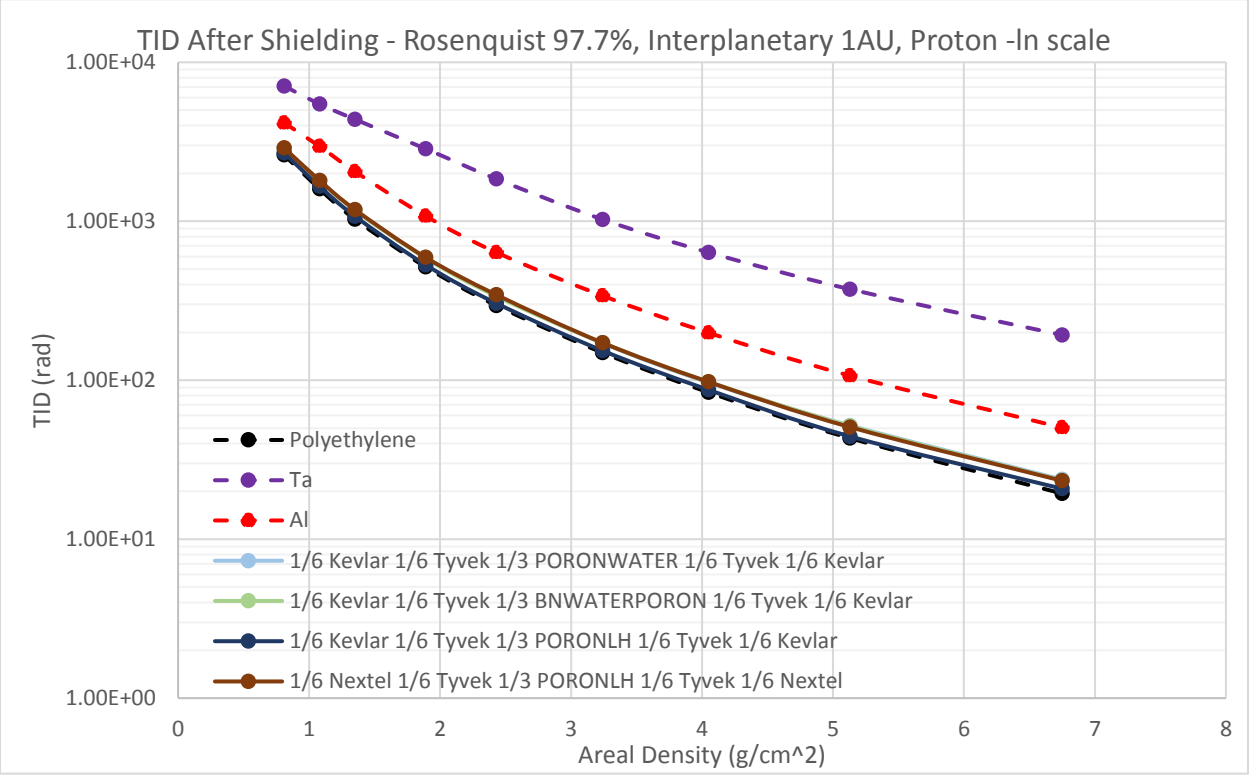

This set of trials represents the full five-layer FFCC that includes two skin layers surrounding the fluid-filled core. As discussed in the MEO environment, these trials act to show the greatest hydrogen density option for the FFCC while also balancing perceived mechanical characteristics of the FFCC. A Kevlar or Nextel face layer is included primarily for structural concerns, with the secondary Tyvek layer for both shielding and isolating of the liquid core. This set of trials predicts that a FFCC composition of Kevlar and Tyvek surrounding the Poron foam core filled with liquid hydrogen (trial 109) will offer shielding of solar protons to an extent meeting that of pure polyethylene (within 3% improved). For the FFCC trial with the Kevlar and Tyvek skin layers surrounding a poron and water core (trial 107), the TID values 15% higher than that of polyethylene. This prediction is similar to what is seen for the same composition as tested in MEO for trapped electrons. Though, in comparison to the traditional shielding metals of aluminum and tantalum, trial 107 is predicted to be 45% lower and 78% lower, respectively. Trial 109 is predicted to show a TID 51% lower than aluminum and 80% lower than tantalum, something not witnessed in MEO.

7.7. Discussion: 1AU Interplanetary, SPE, ESP-PSYCHIC, 4-He

7.7.1. Comparative Baseline: TID, 1AU Interplanetary, SPE, 4-He (Trials 116, 117, 118)

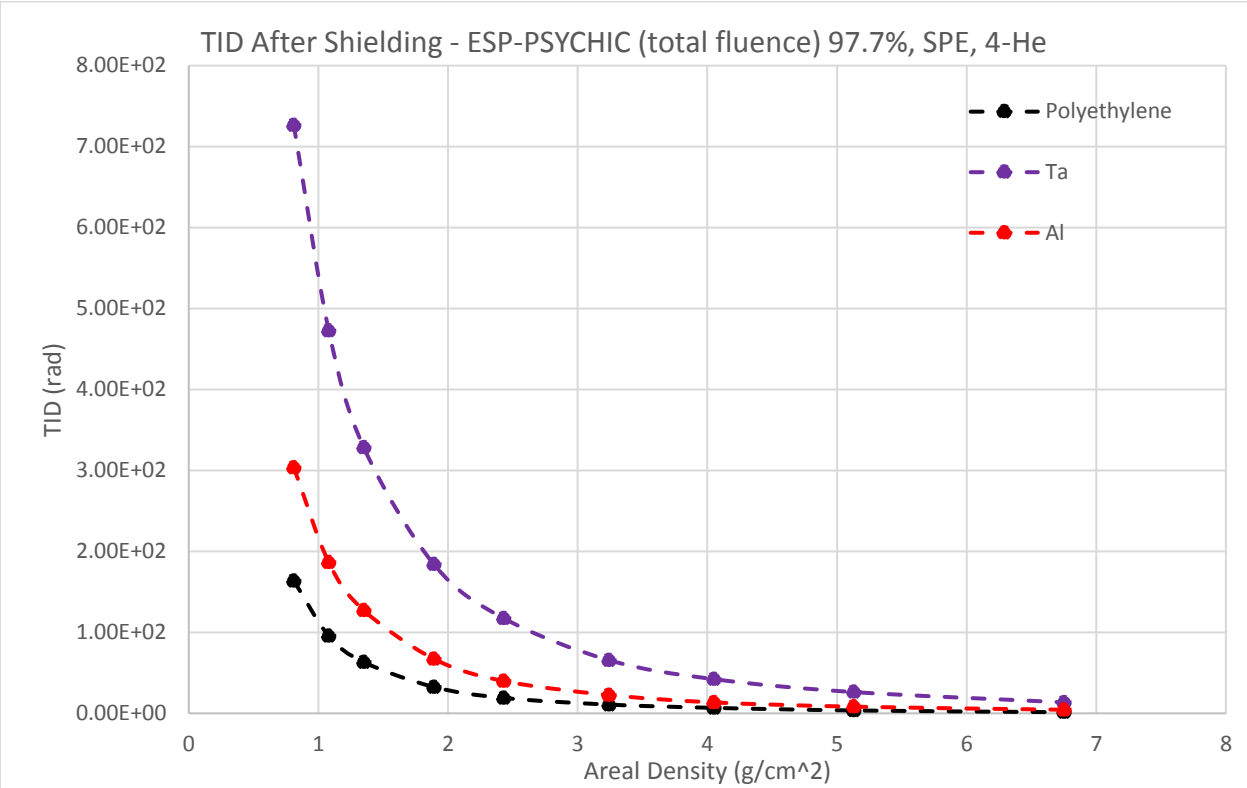

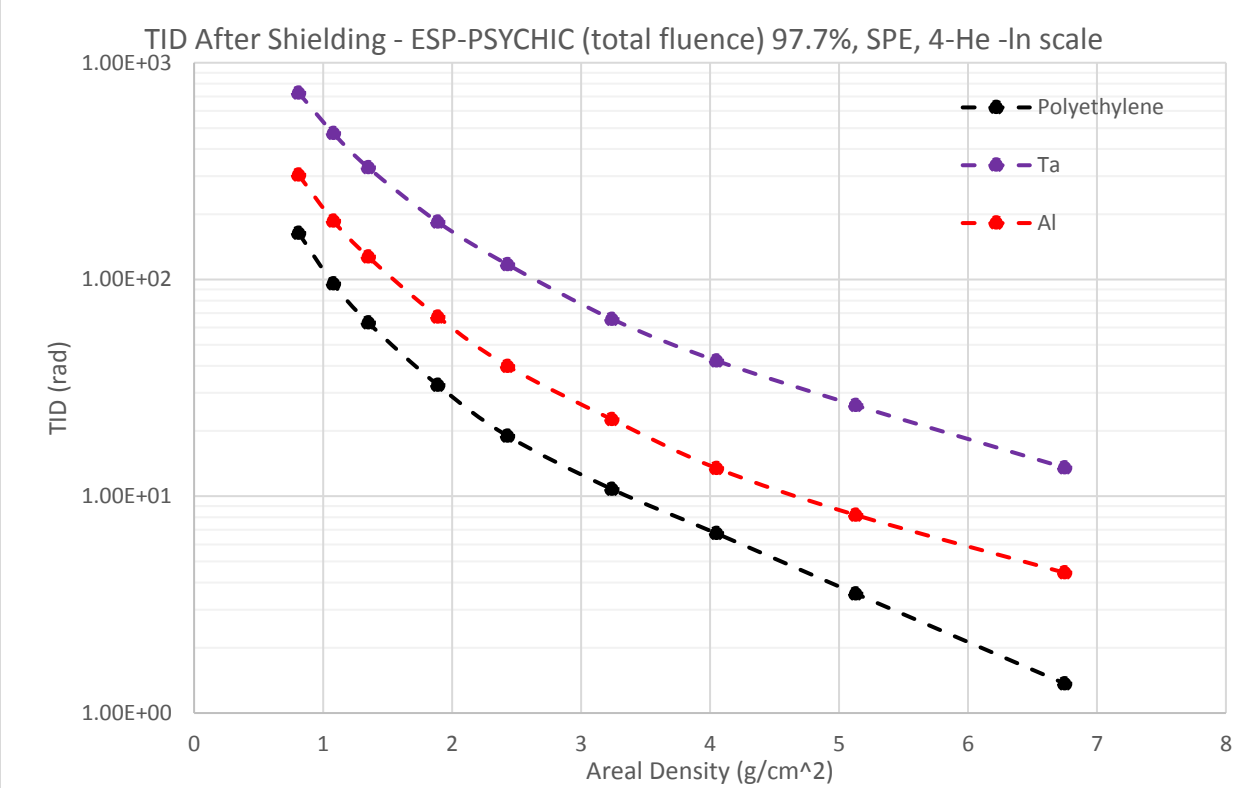

Aluminum, tantalum, and polyethylene are used as the comparative baseline for all other radiation shielding materials in a particular environment. Because solar protons are not the only charged particles ejected in solar particle events, the next most common Helium-4 particles should be considered. Here, the general trend of polyethylene having the lowest dose after shielding is observed, followed by aluminum and tantalum respectively. The spectrum of SPE Helium neutrons presents a greater risk than that of GCR for this particular mission, as shown in the radiation spectrum plot of Figure 3.2.

7.7.2. **TID, Individual Materials at 1AU Interplanetary, SPE, 4-He (Trials 111-119)**

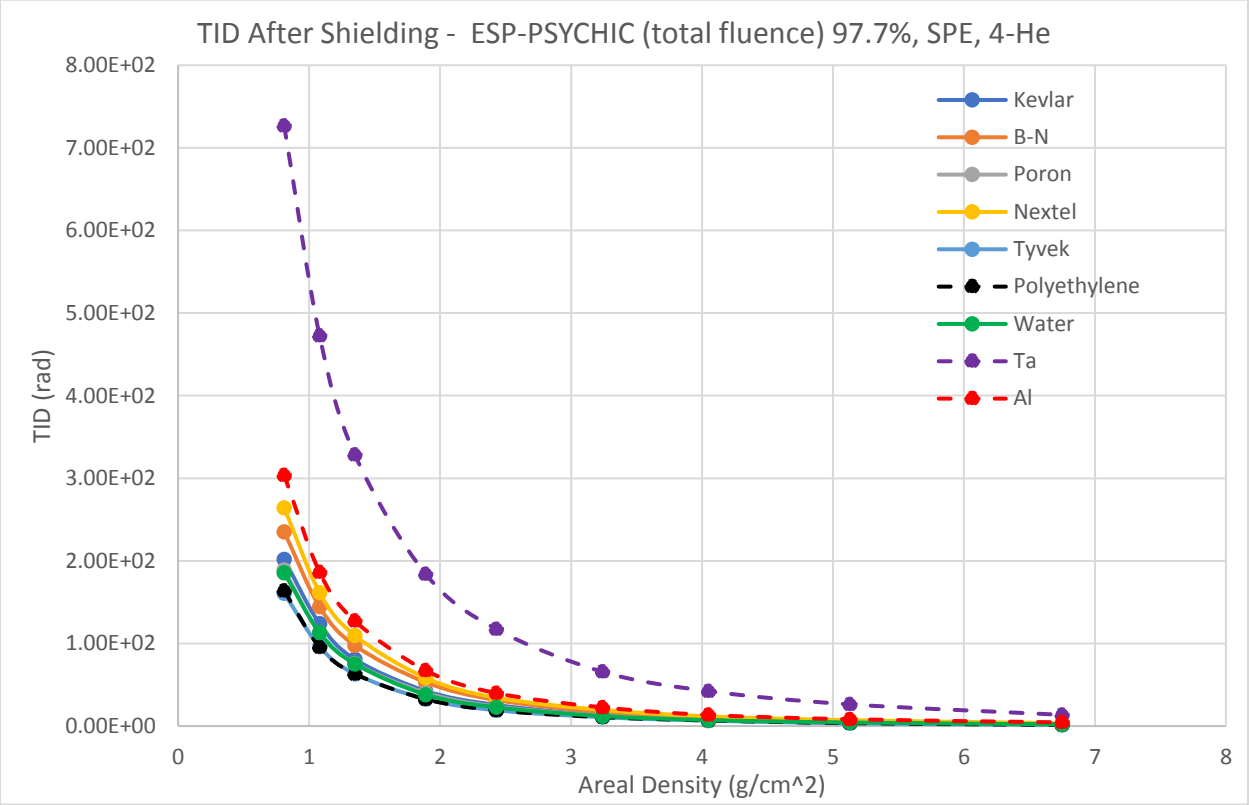

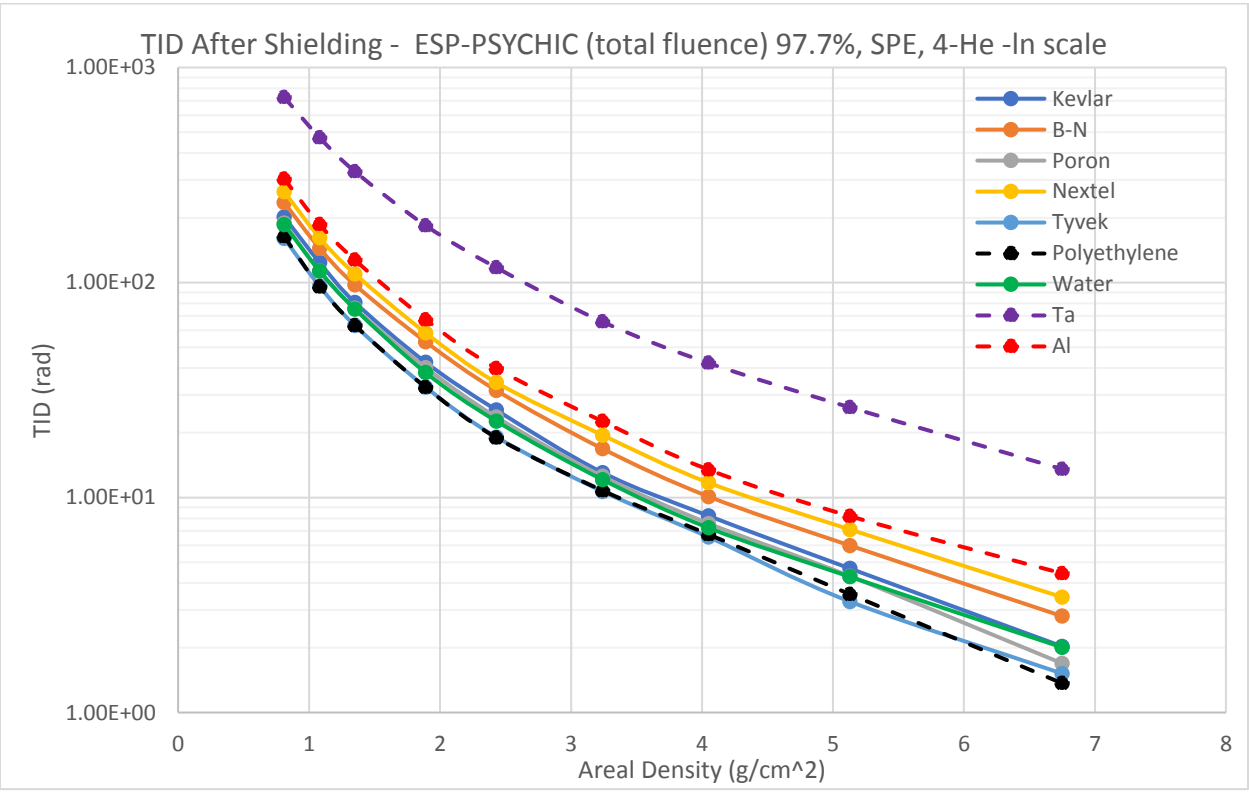

Similar to solar protons, the trend for component materials' shielding response to solar 4-He is between that of polyethylene and aluminum. The discussion for solar protons is mirrored here as well. For an additional note, the shielding response of tantalum is very far off from that of the other materials. This shows the necessity for low Z shielding materials for interplanetary environments.

7.7.3. **TID, Custom Materials at 1AU Interplanetary, SPE, 4-He (Trials 120-125)**

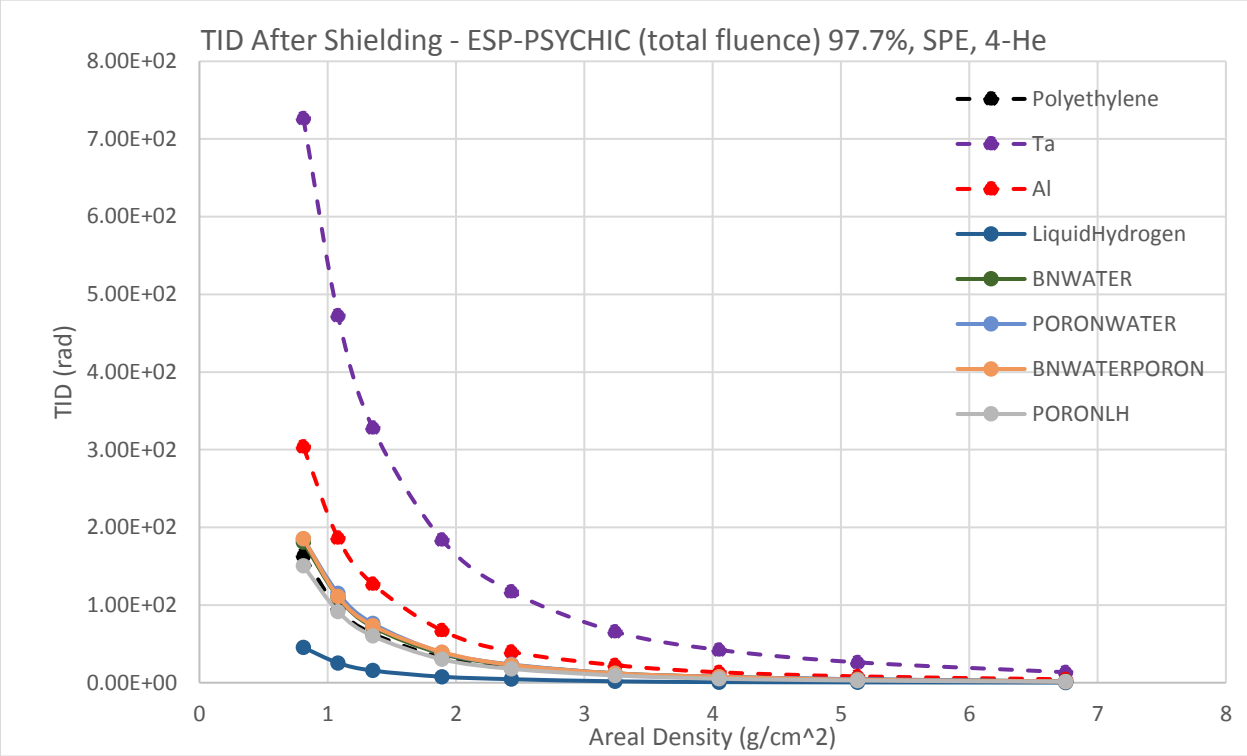

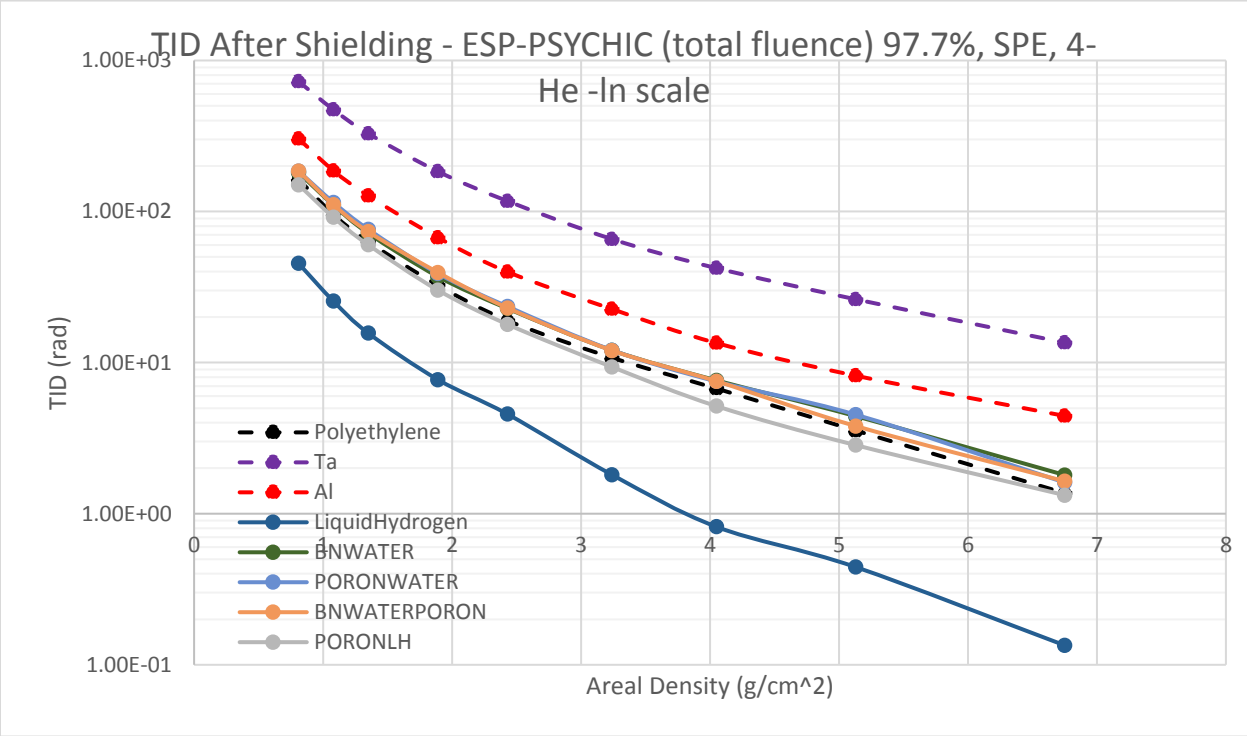

This set of trials shows the shielding response of the custom materials defined in MULASSIS, including the homogenized core layers. All the homogenized core layers perform as expected from the trends seen in both MEO for trapped electrons and SPE for solar protons.

7.7.4. **TID, FFCC w/ Homogenized Poron and Water (3 Layers) in 1AU Interplanetary, SPE, 4-He (Trials 126-129, 134)**

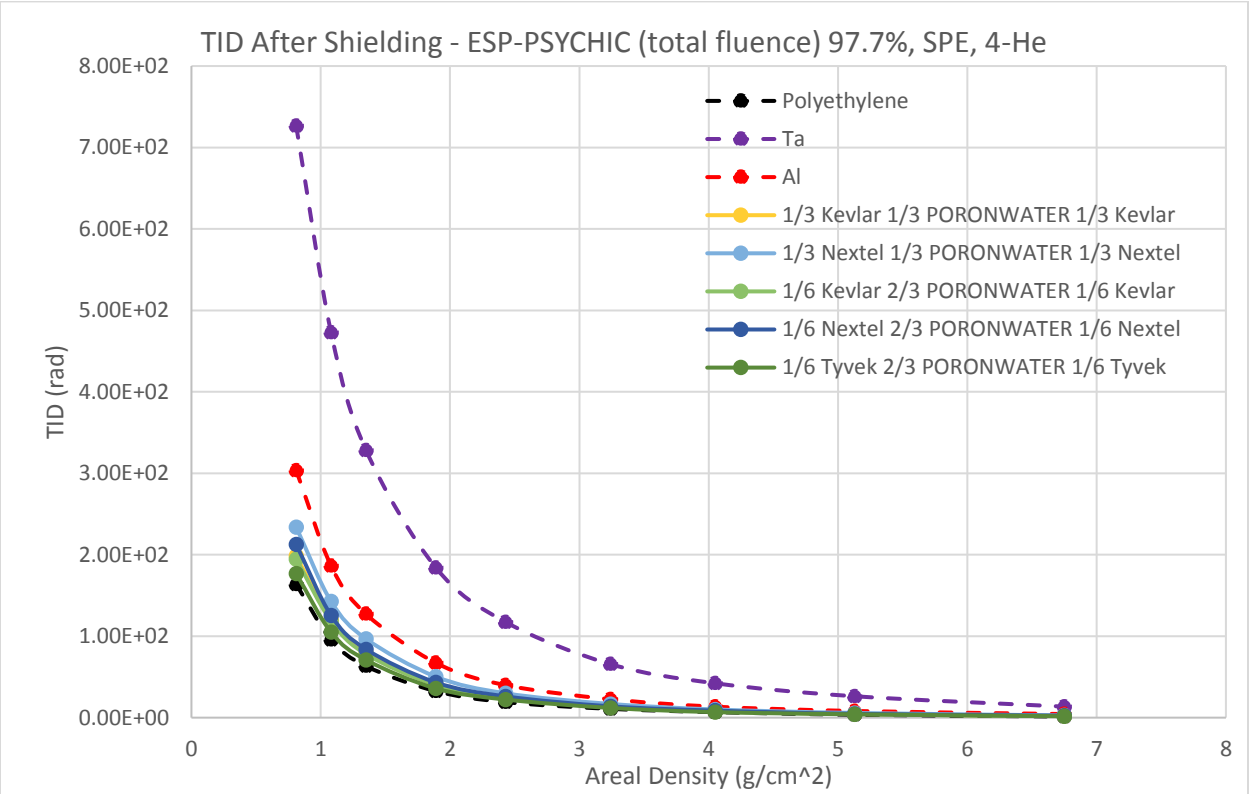

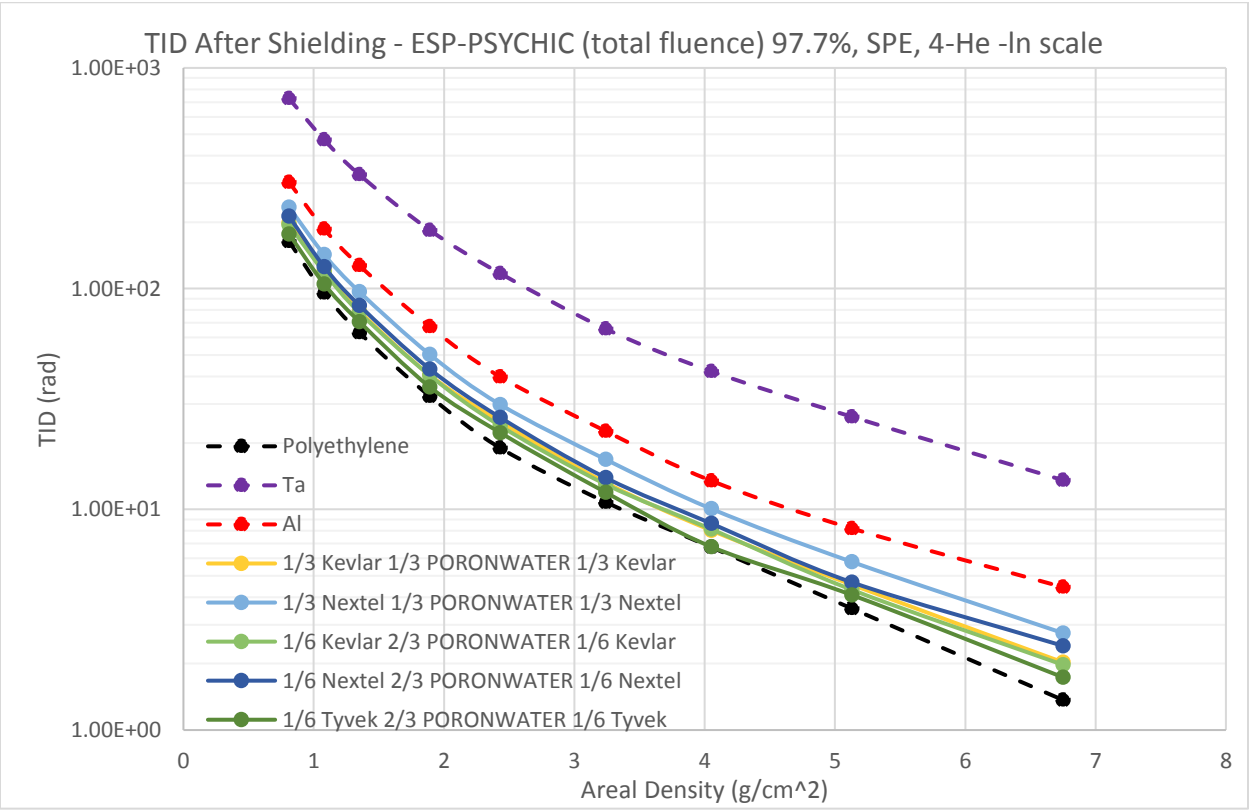

This set of trials predicts the shielding response of a simplified, three-layer FFCC to incident helium nuclei from SPE. The comparative trends seen in both MEO and SPE with solar protons is seen here as well. That is, the FFCC composition with the greatest density of hydrogen performs nearly as well as pure polyethylene (within 10% on average). From these trials, it can be observed that the Nextel face layer (trial 127) offers the least radiation shielding out of each of the three available, due to the poor shielding capability of Nextel. Nextel may still be considered as a skin layer for benefits outside of radiation shielding purposes, especially as it pertains to thermal resistance of the exterior most layer.

7.7.5. **TID, FFCC w/ Homogenized BN, Poron, and Water (3 Layers) in 1AU Interplanetary, SPE, 4-He (Trials 130-133, 135)**

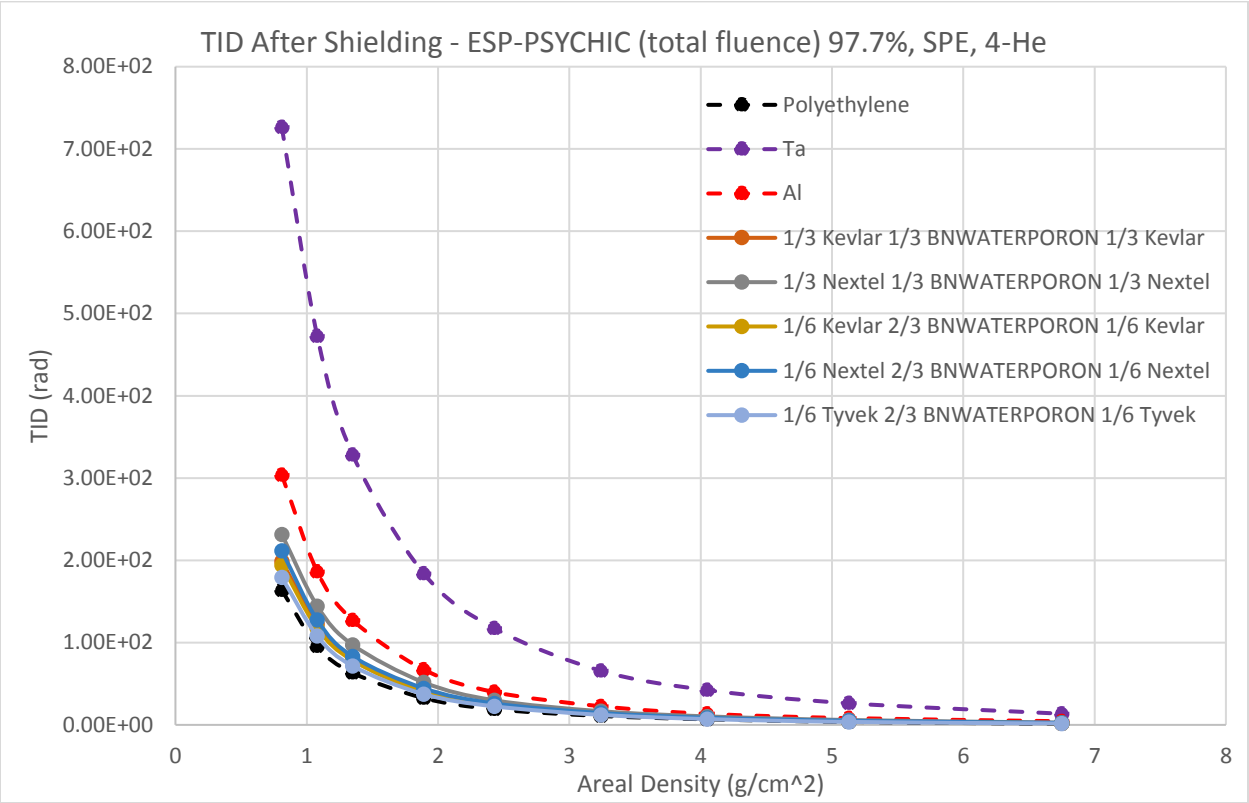

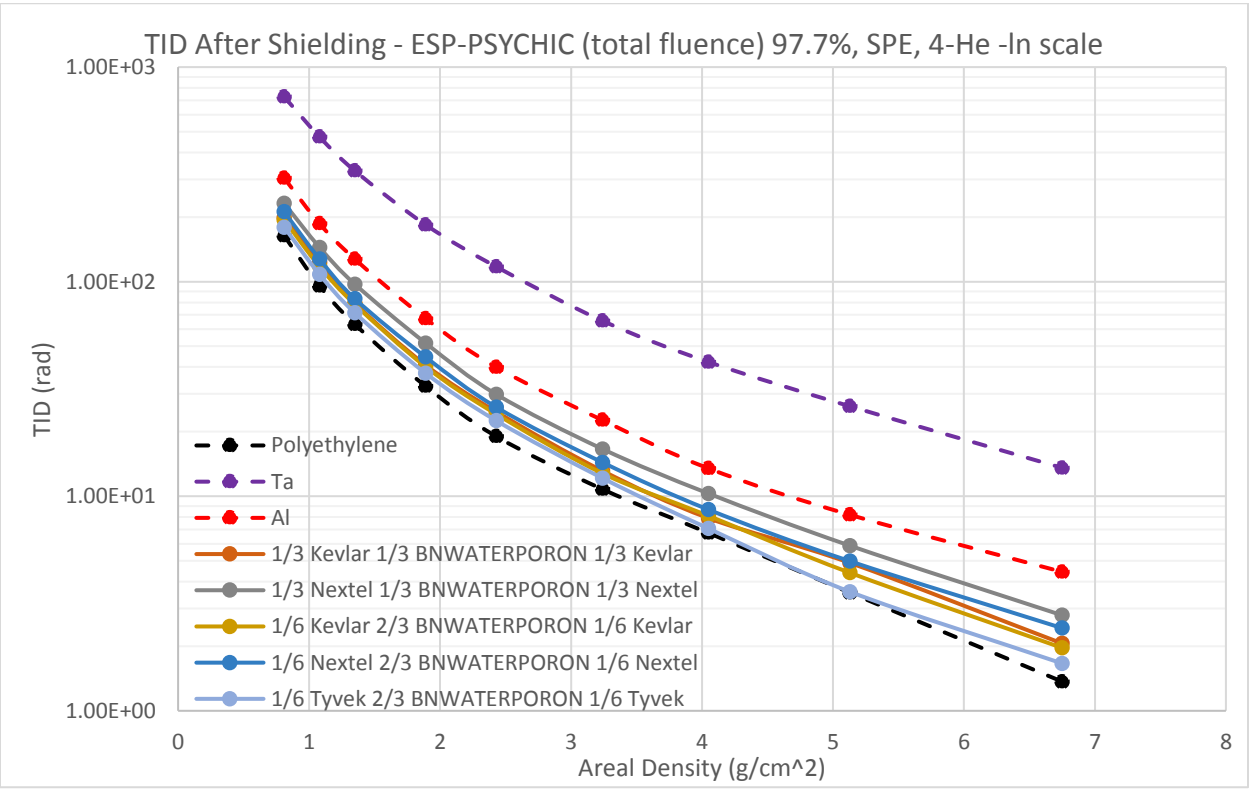

This set of trials is the same as the last, though with the addition of BN as a solute in the liquid core layer. Overall, the comparative trend is similar to that of the solar proton simulations of the same FFCC compositions, though a very slight improvement is seen in shielding of 4-He than that seen for solar protons. It appears that the inclusion of cubic BN only improves the shielding of the FFCC by about 2% in comparison to the set of trials without the BN included in the core liquid (Trials 126-129). This 2% improvement falls within the extent of the relative error and should be considered a negligible difference. Further investigation of high Z incident particles will be needed to determine the value associated with inclusion of BN for radiation shielding.

7.7.6. **TID, FFCC w/ Homogenized Poron and Liquid Hydrogen Core (3 Layers) in 1AU Interplanetary, SPE, 4-He (Trials 136-138)**

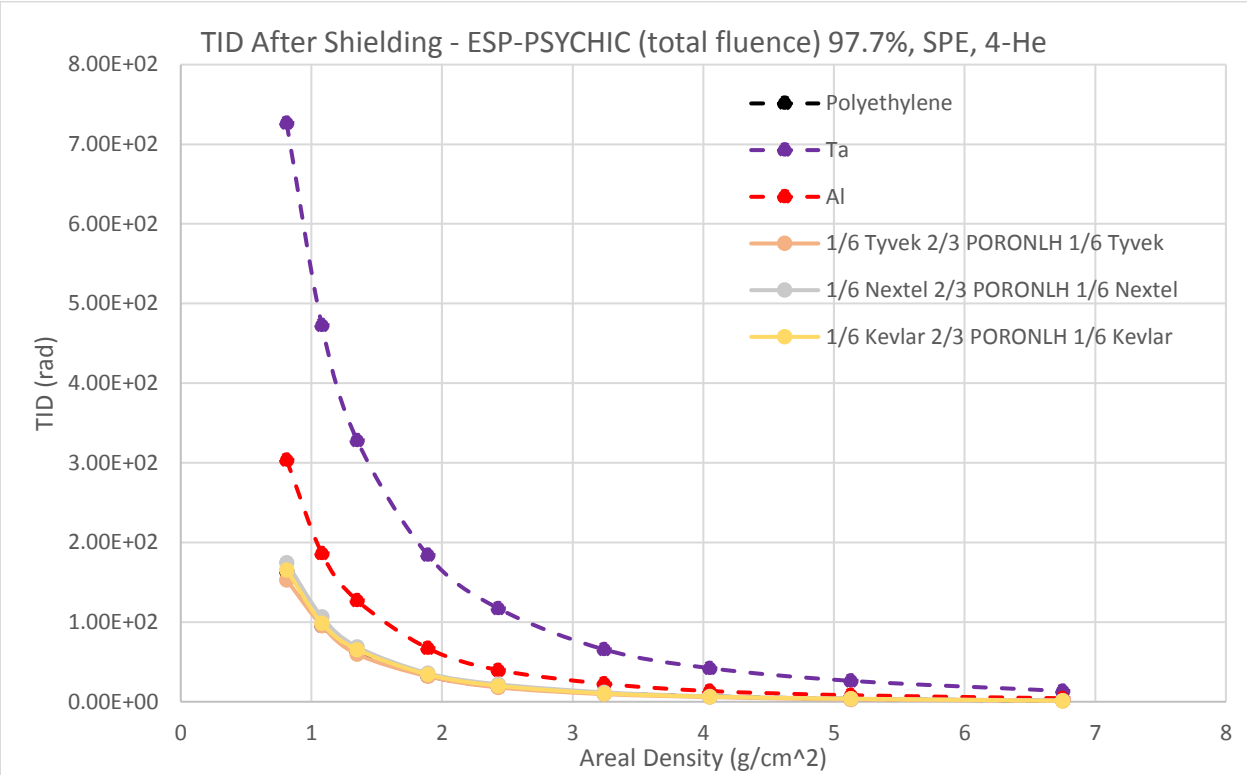

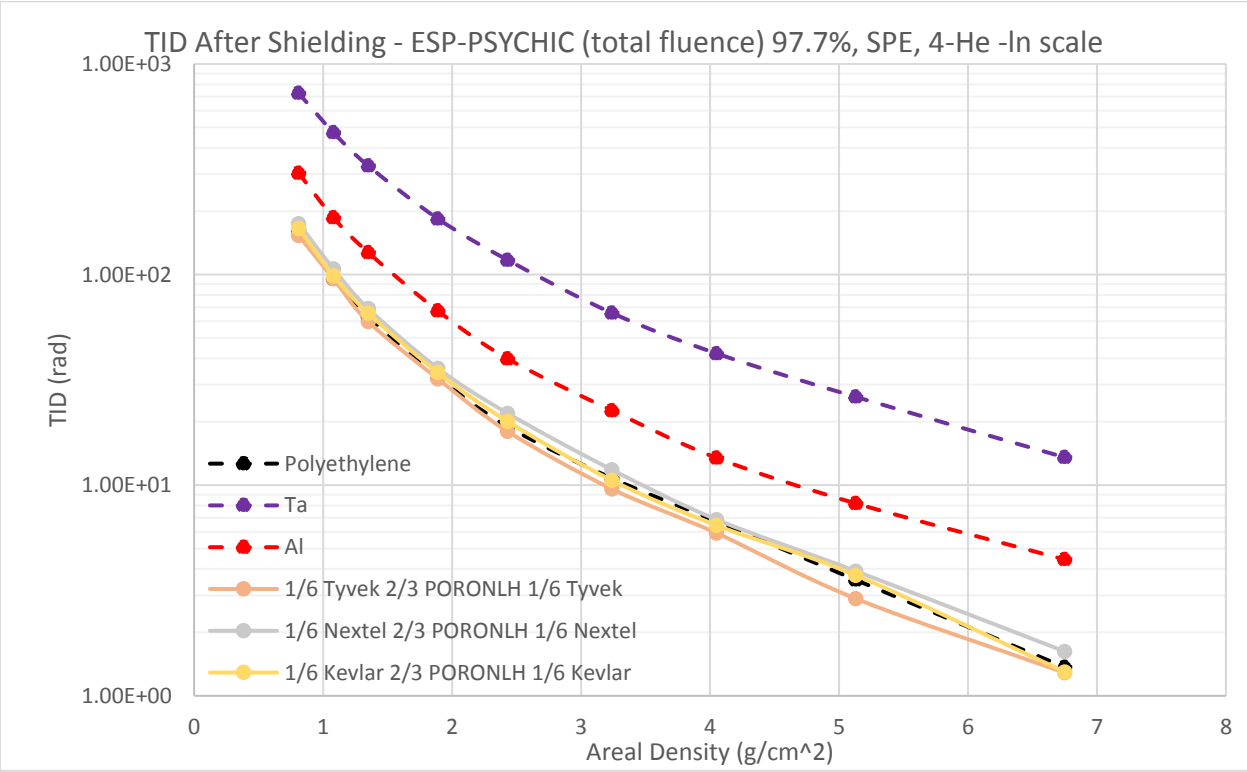

This set of trials looks at the influence of liquid hydrogen in the foam core of the three-layer FFCC. The comparative trend for these trials in SPE due to 4-He mirrors that of the same FFCC compositions in SPE due to solar protons (trials 104-106). All trials predict shielding of Helium neutrons meeting or exceeding the capability of polyethylene with a maximum improvement of 7% on average for trial 136. Once again, this 7% improvement is borderline with the relative error, so a conservative estimate would be to consider the shielding capability as equivalent.

7.7.7. **TID, FFCC w/ Dual Skin Layers and Homogenized Poron and Liquid Hydrogen Core (5 Layers) in 1AU Interplanetary, SPE, 4-He (Trials 139-142)**

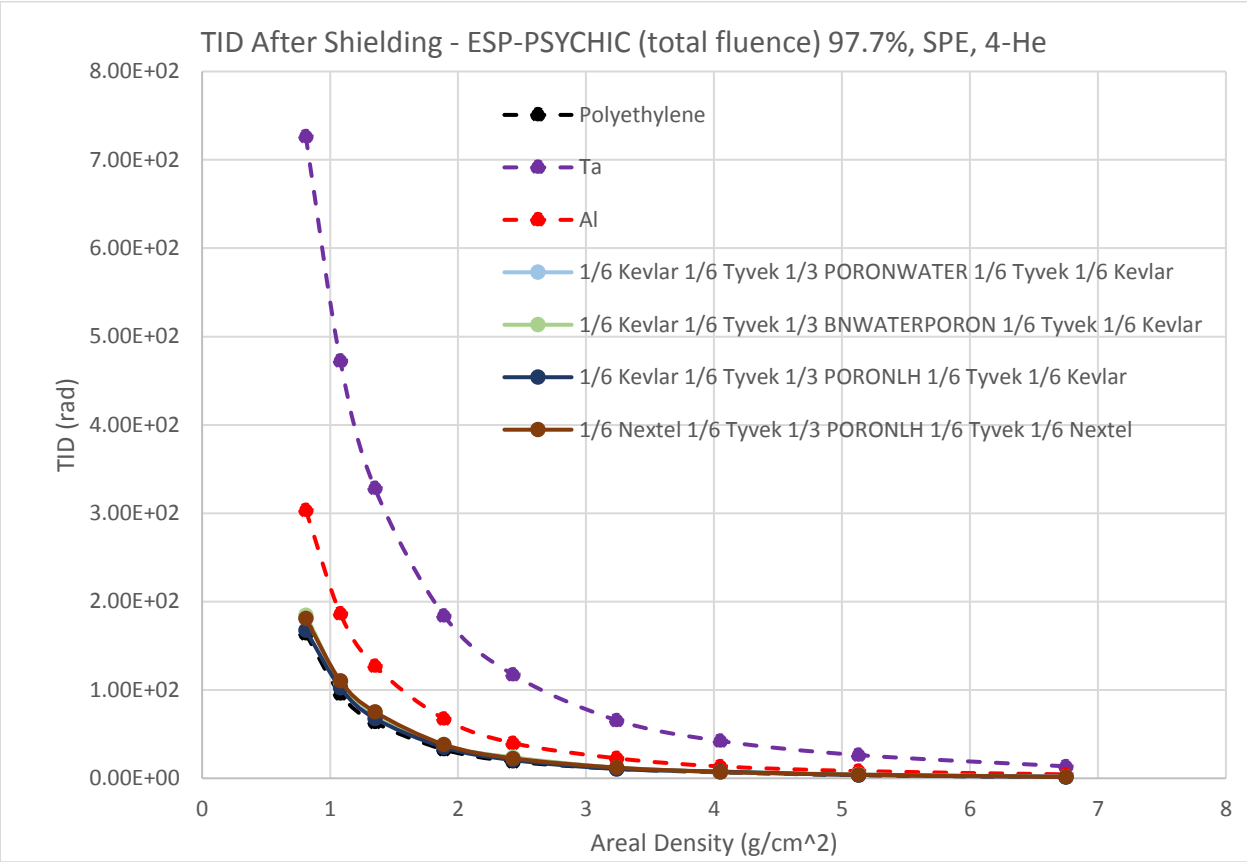

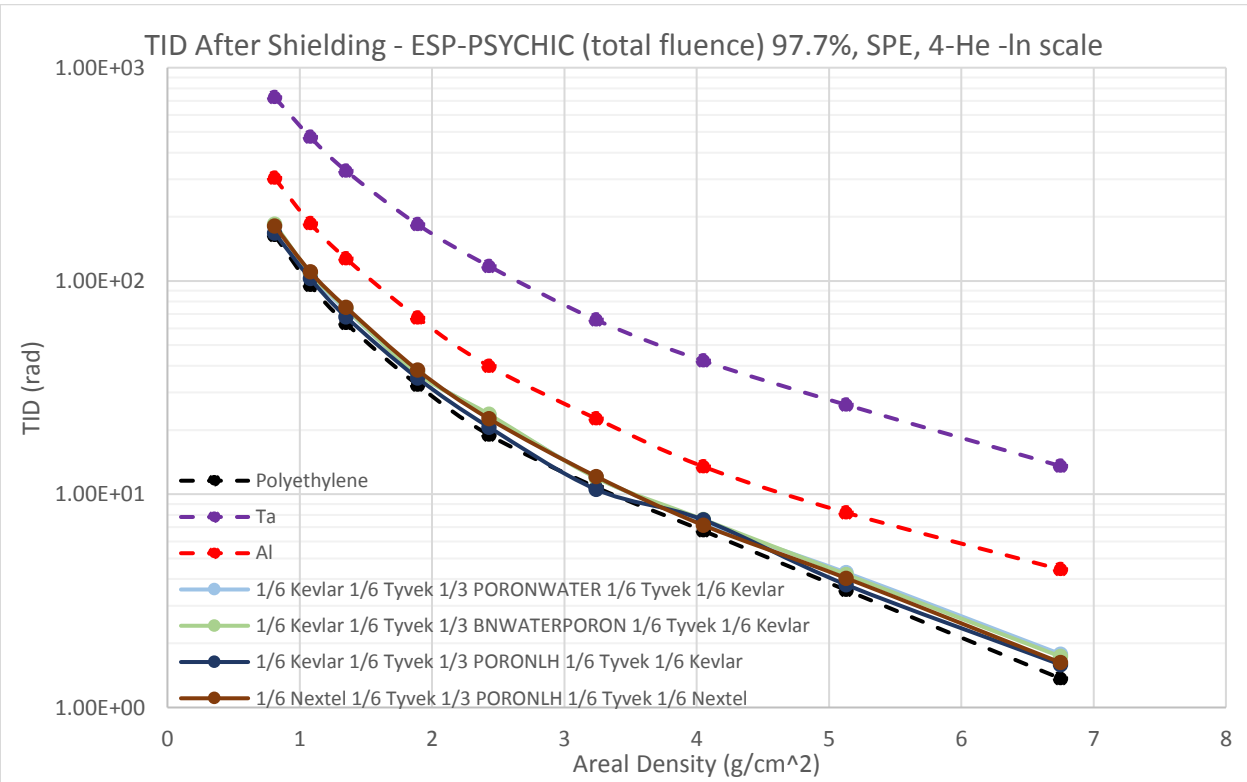

This set of trials is the last analysis of the most hydrogen dense, full (five-layer) FFCC compositions as seen in the MEO environment. The attenuation of incident helium nuclei mirrors that of incident solar protons, where all FFCC trials predict a shielding capability that is at minimum 6% below (trial 141) that of polyethylene and at maximum 10% below (trial 142).

CHAPTER 8: LUNAR REGOLITH FOR RADIATION SHIELDING

8. Lunar Regolith for Radiation Shielding

NASA Kennedy Space Center has expressed goals to develop habitat structures on and off earth from in-situ resources, mined on the moon, mars, or at any space destination. The ability to mine the lunar or Martian regions offers the option to create structural materials from in-situ resources, reducing the need to carry materials from Earth to other terrestrial bodies. One of the primary goals associated with an off-world habitat will be in shielding astronauts from energetic particles, necessitating an understanding of the radiation shielding properties of the proposed geopolymer.

8.1. Lunamer – this is the custom defined material for a geopolymer made from lunar regolith as investigated by Montes et al. [25]. The Lunamer material is made from JSC-1A regolith simulant and offers an in-situ resource for a structural, lunar radiation shielding material.

8.1.1. Chemical Formula input in SPENVIS: Al1800-Ca1026-Fe1571-Mg1354-Na530-O16651-Si5416-Ti124

8.1.2. Density: 1.98 g/cm^3

8.2. Lunamer Shielding Results at 1AU Interplanetary

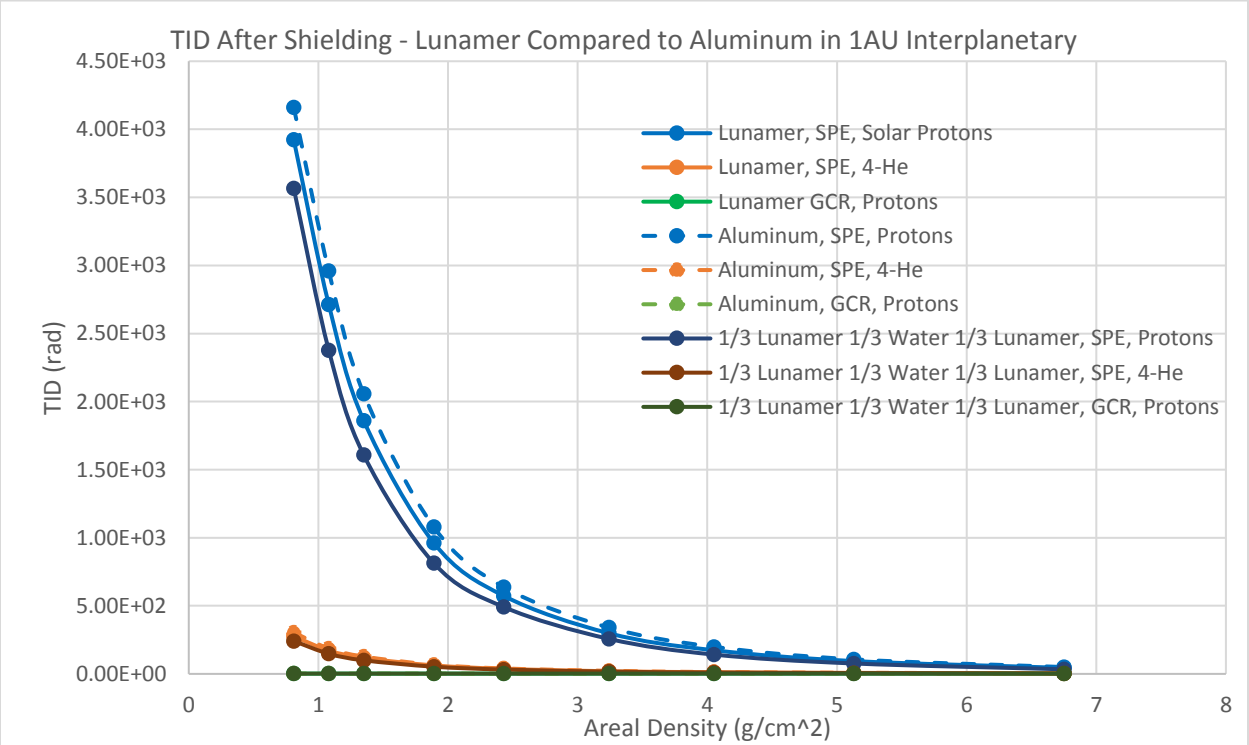

Figure 8.1. Lunamer Compared to Aluminum, TID v. Areal Density

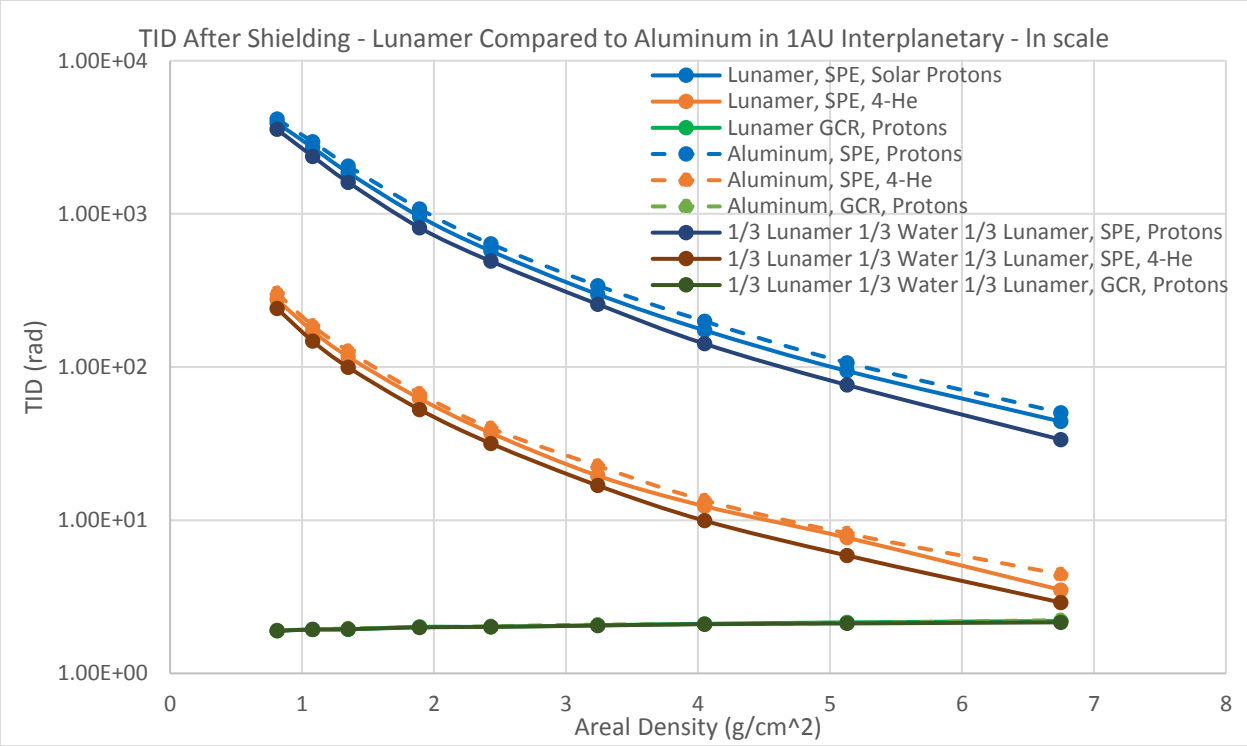

Figure 8.2. Lunamer Compared to Aluminum, TID v. Areal Density -ln Scale

8.3. Discussion: Lunamer Radiation Shielding

The Lunamer geopolymer has a radiation shielding response that is slightly better than that of aluminum. The geopolymer is made from the JSC-1A lunar regolith simulant, which is composed of primarily oxides, including silicon dioxide (43% by weight), aluminum oxide (14.5%), iron oxide (11.5%), calcium oxide (9.1%), and magnesium oxide (8.7%) as the primary contributors by percent weight [30]. This high density of oxygen in addition to the variety of low Z elements results in a TID that is up to 12% lower than Aluminum in the same environment. The 1AU SPE environment represents a conservative estimate of the worst case SPE for the lunar surface, as discussed by De Angelis et al. [26].

For the purposes of off-world habitats, the Lunamer appears to offer a viable material for construction, with an overall wall thickness prediction of 13.4 cm necessary to reduce SPE protons to 100 rad after shielding as seen in Figures 8.1 and 8.2. Addition of a “water wall” will likely benefit habitat construction with Lunamers, as the hydrogen content of water will help increase the shielding capability of such a system. This also permits the storage of liquids within the walls, with the culmination of this being the “Water walls” concept of Flynn et al., where gray and black water processing can be done within wall space to address both life support and radiation concerns [27]. For an initial analysis of a geopolymer wall with a water wall section, an additional set of trials were conducted, as seen in Figures 8.1 and 8.2. These materials are composed of 2/3 Lunamer, and 1/3 Water by areal density. It can be seen that the addition of the middle water layer decreases the TID after shielding by up to 23% from that of a solid Lunamer wall.

CHAPTER 9: CONCLUSION

It can be seen that no FFCC composition shows vastly improved radiation shielding capabilities over traditional materials. This is expected and would not merit the use of most composite materials for shielding alone. It is the combination of somewhat improved radiation shielding with the multifunctionality of structure, high strain rate impact resistance, acoustic dampening, and thermal management that makes the Fluid-Filled Cellular Composite a particularly useful material for deep space structures.

Use of the maximum number of particles for the Monte Carlo Simulation of the FFCC suggests a minimized relative error for TID values calculated in this investigation. Consistent use of 10 million particles in MULASSIS/GEANT4 appears to be limited in other investigations due to the high time cost associated with increasing the number of particles. Other investigations have addressed this difficulty by multithreading through a local version of GEANT4, thus decreasing computation time. This investigation has addressed the issue by creation of a batch run capability through a python code that interfaces with the online version of SPENVIS. Although both methods have their advantages, use of www.SPENVIS simplifies the application of GEANT4 transport code (which alone has a steep learning curve) through the MULASSIS tool. A suggestion for the optimal combination in ease of simulation set-up and improved calculation speed with GEANT4 would be to compile the MULASSIS code in SPENVIS, which can then be exported to a local version of GEANT4 with multithreading.

The homogenization process outlined by SPENVIS support is shown to have pertinence in analysis of the (heterogenous) fluid filled porous core layer, with a TID response that appears to be more accurate for simulation purposes than the prior method. Heritage trials which modeled the core as a variety of individual material layers showed that layer orientation influences results, since the order of the layers would change the TID value by up to 12 percent (for those core layers tested), while the homogenization method provides a consistent value with a decreased potential for layer order discrepancies, thus removing an unnecessary point for uncertainty or error stacking.

It can be seen that the FFCC composition of trial 58 performed the best of all FFCC composites in MEO with a TID of 7045 rad at an areal density of 0.81 g/cm^2 and a 14-26% lower TID than seen with polyethylene. Of all the trials, this composition had the highest density of hydrogen and performed accordingly. This trend can be seen in all the other hydrogen dense FFCC trials, such as those with the homogenized poron and liquid hydrogen core. The trend is consistent across all radiation environments investigated in this research and speaks to the hypothesis that increasing the hydrogen content of the FFCC will result in an increased radiation shielding potential. A Quality Function Deployment (QFD) of shielding, density, and cost has suggested that the FFCC performs up to 1.7 and 1.2 times better than tantalum and aluminum, respectively, in analysis of shielding, density, and cost in MEO. In comparison to polyethylene, the most successful FFCC trials perform similarly or slightly better in shielding capability (up to 1.1 times better) for trapped electron radiation, though without the single function focus of polyethylene. Although the QFD analysis is an imperfect comparison of capability for space, it shows that the FFCC is of the same order of polyethylene for radiation shielding. This

comparative shielding capability is then seen to increase greatly in interplanetary space, where the traditional shielding metals suffer from secondary radiation issues. Here the composition of trial 58 (trial 104) is seen to provide a TID that is (averaged across areal densities) 9% lower than that of polyethylene, 56% lower than that of aluminum, and 82% lower than tantalum. Meaning, the FFCC compositions with the highest hydrogen content consistently perform as well as polyethylene, regardless of environment, while maintaining perceived multifunctionality. It is precisely this multifunctionality that propels the FFCC forward as a potential Mars-class material.

Current research suggests that a Fluid-Filled Cellular Composite layup with a Kevlar, Tyvek, Poron and Liquid Hydrogen (or BN and Water) symmetric construction offers the greatest applicability to space use in consideration of size and weight constraints associated with extended missions such as those to Mars. Such a composite offers radiation shielding which meets or exceeds that of polyethylene, offers consumables storage, acts as a structural material that dampens impacts and sound, and has desirable thermal capabilities. This novel composite is believed to address NASA needs for multifunctional radiation shielding not seen in current spacecraft, suits, or habitats, representative of those characteristics necessary for manned-interplanetary exploration.

CHAPTER 10: FUTURE INVESTIGATION

There are a variety of investigations that can be conducted from the conclusion of this research, though the most applicable for the continuation of the FFCC project is to reconcile the multifunctional characteristics with the radiation shielding capability of the composite. That is, all the compositions tested in this research are engineered for radiation shielding alone. It is unclear whether the various functions of the FFCC that were found in previous research are still pertinent to the compositions determined for radiation shielding. This reconciliation will need to be completed in multiple steps, where the first will likely be a multivariate optimization of the FFCC's structure for shielding, mechanical strength, impact, and thermal properties. Research has been conducted by Cai et al. in an effort to optimize a composite material for radiation shielding, mass and volume, and mechanical properties [21] by two separate methods. The methodologies outlined may provide a reasonable method to optimize the structure of the FFCC. With the optimization of the FFCC structure for multiple functions, a true engineering material will be made, thus propelling the FFCC out of the novel materials phase.

REFERENCES

[1] A.K.Ghosh, A.D.Williams, J.M.Zucker, J.L.Mathews and N. Spinhirne, "An Experimental Investigation into the Acoustic Characteristics of Fluid-filled Porous Structures – A Simplified Model of the Human Skull Cancellous Structures", J. of Experimental Mechanics, April 2008. https://www.nmt.edu/academics/mecheng/faculty/aghosh/2008_EM_Acoustic_Investigation.pdf

[2] Birbahadur, N., "The High-Strain Rate Response of Polyurethane Foam and Kevlar Composite", MS Thesis, New Mexico Tech, 2011. https://www.nmt.edu/academics/mecheng/faculty/aghosh/2011_Birbahadur_MS_Thesis.pdf

[3] Garley, L., "Characterization of a Fluid Filled Composite for Radiation Protection", MS Independence Study, New Mexico Tech, 2015 , [Ghosh is the supervisor]. https://www.nmt.edu/academics/mecheng/faculty/aghosh/2015_Garley_MS_Thesis.pdf

a. Ghosh, Ashok Kumar, "Sandia Final Report", New Mexico Institute of Mining and Technology, 2016, Internal Document

[4] Dr. Sheila Thibeault, Dr. Catherine Fay, Dr. Sharon Lowther, etc. "Radiation Shielding Materials Containing Hydrogen, Boron, and Nitrogen: Systematic Computational and Experimental Study -Phase I", NIAC FINAL REPORT, 2012

[5] J.H. Adams, Jr., D.H. Hathaway, R.N. Grugel, and J.W. Watts , "Revolutionary Concepts of Radiation Shielding for Human Exploration of Space", Marshall Space Flight Center, NASA, 2005.

[6] "Simulated GCR and SPE Radiation Effects on Inflatable Habitat, Composite Habitat, Space Suit, and Space Hatch Cover Materials", Johnson Space Center, National Aeronautics and Space Administration, 2018.

[7] SPENVIS, spenvis.oma.be

[8] Ashok K Ghosh, "Thermal Management Characteristics of a Fluid Filled Porous Composite – An Experimental Investigation", Proceedings of the 23rd National Heat and Mass Transfer Conf., 1st International ISHMT-ASTFE heat and Mass Transfer Conf., Dec 2015, India.

[9] Lawrence, Matthew Lund, "High-Performing Simulations Of The Space Radiation Environment For The International Space Station And Apollo Missions"

[10] Santin, Giovanni., Ansart, Marie., " Investigation on the effects of combinations of shielding materials on the total ionizing dose for the LAPLACE mission" European Space Agency, 2012

[11] T. Paul O'Brien, Christopher Roth, Lisa Winter, "IRENE: AE9/AP9/SPM Radiation Environment Model", Space Vehicles Directorate, AFRL, 2017.

[12] W. Robert Johnston, T. Paul O'Brien, Stuart L. Huston, "Recent Updates to the AE9/AP9/SPM Radiation Belt and Space Plasma Specification Model", Space Vehicles Directorate, AFRL, 2015.

[13] John P. Grotzinger, Joy Crisp, "Mars Science Laboratory Mission and Science Investigation", Space Sci Rev, 2012.

[14] J. Feynmann, G. Spitale, J. Wang, "Interplanetary Proton Fluence Model: JPL 1991"

[15] S. Yoon, Y Shin, J. Jeon, Y. Seo, J, Jeon, J Woo, J, Seon, "Analysis of the charged particle radiation effect for a CubeSat transiting from Earth to Mars", Current Applied Physics, 14 (2014) 575-581.
[16] "GEANT4 Physics Reference Manual", https://geant4-userdoc.web.cern.ch/UsersGuides/PhysicsReferenceManual/html/index.html, Rev5.0, 2020
[17] Elastomeric Material Solutions, "PORON® 4701-30 Very Soft – Supported – Data Sheet", Rogers Corporation
[18] A. Emmanuel, J. Raghavan, "Influence of structure on radiation shielding effectiveness of graphite fiber reinforced polyethylene composite", Advances in Space Research, 2015.
[19] H. Evans, "Materials Definition - Mixture of Gases", https://www.spenvis.oma.be/forum/viewtopic.php?f=5&t=116.
[20] Hyer, Michael W., "Stress Analysis of Fiber-Reinforced Composite Materials", International Editions, WCB/McGraw-Hill, 1998
[21] Yao Cai, Rui Hao, Shaojie Yu, Chang Wang, Guang Hu, "Comparison of two multi-objective optimization methods for composite radiation shielding materials", Applied Radiation and Isotopes, 2020.
[22] A. Borggrafe, M Quatmann, D. Nolke, "Radiation protective structures on the base of a case study for a manned Mars mission", Acta Astronautica, 2009.
[23] A. Emmanuel, J. Raghavan, R. Harris, P. Ferguson, "A comparison of radiation shielding effectiveness of materials for highly elliptical orbits", Advances in Space Research, 2014.
[24] Mamta Saiyad, N.M. Devashrayee, "Lifetime estimation of epoxy based composite materials on irradiating with gamma radiation for shielding applications", Polymer Testing, 2020.
[25] C. Montes, K. Broussard, M. Gongre, "Evaluation of lunar regolith geopolymer binder as a radioactive shielding material for space exploration applications", Advances in Space Research, 2015.
[26] NF-2008-10-464-HQ, "Small Pressurized Rover Concept", National Aeronautics and Space Administration, 2008.
[27] Michael T. Flynn, Marc M. Cohen, "Water Walls Architecture: Massively Redundant and Highly Reliable Life Support for Long Duration Exploration Missions", NASA Ames Research Center, 2012.
[28] M. Kruglanski, N. Messios, E. De Donder, E. Gamby, S. Calders, L. Hetey, and H. Evans "Space Environment Information System (SPENVIS)", Geophysical Research Abstracts, Vol. 11,, 2009.
[29] McCoy, John, "Statistical Mechanics of Ideal Gasses and Other Simple Materials", Second Edition, 2015
[30] J.M. DeWitt, E.R. Benton, "Shielding effectiveness: A weighted figure of merit for space radiation shielding", Applied Radiation and Isotopes, 2020
[31] Durante, Marco, "Space radiation protection: Destination Mars", Life Sciences in Space Research, 2014
[32] Cucinotta, Francis A., Kim, Myung-Hee Y., Chappell, Lori J., "Evaluating Shielding Approaches to Reduce Space Radiation Cancer Risks", NASA TM-2012-217361, 2012.

[33] G. De Angelis, F. F. Badavi, J.M. Clem, "Modeling of the Lunar Radiation Environment", Elsevier, 2006.

APPENDIX

A1. SPENVIS Settings (Advanced Users)

Figure A1.1. Mission Generation: Medium Earth Orbit

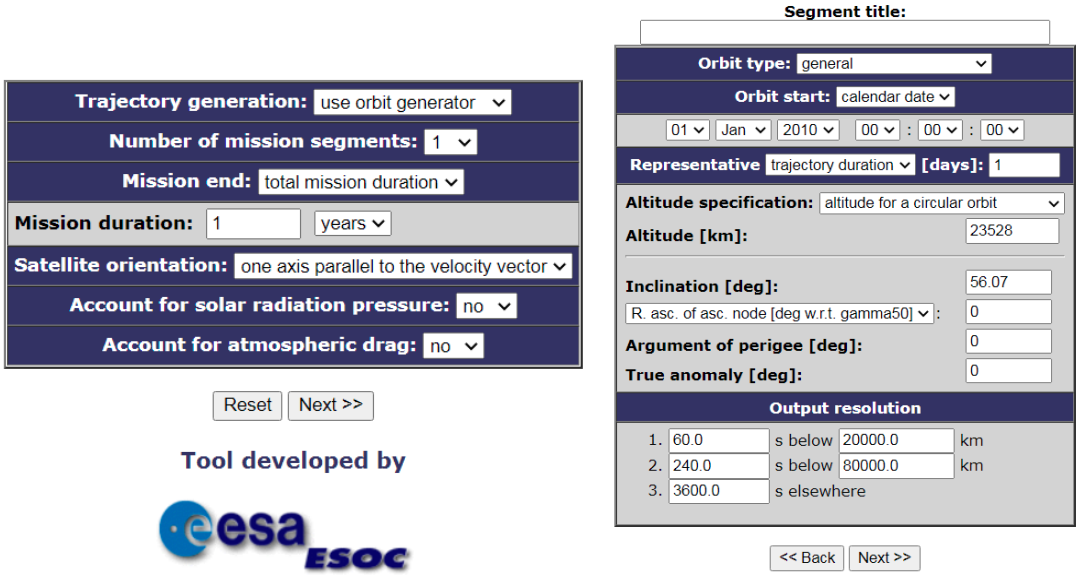

Figures A1.1 and A1.2. Settings for MEO Mission Generation

Figure A1.2. Mission Generation: 1AU Interplanetary Settings

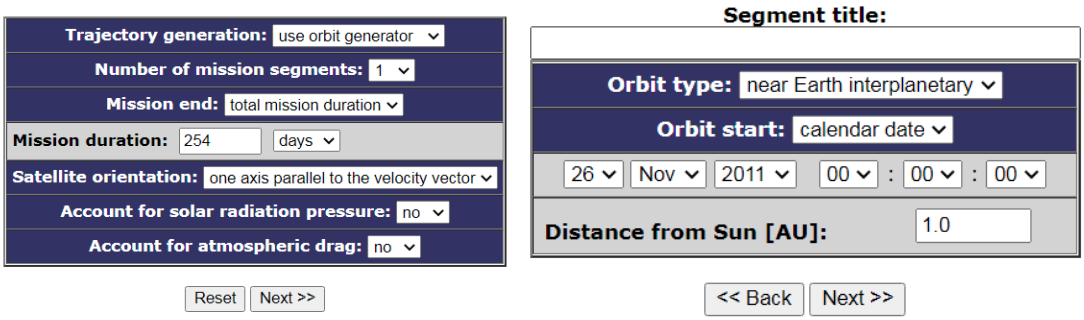

Figures A1.3. and A1.4. Settings for Interplanetary Mission Generation

Figure A1.3. Radiation Models Settings

A1.3.1.Trapped Proton and Electron Fluxes

AE-8 and AE-9 Models, Solar Maximum, 50% Confidence Level.

A1.3.2.Galactic Cosmic Ray Fluxes

CRÈME-96 model.

A1.3.3.Solar Particle Mission Fluences

Rosenquist model, 97.7% Confidence Level.

Sapphire (total fluence) model, 97.7% Confidence Level.

Figure A1.4. MULASSIS Settings

Mission based, x number of particles, don't use energy biasing, linear interpolation.

Planar slab, last two layers are Aluminum (100um) and Silicon (10um) respectively.

Total Ionizing Dose, rad.

No cuts-in-range.

A2. Summary of Verification Process

A2.1.1. Verified SPENVIS settings associated with the User Defined radiation source for known values [5].
A2.1.2. Verified SPENVIS settings associated with orbit generation tool and radiation model application for known values [10].
A2.1.3. Verified Geant4/MULASSIS tool settings for analysis of layered materials [10].
A2.1.4. Verified individual materials of the FFCC behave as expected in comparison to prior research SPENVIS findings.

%error Santin Figure 3- abs value						
Areal Thickness Target:	**Al Fraction = 0**	**Al Fraction = 0.2**	**Al Fraction = 0.4**	**Al Fraction = 0.6**	**Al Fraction = 0.8**	**Al Fraction = 1**
0.81 Al-Ta-Al	8%	14%	18%	20%	19%	10%
2.7 Al-Ta-Al	5%	1%	6%	5%	6%	9%
5.4 Al-Ta-Al	22%	18%	34%	27%	25%	9%

Figure A2. Percent Error Comparison with Figure 3 in *Santin Report [5]*

As expected from the prior research, areal densities above 2.70 g/cm^2 have a greater error associated with the Total Ionizing Dose (TID) output. More on this in Calculation Error section.

A3. Homogenization Method

A method for homogenizing materials for use in SPENVIS/GEANT4/MULASSIS is known via a process outlined by Hugh Evans of ESA with SPENVIS support in their forums. A screenshot is shown below:

First of all you need to define whether it's fraction by mass/weight or volume and then calculate the relative number of individual atoms of each element in the material. If it's volume then you'll have to convert to mass fractions.

For something that's 40% (by mass) propane (C3-H8), and 60% C-O2, then it'd be

- (3×12 + 8×1) = 44 nucleons for propane
  (12 + 2×16) = 44 nucleons for C-O2

So the total material has 88 nucleons. The question then becomes, how many molecule of propane are there to molecules of C-O2 to get a 40:60 ratio by weight.

- 0.4 = X × 44/88 --> X = 0.8
  0.6 = Y × 44/88 --> Y = 1.2

So, the combined chemical formula is:

- 1.2(C-O2)-0.8×(C3-H8)
  (C1.2-O2.4)-(C2.4-H6.4)
  (C12-O24)-(C24-H64)
  (C3-O6)-(C6-H16)

; removing the lowest common factor of 4

regroup and rearrange to get:
C9-O6-H16

Regards,
Hugh

Figure A3. Homogenization Method via SPENVIS Forum Support, via Hugh Evans (ESA) [28]

This process was used to stoichiometrically homogenize materials of multiple compounds or multiple materials (eg. Poron and Water) by percent mass. A resultant density was also calculated by percent mass for each custom material modeled.

It is important to note that SPENVIS considers materials by elemental composition and density for particle interactions. This means that there is no difference to SPENVIS in how a compound is structured, only in the elemental composition and the distance between atoms. For example, H2O has the same TID response as H16O8 (assuming constant density), as the ratio of hydrogen to oxygen is equal for both.

Figure A3.1. Example Homogenization for Poron and Water Core:
Poron: $C_3H_7NO_2$
Number of nucleons: 89
Water: H_2O
Number of nucleons: 18
Total number of nucleons: 107
Submerged water absorption of poron 4701-30 is 14% by weight. This equates to a final proportion by weight that is 87.72% poron and 12.28% water by: Initial amount by weight of poron is 100% plus 14% weight gain from water makes a new 114% total. So the poron portion is 100/114 = 87.71% and the water portion is 14/100 = 12.28%.
The ratio of nucleons of poron by weight percent is then: (% Poron)*(Number of nucleons for Poron)/(Total Number of Nucleons) = 1.055
The ratio of nucleons of water by weight percent is then: (% Water)*(Number of nucleons for Water)/(Total Number of Nucleons) = 0.730

Then, multiplying:

$$(C3\ H7\ N\ O2) * 1.055 = C3.165\ H7.385\ N1.055\ O2.11$$

$$(H2\ O) * 0.730 = H1.46\ O0.730$$

And adding elemental components results in:

$$C317 - H885 - N106 - O284$$

A4. MEO: "Blip" in TID response at 1.22g/cm^2

A noticeable "blip" can be seen in some of the material's TID responses at various areal densities, though most notably for tantalum at 1.22 g/cm^2. Further investigation of this "blip" reveals it is likely a fluctuation associated with Monte Carlo methodology. This was done by increasing the number of points around the desired 1.22 g/cm^2 location through a series of tests as seen in figure x.

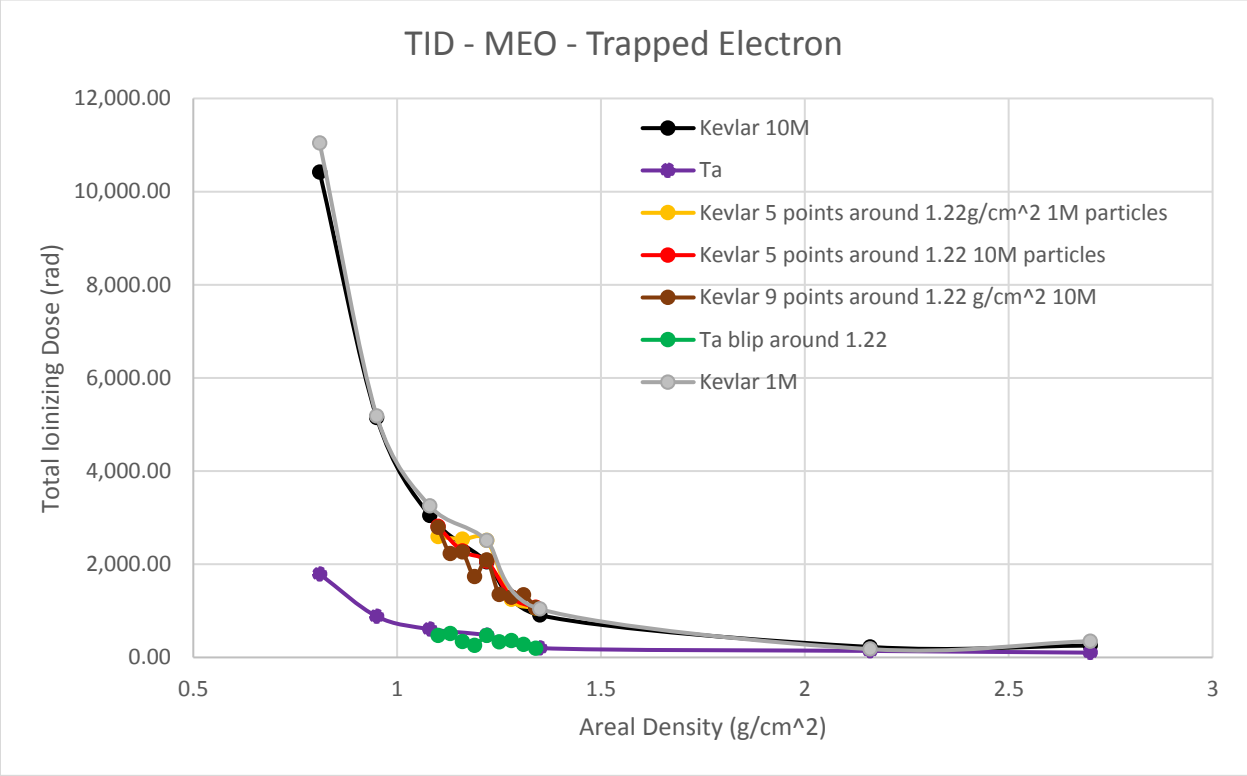

Figure A4.1. Investigation of "Blip" in TID at 1.22g/cm^2

It is understood that the Monte Carle method behind GEANT4 is statistically determined, as opposed to deterministic methods such as those utilized by OLTARIS and HZETRN. This can be seen by varying the number of points around 1.22 g/cm^2 from 1 to 5 to 9, revealing a clear fluctuation in TID values. As expected, more particles used in the calculation results in a decreased magnitude of fluctuation, though the fluctuation remains.

An example of this trend can be seen in Figure A.4.2 from *Statistical Mechanics of Ideal Gasses and Other Simple Materials* [29], where the number Pi is statistically determined by the number of throws of a dart falling in a circle.

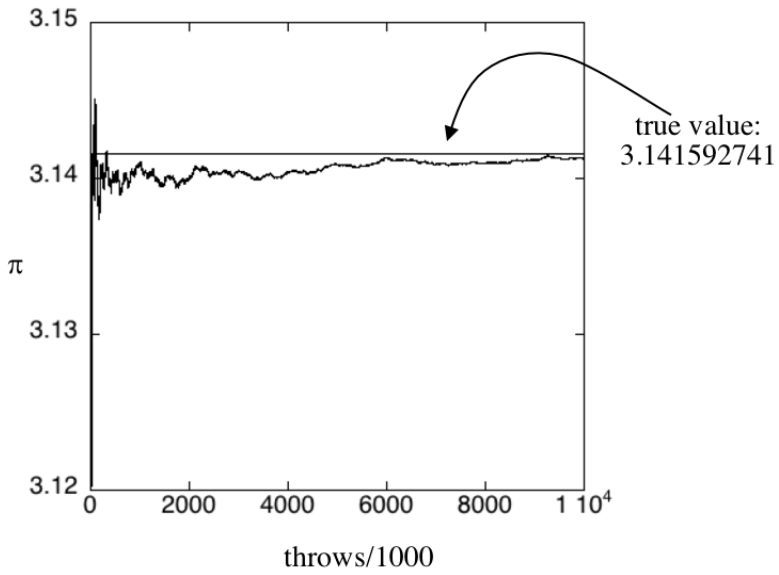

Figure A4.2. Monte Carlo Example [Figure 18.2 in text][29], Convergence of Values Towards Pi vs. Number of Throws of a Dart Landing in a Circle Inscribed in a Square

It is noticed that as the number of throws increases, the accuracy of the output value increases, and fluctuation decreases. This is comparable to number of particles used in GEANT4 calculations, and explains why more particles used in the calculation decreases the magnitude of fluctuation about the true value seen in above Figure A4.2.

A5. Python Code Implementation with SPENVIS:

Figure A5.1. Batchrun Code (where simulation parameters are defined):

```
# Note that if this code fails to get values with SPENVIS, but all settings appear accurate, increase the number of
# particles so that calculation time for SPENVIS increases. This should make the code work.
import time

from helpers_fixed import *


def batchrun(har_file, report_url):
    """Batch run capability for thickness:"""

    # Declare the overrides dict
    overrides = {}
```

```
   # Available materials: NEXTELB, KEVLAR, PORON, G4_WATER, G4_Al,
TYVEK, BN, Lunamer, G4_POLYETHYLENE, G4_Ta, G4_Pb, G4_Si,
PORONWATER, BNWATER, BNWATERPORON, PORONLH, LiquidHydrogen

   materialname = ['Lunamer', 'Lunamer', 'Lunamer', 'Lunamer', 'Lunamer', 'Lunamer',
'Lunamer', 'Lunamer', 'Lunamer']
   thiqness = ['0.81', '1.08', '1.35', '1.89', '2.43', '3.24', '4.05', '5.13', '6.75']
   """
   materialname2 = ['TYVEK', 'TYVEK', 'TYVEK', 'TYVEK', 'TYVEK', 'TYVEK',
'TYVEK', 'TYVEK', 'TYVEK',
                    'TYVEK', 'TYVEK', 'TYVEK', 'TYVEK', 'TYVEK', 'TYVEK', 'TYVEK',
'TYVEK', 'TYVEK',
                    'TYVEK', 'TYVEK', 'TYVEK', 'TYVEK', 'TYVEK', 'TYVEK', 'TYVEK',
'TYVEK', 'TYVEK',
                    'TYVEK', 'TYVEK', 'TYVEK', 'TYVEK', 'TYVEK', 'TYVEK', 'TYVEK',
'TYVEK', 'TYVEK']
   thiqness2 = ['0.135', '0.18', '0.225', '0.315', '0.405', '0.54', '0.675', '0.855', '1.125',
            '0.135', '0.18', '0.225', '0.315', '0.405', '0.54', '0.675', '0.855', '1.125',
            '0.135', '0.18', '0.225', '0.315', '0.405', '0.54', '0.675', '0.855', '1.125',
            '0.135', '0.18', '0.225', '0.315', '0.405', '0.54', '0.675', '0.855', '1.125']

   materialname3 = ['PORONWATER', 'PORONWATER', 'PORONWATER',
'PORONWATER', 'PORONWATER', 'PORONWATER', 'PORONWATER', 'PORONWATER',
'PORONWATER', 'PORONWATER',
                    'BNWATERPORON', 'BNWATERPORON', 'BNWATERPORON',
'BNWATERPORON', 'BNWATERPORON', 'BNWATERPORON',
'BNWATERPORON', 'BNWATERPORON', 'BNWATERPORON',
                    'PORONLH', 'PORONLH', 'PORONLH', 'PORONLH', 'PORONLH',
'PORONLH', 'PORONLH', 'PORONLH', 'PORONLH',
                    'PORONLH', 'PORONLH', 'PORONLH', 'PORONLH', 'PORONLH',
'PORONLH', 'PORONLH', 'PORONLH', 'PORONLH']
   thiqness3 = ['0.27', '0.36', '0.45', '0.63', '0.81', '1.08', '1.35', '1.71', '2.25',
            '0.27', '0.36', '0.45', '0.63', '0.81', '1.08', '1.35', '1.71', '2.25',
            '0.27', '0.36', '0.45', '0.63', '0.81', '1.08', '1.35', '1.71', '2.25',
            '0.27', '0.36', '0.45', '0.63', '0.81', '1.08', '1.35', '1.71', '2.25']

   materialname4 = ['TYVEK', 'TYVEK', 'TYVEK', 'TYVEK', 'TYVEK', 'TYVEK',
'TYVEK', 'TYVEK', 'TYVEK',
                    'TYVEK', 'TYVEK', 'TYVEK', 'TYVEK', 'TYVEK', 'TYVEK', 'TYVEK',
'TYVEK', 'TYVEK',
                    'TYVEK', 'TYVEK', 'TYVEK', 'TYVEK', 'TYVEK', 'TYVEK', 'TYVEK',
'TYVEK', 'TYVEK',
```

'TYVEK', 'TYVEK', 'TYVEK', 'TYVEK', 'TYVEK', 'TYVEK', 'TYVEK', 'TYVEK', 'TYVEK', 'TYVEK']

thiqness4 = ['0.135', '0.18', '0.225', '0.315', '0.405', '0.54', '0.675', '0.855', '1.125',
'0.135', '0.18', '0.225', '0.315', '0.405', '0.54', '0.675', '0.855', '1.125',
'0.135', '0.18', '0.225', '0.315', '0.405', '0.54', '0.675', '0.855', '1.125',
'0.135', '0.18', '0.225', '0.315', '0.405', '0.54', '0.675', '0.855', '1.125']

materialname5 = ['KEVLAR', 'KEVLAR', 'KEVLAR', 'KEVLAR', 'KEVLAR', 'KEVLAR', 'KEVLAR', 'KEVLAR', 'KEVLAR', 'KEVLAR',
'KEVLAR', 'KEVLAR', 'KEVLAR', 'KEVLAR', 'KEVLAR', 'KEVLAR', 'KEVLAR', 'KEVLAR', 'KEVLAR', 'KEVLAR',
'KEVLAR', 'KEVLAR', 'KEVLAR', 'KEVLAR', 'KEVLAR', 'KEVLAR', 'KEVLAR', 'KEVLAR', 'KEVLAR', 'KEVLAR',
'NEXTELB', 'NEXTELB', 'NEXTELB', 'NEXTELB', 'NEXTELB', 'NEXTELB', 'NEXTELB', 'NEXTELB', 'NEXTELB', 'NEXTELB']

thiqness5 = ['0.135', '0.18', '0.225', '0.315', '0.405', '0.54', '0.675', '0.855', '1.125',
'0.135', '0.18', '0.225', '0.315', '0.405', '0.54', '0.675', '0.855', '1.125',
'0.135', '0.18', '0.225', '0.315', '0.405', '0.54', '0.675', '0.855', '1.125',
'0.135', '0.18', '0.225', '0.315', '0.405', '0.54', '0.675', '0.855', '1.125']

_____HELPFUL STUFF FOR COPY AND PASTE_____

['KEVLAR', 'KEVLAR', 'KEVLAR', 'KEVLAR', 'KEVLAR', 'KEVLAR', 'KEVLAR', 'KEVLAR', 'KEVLAR', 'KEVLAR',
'BN', 'BN', 'BN', 'BN', 'BN', 'BN', 'BN', 'BN', 'BN', 'BN',
'PORON', 'PORON', 'PORON', 'PORON', 'PORON', 'PORON', 'PORON', 'PORON', 'PORON', 'PORON',
'NEXTELB', 'NEXTELB', 'NEXTELB', 'NEXTELB', 'NEXTELB', 'NEXTELB', 'NEXTELB', 'NEXTELB', 'NEXTELB', 'NEXTELB',
'TYVEK', 'TYVEK', 'TYVEK', 'TYVEK', 'TYVEK', 'TYVEK', 'TYVEK', 'TYVEK', 'TYVEK', 'TYVEK',
'G4_POLYETHYLENE', 'G4_POLYETHYLENE', 'G4_POLYETHYLENE', 'G4_POLYETHYLENE', 'G4_POLYETHYLENE', 'G4_POLYETHYLENE', 'G4_POLYETHYLENE', 'G4_POLYETHYLENE', 'G4_POLYETHYLENE', 'G4_POLYETHYLENE',
'G4_WATER', 'G4_WATER', 'G4_WATER', 'G4_WATER', 'G4_WATER', 'G4_WATER', 'G4_WATER', 'G4_WATER', 'G4_WATER', 'G4_WATER',
'G4_Ta', 'G4_Ta', 'G4_Ta', 'G4_Ta', 'G4_Ta', 'G4_Ta', 'G4_Ta', 'G4_Ta', 'G4_Ta', 'G4_Ta',
'G4_Al', 'G4_Al', 'G4_Al', 'G4_Al', 'G4_Al', 'G4_Al', 'G4_Al', 'G4_Al', 'G4_Al', 'G4_Al',
'LiquidHydrogen', 'LiquidHydrogen', 'LiquidHydrogen', 'LiquidHydrogen', 'LiquidHydrogen', 'LiquidHydrogen', 'LiquidHydrogen', 'LiquidHydrogen', 'LiquidHydrogen', 'LiquidHydrogen',

```
            'BNWATER', 'BNWATER', 'BNWATER', 'BNWATER', 'BNWATER',
'BNWATER', 'BNWATER', 'BNWATER', 'BNWATER',
            'PORONWATER', 'PORONWATER', 'PORONWATER', 'PORONWATER',
'PORONWATER', 'PORONWATER', 'PORONWATER', 'PORONWATER',
'PORONWATER',
            'BNWATERPORON', 'BNWATERPORON', 'BNWATERPORON',
'BNWATERPORON', 'BNWATERPORON', 'BNWATERPORON',
'BNWATERPORON', 'BNWATERPORON', 'BNWATERPORON',
            'PORONLH', 'PORONLH', 'PORONLH', 'PORONLH', 'PORONLH',
'PORONLH', 'PORONLH', 'PORONLH', 'PORONLH']

            ['0.81', '1.08', '1.35', '1.89', '2.43', '3.24', '4.05', '5.13', '6.75'] *1
            ['0.27', '0.36', '0.45', '0.63', '0.81', '1.08', '1.35', '1.71', '2.25'] *1/3
            ['0.135', '0.18', '0.225', '0.315', '0.405', '0.54', '0.675', '0.855', '1.125'] *1/6
            ['0.54', '0.72', '0.9', '1.26', '1.62', '2.16', '2.7', '3.42', '4.5'] *2/3

            "MATERIALNAME(2)": materialname2[i], "THICKNESS(2)": thiqness2[i],
            "MATERIALNAME(3)": materialname3[i], "THICKNESS(3)": thiqness3[i],
            "MATERIALNAME(4)": materialname4[i], "THICKNESS(4)": thiqness4[i],
            "MATERIALNAME(5)": materialname5[i], "THICKNESS(5)": thiqness5[i]

_____
_____
   """

   ########
   # DOUBLE CHECK NUMBER OF MATERIALS AND THAT ALL ARE
INCLUDED!!!!!!
   # Check that for loop goes through all materials and thicknesses
   ########
   leng = int(len(thiqness))
   dose_val = []
   err_val = []
   for i in range(len(thiqness)):
      remaining = leng - i
      print('Number of calculations remaining: ', remaining)
      t_left = remaining * 3.5
      print('Estimated calculation time remaining (min): ', t_left)

      overrides[4] = {
         "MATERIALNAME(1)": materialname[i], "THICKNESS(1)": thiqness[i]}
      overrides[5] = {"NEVENTS": '10000000'}
      #overrides = {}
```

```
        execute_har(har_file, modify_parameters=overrides)

        fil = get_vals(report_url)
        fil = fil.split('\n')
        # print('fil: ', fil)
        temp = []
        for i in range(len(fil)):
            temp.append(fil[i].split(','))
        dose_val.append(float(temp[-3][-2]))
        err_val.append(float(temp[-3][-1]))
        print('calc dose: ', dose_val)
        print('calc error: ', err_val)

        # download_link(report_url, file_name='%s.txt' )

    print("Final dose (rad): ", dose_val)
    print('Error in calcs: ', err_val)
    return dose_val


def batchrun_fluence(har_file, report_url, image_url):
    """Try setting up batch run capability for thickness: """

    # Declare the overrides dict
    overrides = {}

    # Available materials: NEXTELB, KEVLAR, PORON, G4_WATER, G4_Al,
TYVEK, BN, LunarRegolith, G4_POLYETHYLENE, G4_Ta, G4_Pb, G4_Si

    materialname = ['KEVLAR', 'BN', 'PORON', 'NEXTELB',
                    'TYVEK', 'G4_POLYETHYLENE', 'G4_WATER', 'G4_Ta', 'G4_Al']

    thiqness = ['0.81', '0.81', '0.81', '0.81',
                '0.81', '0.81', '0.81', '0.81', '0.81']

    ########
    # DOUBLE CHECK NUMBER OF MATERIALS AND THAT ALL ARE
INCLUDED!!!!!!
    # Check that for loop goes through all materials and thicknesses
    ########

    for i in range(len(thiqness)):
        overrides[4] = {
```

```
            "MATERIALNAME(1)": materialname[i], "THICKNESS(1)": thiqness[i]}
        overrides[5] = {"NEVENTS": '10000000'}
        execute_har(har_file, modify_parameters=overrides)

        execute_har('mulassis_fluence_plot.har')
        download_link(image_url, file_name='%s_%s_10M_proton.png' %
                      (materialname[i], thiqness[i]))
        print("Fluence image saved ")


def iteration(har_file, report_url):
    """Try setting up iterating run capability for thickness:"""

    # Declare the overrides dict
    overrides = {}
    materialname1 = ['G4_Ta', 'G4_Al', 'G4_Si']
    thiqness = '0.81'

    overrides[4] = {"MATERIALNAME(1)": "G4_Ta", "THICKNESS(1)": thiqness}
    # overrides[5] = {"NEVENTS": "1000000"}
    # overrides[7] = {"#waitWhileRunning(200)" : "Refresh"}
    execute_har(har_file, modify_parameters=overrides)
    # execute_har(can make a har file of just the refresh button and run it after)

    # increase wait timer for more particle, 100,000: 1, 1,000,000:10, 10,000,000:?
    time.sleep(10)
    execute_har('mulassis_refresh')
    # download_link(report_url, file_name='spenvis_mlot.txt')
    # fil = open('results\spenvis_mlot.txt', 'r').readlines()

    fil = get_vals(report_url)
    print('fil: ', fil, 'type: ', type(fil))

    # print('is this the right line? ', fil[-2])
    temp = fil.split(',')
    print('temp: ', temp)
    dose_val = float(temp[-2])
    print("dose: ", dose_val)

    while dose_val > float(4e2):
        thiqness = str(float(thiqness) + 0.250)
        print('overides: "MATERIALNAME(1)": "G4_Ta", "THICKNESS(1)": ', thiqness)
        overrides[8] = {"MATERIALNAME(1)": "G4_Ta", "THICKNESS(1)": thiqness}
```

```
            # overrides[5] = {"NEVENTS": "1000000"}
            execute_har(har_file, modify_parameters=overrides)
            time.sleep(150)
            fil = get_vals(report_url)
            temp = fil.split(',')
            dose_val = float(temp[-2])
            print("dose: ", dose_val)


        def main():
            # The har file is the file with the network requests we're trying to copy
            har_file = input("input har file to use: ")

            # This is the link we would click to download the file
            report_url =
        'https://www.spenvis.oma.be/htbin/spenvis.exe/TEST1?%23sendResult(spenvis_mlo.txt)'
            # For TEST1:
        'https://www.spenvis.oma.be/htbin/spenvis.exe/TEST1?%23sendResult(spenvis_mlo.txt)'
            # For TEST2:
        'https://www.spenvis.oma.be/htbin/spenvis.exe/TEST2?%23sendResult(spenvis_mlo.txt)'
            image_url =
        'https://www.spenvis.oma.be/htbin/spenvis.exe/TEST1?%23sendResult(mulassis_flu.png
        )'

            batchrun(har_file, report_url)
            # batchrun_fluence(har_file, report_url, image_url)


        if __name__ == '__main__':
    main()
```

Figure A5.2. Helpers Code (for connecting to SPENVIS with .har files) [Paul Reimann]:

```
        import requests
        import json
        from urllib.parse import urlparse, unquote
        import os
        import urllib3
        import time
        import re
        urllib3.disable_warnings(urllib3.exceptions.InsecureRequestWarning)

        # Python SPENVIS helper functions
```

```
# Set global variables
username = REDACTED
password = REDACTED

# Function to parse the HAR file for relevant data


def parse_pages(har_data, remove_quote=True):
    pages = {}
    for entry in har_data['log']['entries']:
        # Make sure we are only looking at documents
        if entry['_resourceType'] == 'document':
            current_page = {}

            # Get the page's ID and URL
            id = entry['pageref']
            current_page['url'] = entry['request']['url']
            current_page['method'] = entry['request']['method']

            # Get the form data
            page_data = {}
            if 'postData' in entry['request']:
                for param in entry['request']['postData']['params']:
                    key = unquote(
                        param['name']) if remove_quote else param['name']
                    value = unquote(
                        param['value']) if remove_quote else param['value']
                    page_data[key] = value

            # Add to the dictionary
            current_page['data'] = page_data
            pages[id] = current_page
    return pages

# Simulate submitting one page


def execute_form(url, data, modify_parameters=None, method='POST'):
    # Modify parameters if necessary
    if modify_parameters:
        for key, value in modify_parameters.items():
            data[key] = value
```

```
    # Make the request and return the result
    try:
        if method.upper() == 'POST':
            response = requests.post(url, auth=(
                username, password), verify=False, data=data)
        else:
            response = requests.get(url, auth=(
                username, password), verify=False)
        respstring = response.text
    except Exception as e:
        print('Error:', e)
        return ''
    return respstring

# Determine the refresh time and URL from the HTTP returned


def parse_refresh_str(refresh_str):
    time = 0
    url = ''
    if refresh_str:
        parts = refresh_str.split(';')
        time = int(parts[0].strip())
        temp_url = parts[1].strip()
        if len(parts) > 1:
            loc = temp_url.lower().find('url=')
            if loc >= 0:
                url = temp_url[loc + 4:]
    return time, url


# Run all pages in the HAR file one at a time, replacing any parameters from the
modify_parameters dict
def execute_har(file_name, modify_parameters=None, base_path='HAR files/',
parse_refresh=True):
    # Init regex
    regex = r'<meta[^>]*?content=[\'\'](.*?)[\'\']'

    # Add '.har' if not already included
    if '.' not in file_name:
        file_name += '.har'
```

```
    # Read the file in
    with open(base_path + file_name) as file:
        data = json.load(file)

    # Get the pages that were loaded
    pages = parse_pages(data)

    # Simulate running each page in order, modifying parameters as necessary
    for index, page_id in enumerate(sorted(pages)):
        run_page = True
        url = pages[page_id]['url']
        while run_page:
            page_modification = None
            if modify_parameters and index + 1 in modify_parameters:
                page_modification = modify_parameters[index + 1]
            resp = execute_form(url, pages[page_id]
                                ['data'], page_modification, pages[page_id]['method'])

            # print(resp)

            if not parse_refresh:
                run_page = False
                continue
            match = re.search(regex, resp, re.MULTILINE | re.IGNORECASE)
            if match and match.groups():
                wait_time, _ = parse_refresh_str(match.groups()[0])
                time.sleep(wait_time + 1)
            else:
                run_page = False


# Directly download the link to a string without saving to a file
def get_vals(url):
    response = requests.get(url, auth=(username, password),
                            verify=False, allow_redirects=True)
    return response.text

# Download the given link to the given file_name (will automatically find the name if
none is provided)


def download_link(url, file_name=None, base_path='results/'):
```

```
        # Get the response
        response = requests.get(url, auth=(username, password),
                                verify=False, allow_redirects=True)

        # Figure out the file path
        if not file_name:
            file_name = os.path.basename(urlparse(response.url).path)
        file_path = base_path + file_name

        # Save the file
        with open(file_path, 'wb') as file:
            file.write(response.content)
    print('Result saved in', os.path.abspath(file_path))
```

Figure A5.3. Show Har Code (for displaying the .har file for reference or reminder) [Paul Reimann]:

```
import json
from helpers_fixed import *

# Prompt for the page name
page_name = input('Enter the HAR file name: ')

# Add '.har' if not already included
if '.' not in page_name:
    page_name += '.har'

# Read the file in
with open('HAR files/' + page_name) as file:
    data = json.load(file)

# Get the pages that were loaded
pages = parse_pages(data)

# Print the information
for index, page_id in enumerate(sorted(pages)):
```

```
print('Data for page ' + str(index + 1) + ':')
for key, value in pages[page_id]['data'].items():
    print('\t"' + key + '" = "' + value + '"')
print('\n')
```

Figure A5.4. Example of Desired .har File Format:

Enter the HAR file name: mulassis_1AU_SPE_ROSENQUIST_proton_1material >
Data for page 1:

Data for page 2:

Data for page 3:

Data for page 4:
"_JS_SUBMIT" =
"#saveform(mulassis_geo.html)#resetToPrevious(mulassis_geo.html)"
"USER" = "1"
"SHAPE" = "slab"
"NLAYER" = "3"
"MATERIALNAME(1)" = "G4_Al"
"THICKNESS(1)" = "0.81"
"TUNIT(1)" = "g/cm2"
"COLOURINDEX(1)" = "1"
"MATERIALNAME(2)" = "G4_Al"
"THICKNESS(2)" = "100"
"TUNIT(2)" = "um"
"COLOURINDEX(2)" = "1"
"MATERIALNAME(3)" = "G4_Si"
"THICKNESS(3)" = "10"
"TUNIT(3)" = "um"
"COLOURINDEX(3)" = "1"
"FILE" = "1"
"TRACK" = "0"
"VIS" = "1"
"#saveForm(mulassis_geo.html)#resetToPrevious(mulassis123_def.html)" =
"Save+>>"

Data for page 5:

"MAX_RUN_TIME" = "141"
"PARTICLETYPE" = "proton"
"NEVENTS" = "10000000"
"ANGULAR_DISTRIBUTION" = "cos"
"MIN_THETA" = "0.0"
"FLUNIT" = "cm2"

"#saveForm(mulassis123_def.html)#namelist(mulassis[mulassis_geo+mulassis_ana+mulassis123_cutoffs+mulassis123_def],USERMAT[g4_material_dat])#runModel(mulassis123_macro)#resetToPrevious(mulassis123_in.html)" = "Create+macro"

Data for page 6:

"_JS_SUBMIT" =
"#saveform(mulassis123_in.html)#resetToPrevious(mulassis123_in.html)"
"MULASSIS_version" = "126"
"#runModel(xeq_mulassisRun)#resetToPrevious(mulassis_out.html)" = "Run"

Data for page 7:

"#waitWhileRunning(2)" = "Refresh"

A6. Individual Material Fluence, MEO

This section is meant to show the fluence through each individual material, in Medium Earth Orbit. This helps shed light on the specific portions of the incident particle energy spectrum that are attenuated by each layer material. In prior research, it was noticed that different materials shield different portions of the incident particle energy spectrum to different degrees, suggesting that analysis of fluence through the individual materials will offer a method to engineer the FFCC into better shielding characteristics. This ended up being true to an extent, though the effect was shadowed by the discovery that hydrogen dense materials improve shielding to a great extent in all energy bands of the incident radiation, while fluence through individual layers suggests all materials tested shield a similar energy spectrum to varying levels. That is, most materials are seen to shield the lower energy particles satisfactorily while providing poor shielding for high energy particles, but the hydrogen dense materials are seen to have improved shielding across all energies in comparison to those materials with less hydrogen content.

Figure A6.1. MEO, Incident Trapped Proton Fluence

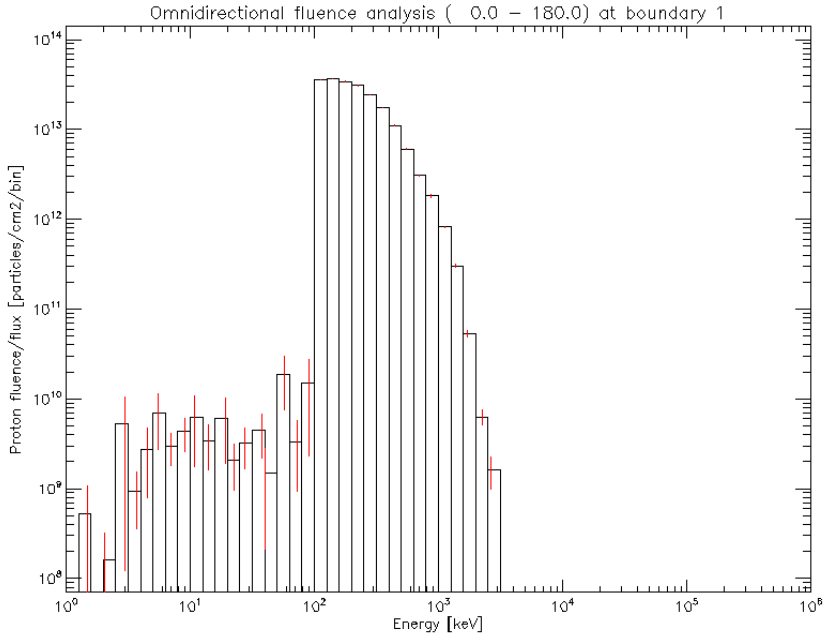

Figure A6.2. Al 0.81g/cm^2, 10M Particles, in MEO, Trapped Proton Fluence

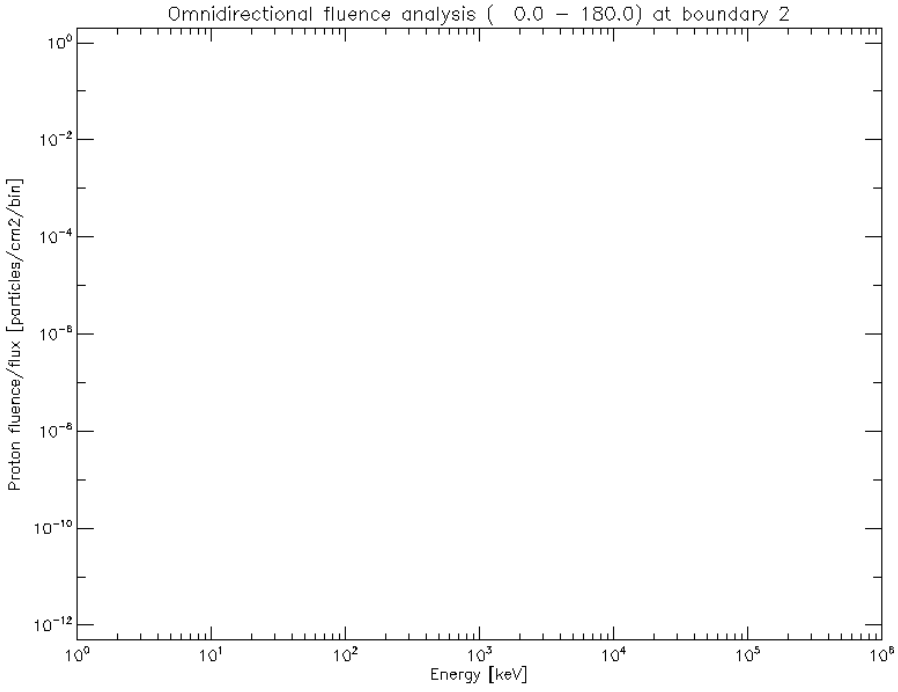

This is representative of all tested individual materials in MEO for trapped proton radiation, that is, all incident protons are completely attenuated.

Figure A6.3. MEO, Incident Trapped Electron Fluence

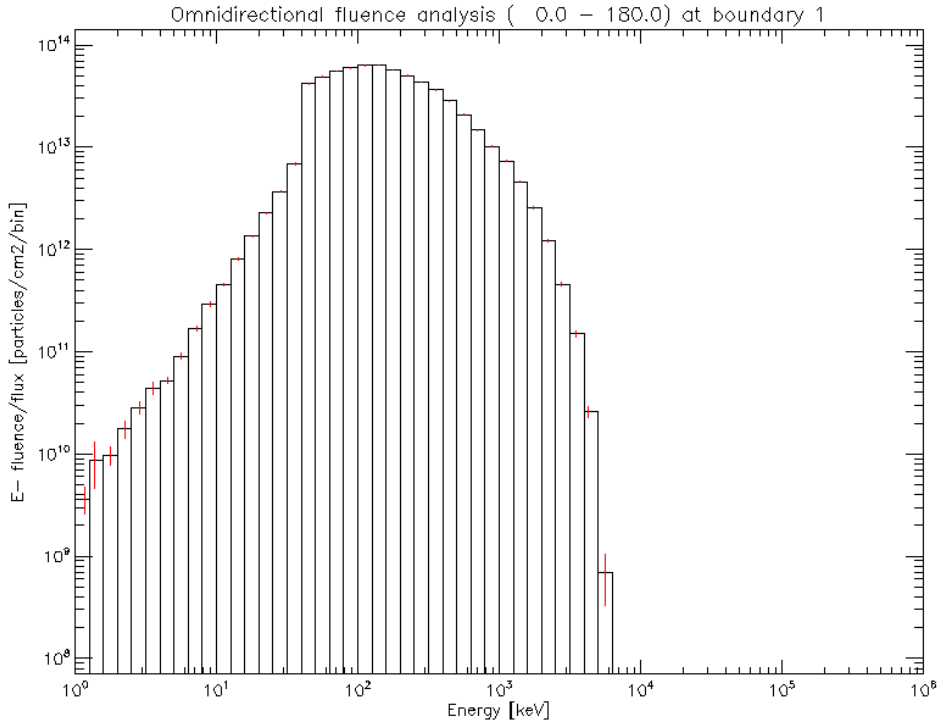

Figure A6.4. BN 0.81g/cm^2, 10M Particles, in MEO, Trapped Electron Fluence

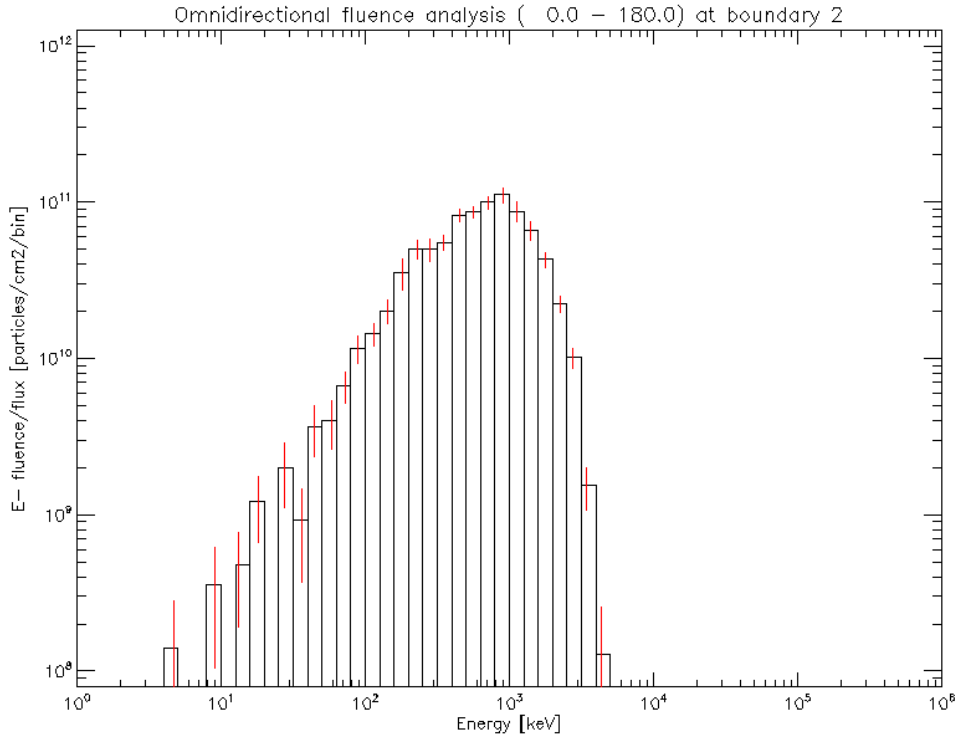

Figure A6.5. Al 0.81g/cm^2, 10M Particles, in MEO, Trapped Electron Fluence

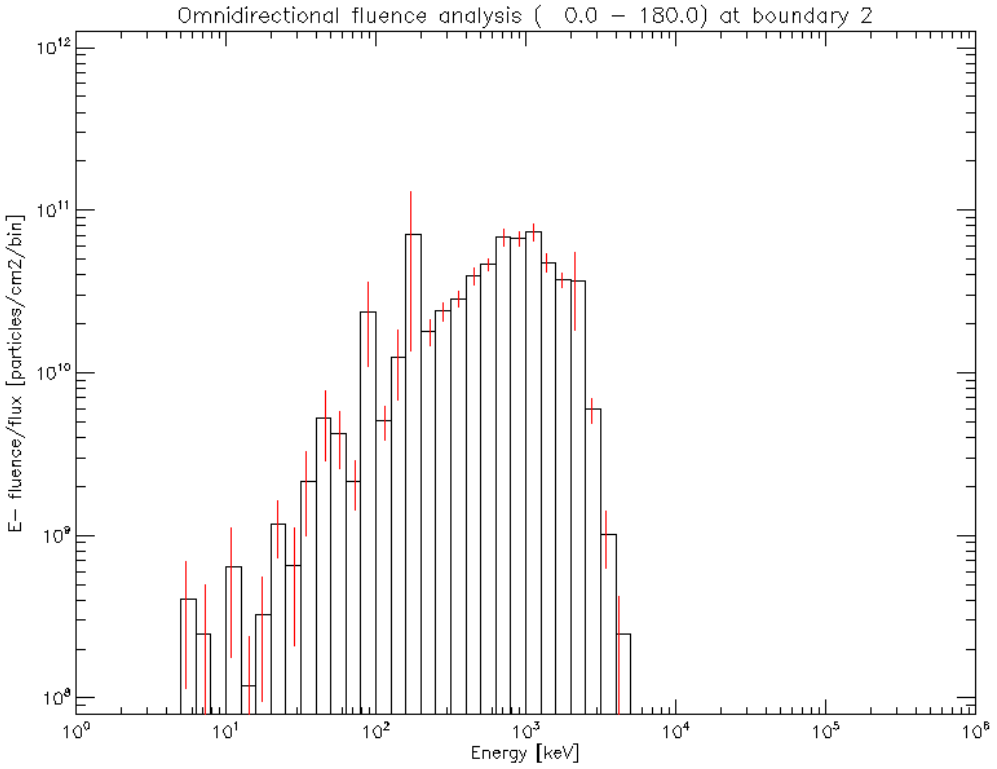

Figure A6.6. Polyethylene 0.81g/cm^2, 10M Particles, in MEO, Trapped Electron Fluence

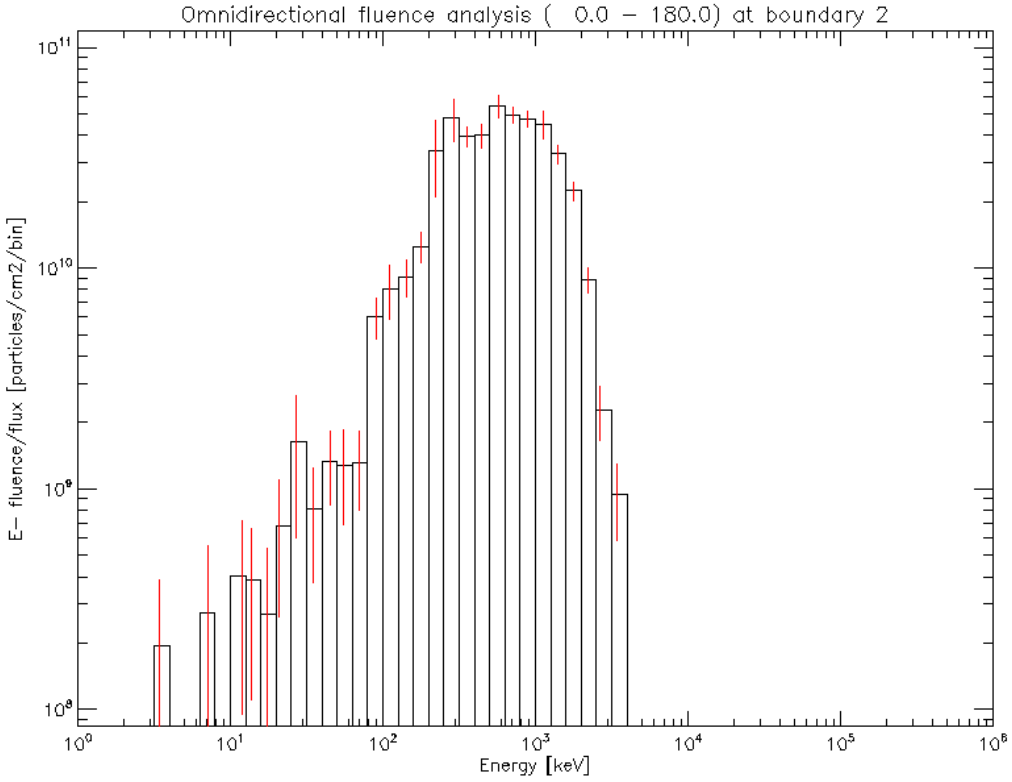

Figure A6.7. Ta 0.81g/cm^2, 10M Particles, in MEO, Trapped Electron Fluence

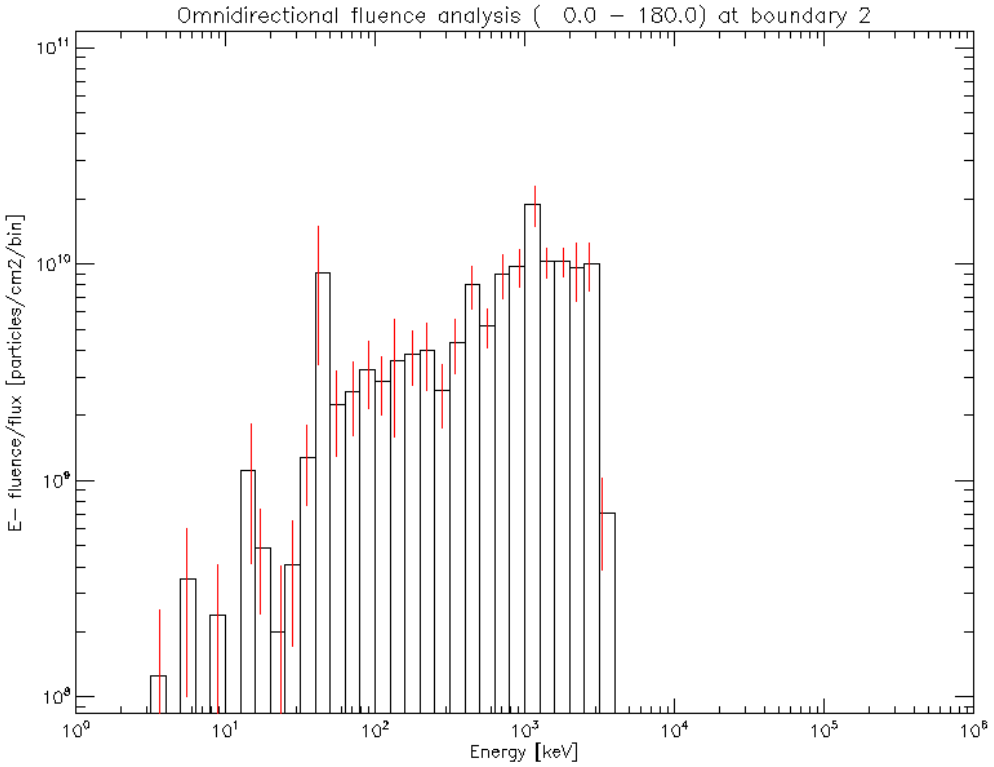

Figure A6.8. Water 0.81g/cm^2, 10M Particles, in MEO, Trapped Electron Fluence

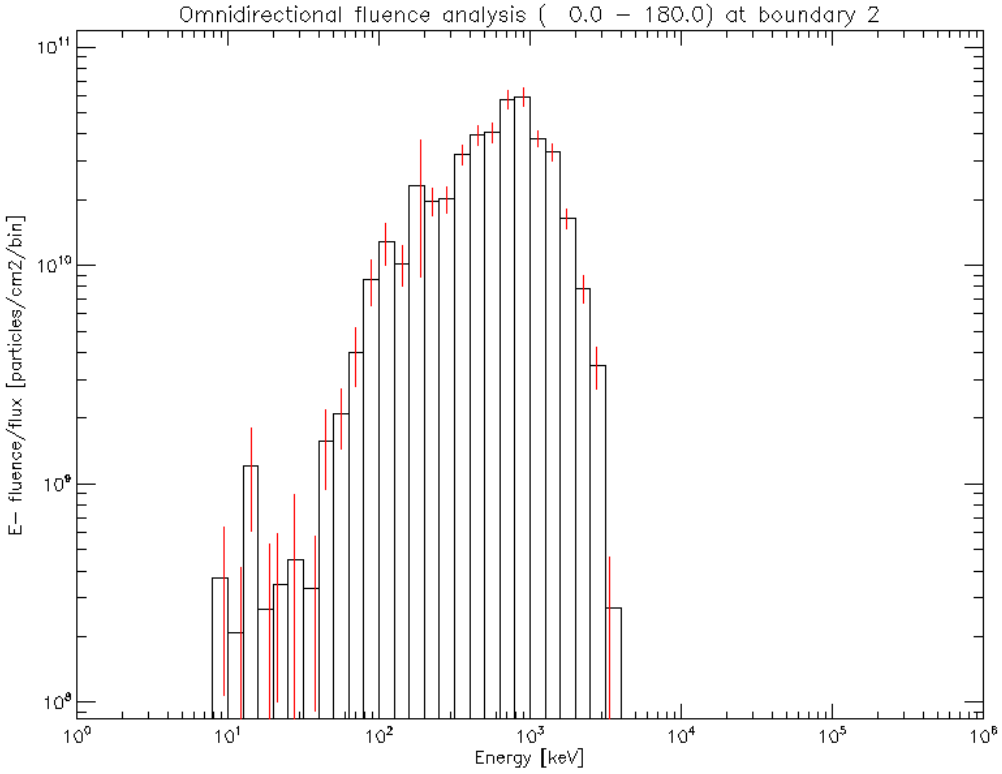

Figure A6.9. Kevlar 0.81g/cm^2, 10M Particles, in MEO, Trapped Electron Fluence

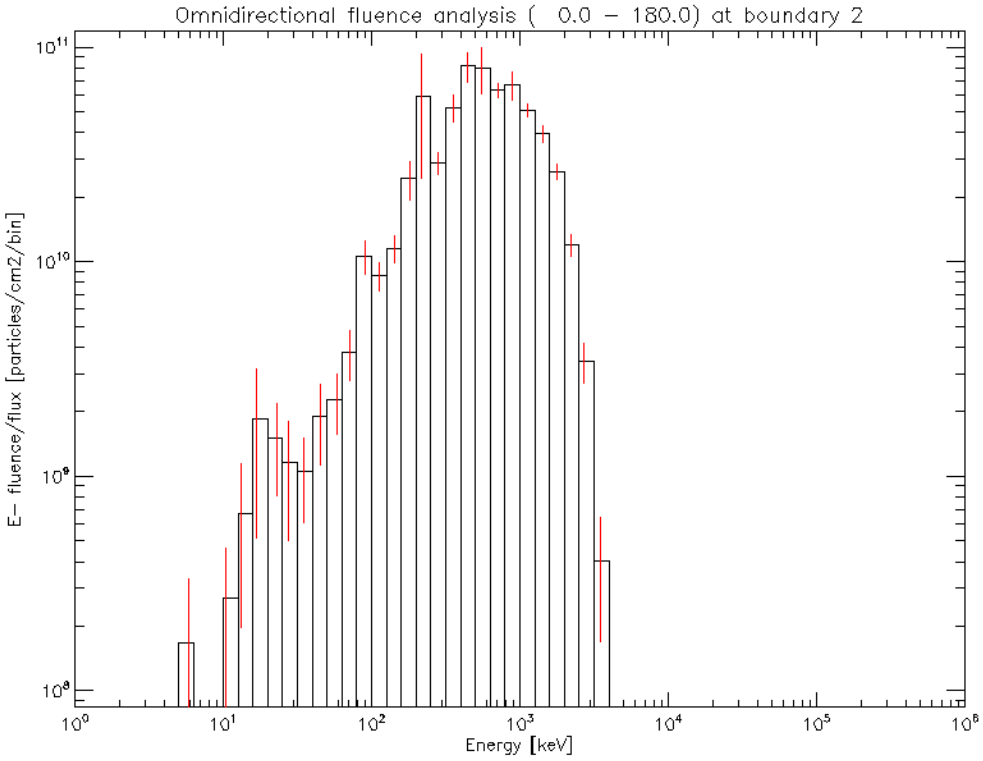

Figure A6.10. Nextel 0.81g/cm^2, 10M Particles, in MEO, Trapped Electron Fluence

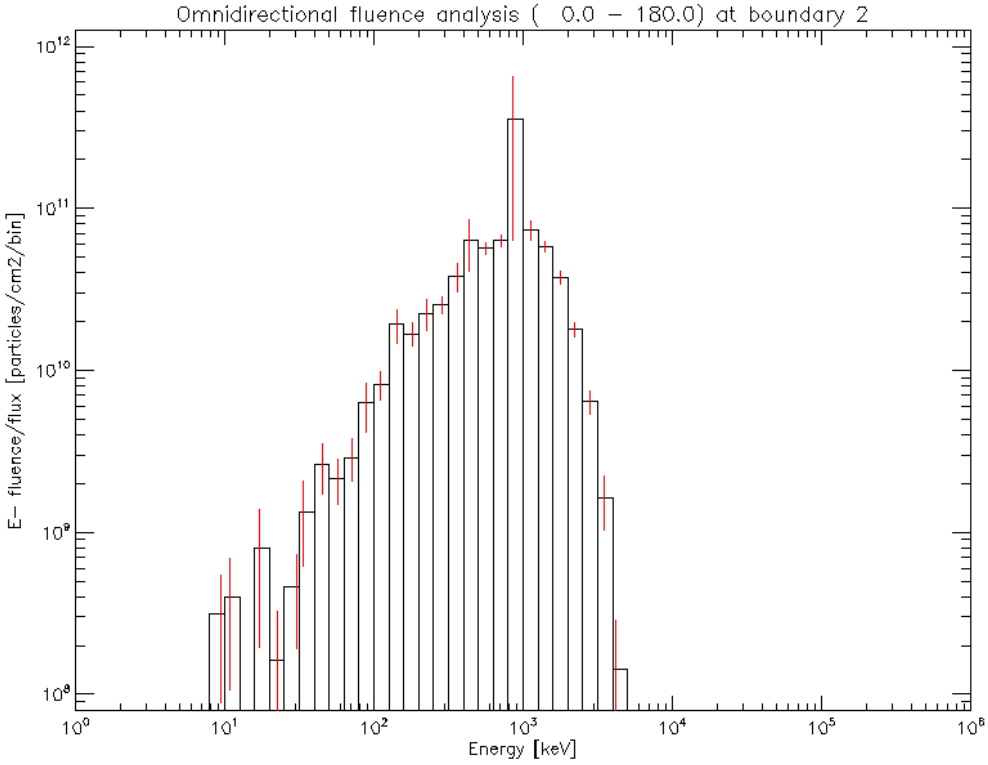

Figure A6.11. Poron 0.81g/cm^2, 10M Particles, in MEO, Trapped Electron Fluence

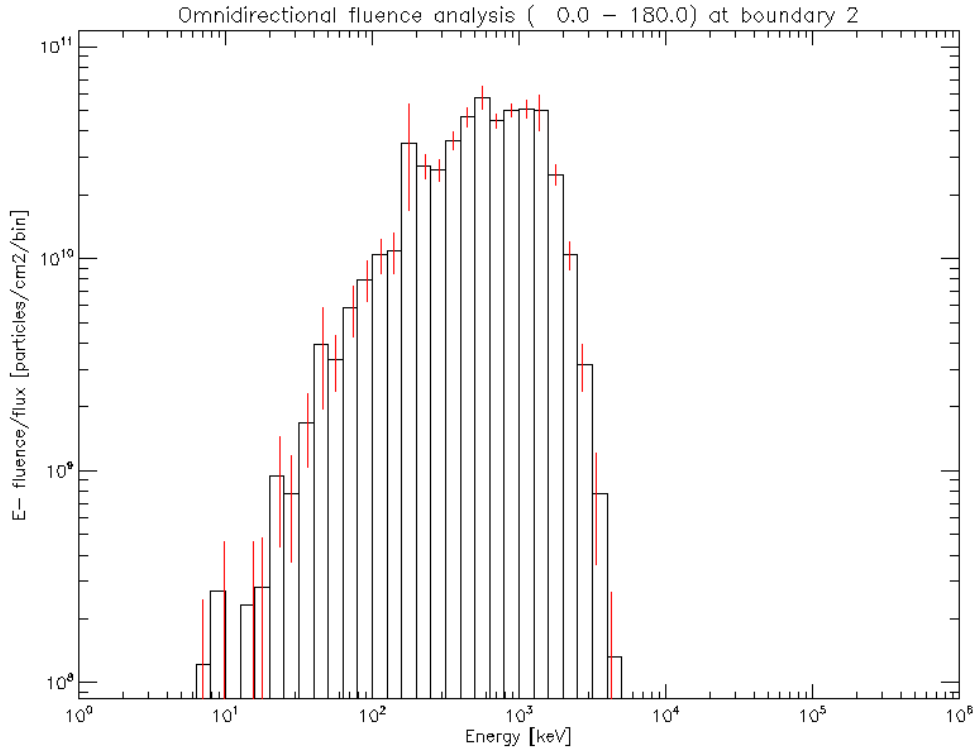

Figure A6.12. Tyvek 0.81g/cm^2, 10M Particles, in MEO, Trapped Electron Fluence

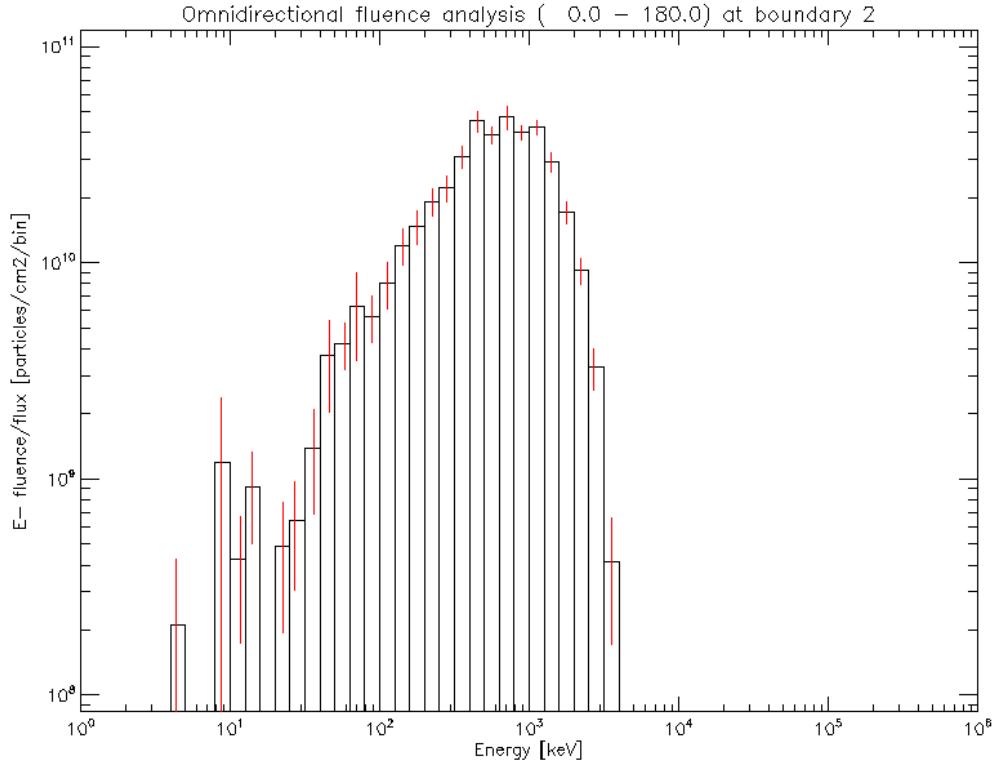

A7. Quality Function Deployment

The Quality Function Deployment was used to determine material capabilities with consideration of radiation shielding, density, and cost. Not considered in this QFD is structural applicability, or multifunctionality as no quantifiable measures have been made in this research. For each category, the values have been normalized to the minimum and maximum values and scaled to the priority seen in Figure A7 (min-max scaling). The cost of the FFCC was determined by the sum of the cost of its components, without regard to manufacturing costs (not yet determined). The density values are determined by the material definitions seen in Chapter 4. The shielding values used are from the TID values for trapped electrons in MEO.

Quality Function Deployment FFCC in MEO, Trapped Electron Radiation	Requirements	Shielding	Density	Cost	Total
	Priority	**100**	**75**	**50**	**225**
	Tantalum	100.00	0.0	10.51	**110.5**
	Aluminum	43.44	64.4	49.46	**157.3**
	Polyethylene	48.00	72.5	49.56	**170.1**
	1/6 Tyvek 2/3 PORONLH 1/6 Tyvek	65.19	74.2	48.18	**187.6**
	1/6 Kevlar 2/3 PORONLH 1/6 Kevlar	53.54	73.5	46.01	**173.1**
	1/6 Tyvek 2/3 BNWATER 1/6 Tyvek	52.82	72.2	49.53	**174.6**
	1/6 Nextel 2/3 PORONLH 1/6 Nextel	58.88	71.6	38.00	**168.5**
	1/6 Kevlar 1/6 Tyvek 1/3 PORONLH 1/6 Tyvek 1/6 Kevlar	48.95	72.6	46.58	**168.1**
	1/6 Kevlar 2/3 PORONWATER 1/6 Kevlar	52.82	72.2	49.53	**174.6**

Figure A7. QFD of Shielding, Density, and Cost

This is not a perfect comparison of the FFCC with traditional shielding materials, because the QFD does not account for the structural, thermal, acoustic, or impact characteristics of each material. A QFD that compares the multifunctional nature of the FFCC to traditional shielding is expected to show a greater difference in capability. This QFD does have value in showing the balance of radiation shielding with size and weight concerns inherent to space missions.

A8. Divergence from Prior Research

Those familiar with the FFCC project will notice the difference between the optimal FFCC compositions engineered in this investigation and those from the prior investigation [2]. The investigation of the FFCC for radiation shielding immediately prior to this research suggests that the best FFCC compositions tested have a drastically greater capacity for radiation shielding than what was found in the current investigation. With a deeper look, it has been determined that this is likely from a mistake in the custom material definition of Nextel in SPENVIS. Notably, the Chemical Formula was written as Al5-O11-Si-Bi in the prior research, instead of the correct Al5-O11-Si-B. The difference between bismuth and boron is apparent in shielding capability in

MEO, with the current research suggesting that Nextel and the FFCC as a whole (including Nextel) does not perform as well as suggested by Sid/Ghosh (2016) [3a].

INVESTIGATION OF A FLUID-FILLED CELLULAR COMPOSITE FOR RADIATION SHIELDING IN MEDIUM EARTH ORBIT AND INTERPLANETARY SPACE

by

Gabriel D. Maestas


NEW MEXICO TECH
SCIENCE • ENGINEERING • RESEARCH UNIVERSITY